

Predictive Models of Cell Alignment and Scar Formation under Mechanical Loading

A Dissertation

Presented to

the faculty of the School of Engineering and Applied Science

University of Virginia

in partial fulfillment
of the requirements for the degree

Doctor of Philosophy

by

Kellen Chen

December 2018

APPROVAL SHEET

This Dissertation
is submitted in partial fulfillment of the requirements
for the degree of
Doctor of Philosophy

Author Signature:  _____

This Dissertation has been read and approved by the examining committee:

Advisor: Jeffrey Holmes

Committee Member: Silvia Blemker

Committee Member: Doug DeSimone

Committee Member: George Christ

Committee Member: Thomas Barker

Committee Member: _____

Accepted for the School of Engineering and Applied Science:



Craig H. Benson, School of Engineering and Applied Science

December 2018

Table of Contents

Table of Contents	i
Abstract	v
Acknowledgements	ix
Chapter 1: Background.....	1
Scar Structure and Healing in Heart.....	2
Scar Structure and Healing in Tendon	3
Wound Healing Process.....	6
Mechanical Modulation of Fibroblast and Collagen Alignment	7
Fibroblast Alignment	8
Collagen Deposition and Alignment	10
Collagen Synthesis	12
Aims and Approaches	13
Significance	15
References.....	18
Chapter 2: Computational Modeling of Stress Fiber Alignment	28
2.1 Introduction	29
2.2 Methods	31
2.2.1 Stress Fiber Alignment Model Description	32
2.2.2 Description of Test Conditions	33
2.2.3 Implementation of Model.....	35
2.3 Results and Discussion	38
2.3.1 Stress Fiber Alignment in the Absence of Compaction	38
2.3.2 Stress Fiber Alignment in the Presence of Transverse Compaction ...	38
2.3.3 Stress Fiber Alignment in the Presence of Isotropic Compaction	41
2.3.4 Conclusions and Future Directions and Limitations	41
2.4 References.....	45

Chapter 3: Role of Boundary Conditions in Determining Cell Alignment in Response to Stretch	46
3.1 Introduction	47
3.2 Methods	49
3.2.1 Adult Cardiac Fibroblast Isolation and Culture	49
3.2.2 Fabrication of Fibroblast-Populated Collagen Hydrogels	50
3.2.3 Loading of Collagen Gels and Description of Test Conditions	53
3.2.4 Fabrication of Customized Stretching Frame	54
3.2.5 Quantification of Gel Compaction	56
3.2.6 Microscopy and Quantification of Cell Alignment	57
3.2.7 Quantifying Parallel vs. Perpendicular Alignment of Cells and Stress Fibers	60
3.2.8 Experimental Measurements of Cell Alignment in 2D	60
3.2.9 Statistics.....	61
3.2.10 Improved Thermodynamic Computational Model of Stress Fiber Alignment	61
3.2.11 Comparison of Cell Alignment to In Vitro Stress Fiber Alignment	62
3.3 Results and Discussion	65
3.3.1 Cellular Alignment in the Presence of Transverse Compaction	65
3.3.2 Cellular Alignment in the Presence of Isotropic Compaction.....	69
3.3.3 Cellular Alignment in the Absence of Compaction	70
3.3.4 Effect of Stretching Frequency on Cellular Alignment in 3D Gels	72
3.3.5 Mechanical Determinants of Cell Alignment in 2D and 3D.....	75
3.3.6 Modified Computational Predictions of Cell Alignment.....	76
3.3.7 Comparison of Cell Alignment with In Vitro SF Alignment.....	81
3.3.8 Limitations and Sources of Error	84
3.4 References	85
 Chapter 4: Development of Experimental Protocols to Study Fibroblast Alignment, Deformation, and Extracellular Matrix Synthesis	 89
4.1 Introduction	90
4.2 Methods	91

4.2.1 Utilizing Dil to Live Stain Fibroblasts in Collagen Gels.....	91
4.2.2 Using Fluorescent Microspheres to Quantify ECM and Cell Strains ...	91
4.2.3 Second Harmonic Generation Microscopy of Collagen.....	94
4.2.4 Stimulating Synthesis of Collagen and Fibronectin by Fibroblasts.....	94
4.3 Results and Discussion.....	96
4.3.1 Fibroblast Alignment After Tension Release.....	96
4.3.2 Global Gel Strains versus Strains Near and Away from Cells.....	99
4.3.3 SHG Microscopy of Fibroblasts Remodeling Collagen Gels.....	102
4.3.4 Deposition of Collagen by Fibroblasts.....	102
4.3.5 Deposition of Fibronectin by Fibroblasts.....	107
4.4 References.....	110
4.5 Appendix.....	112
Appendix 4.5.1.....	112
Appendix 4.5.2.....	113
Appendix 4.5.3.....	114
Chapter 5: Multiscale Computational Model of Achilles Tendon Healing: Integrating Biology and Mechanics.....	115
5.1 Introduction.....	116
5.2 Methods.....	117
5.2.1 Literature Collection.....	118
5.2.2 OpenSim Simulations and Strains.....	120
5.2.3 Thermodynamic Computational Model of Cell Alignment.....	125
5.2.4 Agent Based Model of Achilles Tendon Wound Healing.....	127
5.3 Results and Discussion.....	133
5.3.1 Effect of Unloading and Loading on Unrepaired Achilles Tendons ...	133
5.3.2 Effect of Unloading and Loading on Surgically Repaired Achilles Tendons.....	137
5.3.3 Effect of Intermittent Loading on Cell Alignment.....	142
5.3.4 Limitations.....	145
5.3.5 Conclusions.....	148

5.4 References	149
Chapter 6: Summary and Final Conclusions	156
Motivation	157
Role of Boundary Conditions in Determining Cell Alignment in Response to Stretch	158
Effect of Repair and Loading on Achilles Tendon Wound Healing	160
References	162

Abstract

Following injury to many different tissues in the body – including heart, tendons and ligaments, spinal cord, and skin – the body builds scar tissue through a complex wound healing process. The structural and mechanical properties of the resultant scar are critical in determining the overall function of the repaired tissue, particularly for tissues that are under high mechanical load. In the case of healing after myocardial infarction in the heart, our lab has found that longitudinally reinforcing the damaged region can significantly improve cardiac output and pump function, suggesting that manipulating the healing process to generate longitudinally aligned collagen could represent a novel therapeutic approach. In tendons and ligaments, collagen in the scar tissue that forms following injury is generally less aligned and mechanically weaker than native tissue, again suggesting that controlling collagen alignment in healing scar could be an important therapeutic advance. Currently, the exact determinants of scar structure are not understood well enough to design protocols to achieve a desired outcome.

Fibroblasts are the primary drivers of collagen deposition and scar formation. These cells align in response to cues from their environment and synthesize, assemble, remodel, and cross-link collagen within the developing scar, mediating the development of scar mechanical properties. In both healthy and scar tissue, fibroblasts are typically found aligned with local collagen fibers, suggesting that fibroblast alignment and collagen organization are mechanistically related. While

we know that the mechanical environment plays a key role in driving cellular behaviors and scar formation, a more complete understanding of how the mechanical environment influences cell and collagen alignment may enable us to develop better interventions for healing scar tissue. The overall goal of this dissertation was to develop predictive models of fibroblast alignment and scar formation during wound healing. The overall approach of this dissertation was to first experimentally test the effect of the mechanical environment on cell alignment across a broad range of mechanical conditions. We then used this data to develop a computational model of cell alignment and incorporated that validated cellular model into a multiscale computational framework to predict scar formation in the healing tendon.

Fibroblasts, endothelial cells, mesenchymal stem cells, and osteoblasts all orient perpendicular to an applied cyclic stretch when plated on stretchable elastic substrates, suggesting a common underlying mechanism. Yet many of these same cells orient parallel to stretch *in vivo* and in 3D culture, and a compelling explanation for the different orientation responses in 2D and 3D has remained elusive. Here, we employed a novel experimental system to conduct a series of experiments designed specifically to test the hypothesis that differences in strains transverse to the primary loading direction give rise to the different alignment patterns observed in 2D and 3D cyclic stretch experiments (“strain avoidance”). We found that in static or low-frequency stretch conditions, cell alignment in fibroblast-populated collagen gels correlated with the presence or

absence of a restraining boundary condition, rather than with compaction strains. Cyclic stretch could induce perpendicular alignment in 3D culture, but only at frequencies an order of magnitude greater than reported to induce perpendicular alignment in 2D. We modified a published model of stress fiber dynamics and were able to reproduce our experimental findings across all conditions tested, as well as published data from 2D cyclic stretch experiments. These experimental and model results suggest a new explanation for the apparently contradictory alignment responses of cells subjected to cyclic stretch on 2D membranes and in 3D gels.

Next, we used this knowledge about cell alignment and applied it to make predictions about scar formation within the healing tendon. Mechanical stimulation of the healing tendon is thought to regulate scar anisotropy and strength and is relatively easy to modulate through physical therapy. However, *in vivo* studies of various loading protocols in animal models have produced mixed results. To integrate and better understand the available data, we developed a multiscale model of rat Achilles tendon healing that incorporates the effect of changes in the mechanical environment on fibroblast behavior, collagen deposition, and scar formation. We modified an OpenSim model of the rat right hindlimb to estimate physiologic strains in the lateral/medial gastrocnemius and soleus musculo-tendon units during loading and unloading conditions. We used the tendon strains as inputs to a thermodynamic model of stress fiber dynamics that predicts fibroblast alignment, and to determine local collagen synthesis rates

according to a response curve derived from *in vitro* studies. We then used an agent-based model (ABM) of scar formation to integrate these cell-level responses and predict tissue-level collagen alignment and content. We compared our model predictions to experimental data from ten different studies. We found that a single set of cellular response curves can explain features of observed tendon healing across a wide array of reported experiments in rats – including the paradoxical finding that repairing transected tendon reverses the effect of loading on alignment – without fitting model parameters to any data from those experiments. The key to these successful predictions was simulating the specific loading and surgical protocols to predict tissue-level strains, which then guided cellular behaviors according to response curves based on *in vitro* experiments. Our model results provide a potential explanation for the highly variable responses to mechanical loading reported in the tendon healing literature and may be useful in guiding the design of future experiments and interventions.

Acknowledgements

When I first started this journey at the University of Virginia, I could never have imagined the support I would receive. Thank you to everyone who has helped me along the way! First, I would like to thank my advisor, Jeffrey Holmes. Since the beginning, you have always been there to challenge me, teach me, and provide valuable insight during my graduate career. Thank you for all the guidance to help me grow as a scientist and researcher. I have also learned so much by just observing how you mentor others or deal with difficult situations. Finally, I appreciate his support in allowing me to explore my various interests, ranging from externships to teaching to clinician shadowing to entrepreneurial seminar courses.

I would like to thank the rest of my committee for their guidance on my research and professional development. Your comments and suggestions helped focus my research goals and formulate a holistic story for this dissertation. Thank you Silvia, for introducing me to Xiao and providing guidance and advice during our collaboration for the tendon multiscale model; George, for providing me with valuable teaching experience when I was a TA for your BME Physiology II class; Doug, for serving as my BTP minor mentor and helping me think more deeply about intracellular mechanisms; Tom, for all the brainstorming sessions about interesting new possibilities and experiments for my research.

I would like to thank all the members of the Cardiac Biomechanics Group for all their support and the good times we've spent together in lab. I have valued all of your advice and friendship over the years. Thank you to Dr. Will Richardson for being one of my first mentors in the lab, giving me incredible advice on just how to be a good graduate student, balance my time, and deal with negative data. Thank you Dr. Colleen Witzenburg and Dr. Kyoko Yoshida for all their career advice and encouragement; Dr. JJ Lee for all the conversations about life; Dr. Christian Moyer, Dr. Sam Clarke, and Dr. Pim Oomen for being valuable

mentors. Thank you to Ana Estrada, TK Phung, Laura Caggiano, Derek Bivona, Arlynn Baker, and Mike Torres—I cannot express how lucky I am to have such friendly and fun lab mates to not only help me with research but also to hang out with outside of the lab. I would also like to thank George Morcos and Sarah Schroter for being highly motivated and passionate undergraduate researchers. I wish I could individually thank all of the other great friends and colleagues I've made over the years. I could not have done it without your guidance, support, lunch and coffee conversations, and I thank you.

I would like to thank Erin for her love, care, and support. I am so thankful for our fun adventures and traveling, your enthusiasm about science, and all the encouragement you've given me during such a busy and exciting time in my life.

Finally, I would like to thank my family. Thank you to my dad for always pushing me towards my goals, helping me navigate difficult situations, and being there to celebrate all of our sports teams. Thank you to my mom for always being excited and enthusiastic about my successes while still providing me support and care to get me through the stressful times. Last but not least, thank you, Kenny for being one of my closest friends. I cannot stress how valuable it is to have someone I can confide in about any and all aspects of my life. Someone I can fully trust and always has my back.

Thank you everyone, and I hope you enjoy my dissertation.

Chapter 1

Background: Predictive Models of Cell Alignment and Scar Formation under Mechanical Loading

Scar Structure and Healing in Heart

Over a million people annually suffer from a myocardial infarction in America. With improvements in treatment and therapy, most people survive the initial event but then experience life-threatening complications later (Lloyd-Jones et al. 2010). During a myocardial infarction, the healthy heart tissue loses its oxygen supply and dies. Passive scar tissue replaces the previously healthy, contracting heart tissue, and the structural and mechanical properties of this scar tissue play a critical role in maintaining cardiac function and structural integrity (Holmes, Borg, and Covell 2005). Some infarcts cannot withstand the continual mechanical loading placed on them and rupture in the first few days (Wehrens and Doevendans 2004). Other infarcts withstand the continual load, but stretch and thin in a way that can severely alter the mechanical environment of the heart. This altered state leads to dilation of the left ventricle, loss of cardiac function, and progressive heart failure (Weisman and Healy 1987; Richardson and Holmes 2015; Caggiano, Lee, and Holmes 2018). Many therapies have emerged in an attempt to prevent remodeling or restore the normal mechanical environment, such as directly stiffening the scar using a polymer injection or limiting excessive deformation using cardiac restraint devices. Our lab has recently found that anisotropically reinforcing healing scar (stiffer longitudinally than circumferentially) can acutely improve cardiac output and pump function (Fomovsky et al. 2012; Fomovsky et al. 2011), leading us to believe that developing a longitudinally anisotropic scar could lead to better outcomes. Understanding how the collagen structure forms within the healing scar will allow

us to develop therapies to produce this desired anisotropic scar structure and potentially reduce complications after myocardial infarction.

Scar Structure and Healing in Tendon

Tendons and ligaments transmit force between muscles and bones throughout the body and are comprised of highly aligned collagen fibers that help bear high loads. Damage to the tendon due to injuries such as rupture or overuse causes major pain, disability, and loss of productivity in our society. The ability of the Achilles tendon to bear load is especially important, as it can be exposed to loads up to 70 MPa, whereas most other tendons only experience loads up to 30 MPa (Kongsgaard et al. 2005). Achilles tendon ruptures account for up to 45% of all tendon ruptures (Jozsa et al. 1989) and afflict up to 2.5 million annually (McCormack and Bovard 2015; Rigglin et al. 2014). Prevalence of Achilles tendon ruptures has also increased in recent years, directly related to the increase of recreational sports and other physically demanding activities. Tendon and ligament ruptures affect our active military population (White et al. 2007), and professional athletes suffer from Achilles tendon ruptures every year (Jozsa et al. 1989; Leppilahti, Puranen, and Orava 1996; Moller, Astron, and Westlin 1996; Amin et al. 2013; Parekh et al. 2009). Many who suffer from an Achilles tendon rupture never regain complete function.

About 80% of Achilles tendon ruptures occur 3-6 cm above the calcaneal insertion, potentially because this area experiences high amounts of stress and a

low blood supply that leads to chronic inflammation and tendinopathy. Healthy Achilles tendon is comprised of dense, tightly aligned collagen, and it is hypothesized that this chronic tendinopathy leads to chronic deterioration of the collagen fibers and eventually catastrophic injury. After the rupture event, healing tendons form scar with reduced collagen fiber organization and stiffness compared to uninjured tendons (Soslowky et al. 2000). Despite many studies intended to identify optimal treatment methods after injury in patients, current treatments have produced only moderate results (Freedman, Gordon, and Soslowky 2014). While there seems to be general agreement that mechanical stimulation is important for controlling the scar anisotropy (Thomopoulos, Williams, and Soslowky 2003), the effects of the exact timing and magnitude of this stimulation are still not well understood (Kongsgaard et al. 2005). McCormack and Bovard (McCormack and Bovard 2015) observed that physical therapy regimens involving early mobilization after rupture can lead to better functional outcomes compared to cast immobilization followed by delayed mobilization. However, this early mobilization comes with an increased risk of re-rupture, since patients with previously injured tendons are already more likely to re-rupture the tendon (McCormack and Bovard 2015; Wills et al. 1986) and 200 times more likely to overload and rupture the contralateral tendon (Årøen et al. 2004). Consequently, suture repair of tendons has emerged as a common treatment for Achilles tendon ruptures to reduce chances of re-rupture, although little characterization has been done on the effect of this procedure on functional outcomes outside of decreasing re-rupture likelihood.

Recently, researchers and surgeons have become increasingly interested in using non-surgical repair methods and allowing the tendons to heal naturally to reduce chances of infection. Studies that have attempted to evaluate the differences between suture-repaired and non-surgical repaired tendons during loading, however, have produced variable outcomes. While some observed no significant differences in functional outcomes from loading (Olsson et al. 2013; Weber et al. 2003; Twaddle and Poon 2007), others have observed the opposite, claiming that early loading of the tendon only provided beneficial effects for suture-repaired tendons and had no effect for non-repaired (M. L. Costa et al. 2006; Metz et al. 2008). Furthermore, since performing actual biomechanical testing on the subjects can be challenging, many of these studies also mainly used qualitative or subjective metrics, such as patient satisfaction or time to return to work.

Because obtaining long term, non-destructive, and quantitative data in human subjects is challenging, animal models—such as rat—of Achilles tendon rupture have been utilized to better understand the impact of loading. These studies have also led to a wide variety of results, with mechanical loading sometimes appearing to increase, but at other times appearing to decrease, tendon properties such as stiffness or rupture strength. One of the potential explanations for this variability could be due to differences in mechanics during healing. In some studies, tendons have been completely unloaded by tail suspension or botulinum toxin (Botox) injection into the gastrocnemius muscle (Eliasson,

Andersson, and Aspenberg 2009; Eliasson, Andersson, and Aspenberg 2012; Andersson et al. 2012; Andersson, Eliasson, and Aspenberg 2009; Tuzuner et al. 2013). In others, the injured leg was put into a cast that prevented excessive load but still allowed for isometric contractions to occur (Freedman et al. 2016; Meier Bürgisser et al. 2016; Murrell et al. 1994; Palmes et al. 2002; Bring et al. 2009; Ikoma et al. 2013; Schizas et al. 2010; Min et al. 2013). Increasing loads have also been applied by allowing the rat to freely walk around its cage (Andersson, Eliasson, and Aspenberg 2009; Tuzuner et al. 2013; Freedman et al. 2016; Schizas et al. 2010; Freedman et al. 2013) or subjecting the rat to an exercise regimen by running on a treadmill daily (Eliasson, Andersson, and Aspenberg 2012; Freedman et al. 2016; Heinemeier et al. 2012; Glazebrook et al. 2008; T. F. Huang, Perry, and Soslowsky 2004). These interventions have also been studied in both non-repaired and suture-repaired tendons (Freedman et al. 2016; Meier Bürgisser et al. 2016), which could potentially affect the mechanical environment by altering the length at which the tendon begins to exert passive elastic force.

Wound Healing Process

Whether in a myocardial infarction, a tendon or ligament rupture, spinal-cord injury, or a burn wound, the wound healing process remains relatively similar across the body and comes in three stages: inflammation, scar formation, and remodeling (Richardson et al. 2015; Gurtner et al. 2008). Immediately following the initial injury event, healthy cells die, and inflammatory cells, such as

neutrophils, macrophages, and lymphocytes, infiltrate the wound area. These inflammatory cells phagocytose necrotic material (e.g. dead myocytes in the heart) and deposit a provisional matrix, primarily composed of fibrin and fibronectin, which prevents fluid/blood loss within the wound and maintain a temporary initial structure (Grinnell 1984). The inflammatory cells also release cytokines, such as TGF- β , interleukins, or TNF- α , which promote early inflammation and recruit other cell types, such as fibroblasts, to initiate fibrosis. Fibroblasts sense these chemokines, migrate into the wound area, and proliferate. These fibroblasts could originate from the healthy, surviving tissue or even other nearby tissues, such as the pericardium in heart or paratenon in Achilles tendon (Müller et al. 2018). On the time scale of weeks, fibroblasts continue to proliferate while synthesizing and depositing collagen to form the scar tissue. The inflammatory cell population steadily decreases during this period. On the time scale of months, the fibroblast population begins to wane (Caggiano, Lee, and Holmes 2018). Within this final remodeling phase, smaller populations of fibroblasts maintain the scar tissue by producing a steady state of collagen and creating mature scar tissue through cross-linking (Richardson et al. 2015).

Mechanical Modulation of Fibroblast and Collagen

Alignment

Fibroblasts align in response to their environment and synthesize, assemble, remodel, and cross-link collagen within the developing scar (Langberg et al. 1999; Layman, McGoodwin, and Martin 1971), mediating the development of

scar mechanical properties. Specifically, the mechanical environment plays a key role in driving some of these cellular behaviors. In both healthy and scar tissue, fibroblasts are typically found aligned with local collagen fibers, suggesting that fibroblast alignment and collagen organization are mechanistically related (Soslowsky et al. 2000). Improving our understanding of how fibroblasts align and produce subsequent scar structures could give us better insights into how to optimize collagen alignment and scar anisotropy during wound healing.

Fibroblast Alignment

Various studies have attempted to determine how the mechanical environment drives cell alignment. Traditionally, most of these experiments have been conducted by seeding cells on 2D silicone elastomer membranes, gripping the ends of the membrane, and pulling to initiate stretch. While equibiaxial static or cyclic stretch resulted in random alignment, many early experiments that subjected cell-seeded membranes to uniaxial cyclic stretch observed perpendicular alignment of cells (C. Huang et al. 2013; Moretti et al. 2004; Kaunas et al. 2005; Ives, Eskin, and McIntire 1986; Karlou et al. 1999; Hsu, Lee, and Kaunas 2009; Jungbauer et al. 2008), which seemed to clearly demonstrate that cells avoided cyclic strain. A recent study by Livne et al. even observed that cells stretched on flexible substrates with a larger Poisson ratio actually aligned obliquely in the direction of lowest strain, away from both the stretching and Poisson strains (Livne, Bouchbinder, and Geiger 2014). Researchers have also explored the effect of stretching cells within 3D environments, most typically within collagen or fibrin hydrogels, to better mimic physiological conditions.

Surprisingly, while cells plated on a flexible 2D substrate oriented perpendicular to an applied uniaxial cyclic stretch (C. Huang et al. 2013; Moretti et al. 2004; Kaunas et al. 2005; Ives, Eskin, and McIntire 1986; Karlou et al. 1999; Hsu, Lee, and Kaunas 2009), these same types of cells embedded in a 3D matrix oriented parallel to stretch (E. J. Lee, Holmes, and Costa 2008; Foolen et al. 2012; Matsumoto et al. 2007; Roby, Olsen, and Nagatomi 2008; Bellows, Melcher, and Aubin 1982; Hu, Humphrey, and Yeh 2009; Pang et al. 2011).

Within these 3D matrix hydrogel environments, cells interact with their environment and bind to the matrix fibers surrounding them. Cells cultured in free floating, unconstrained gels exert traction forces on their environment, pulling on fibers and compacting the gels to as little as 30% of their original size after a few days and aligning randomly (Knezevic et al. 2002; Bellows, Melcher, and Aubin 1982). Cells constrained equibiaxially also align randomly, while cells constrained uniaxially align parallel to the direction of the constraint, leading some to believe that these cells align depending on their boundary conditions and the direction they can exert traction forces. Hu *et al.* observed that the stretch ratio from non-equibiaxial stretch conditions (stretch of different magnitudes in x_1 and x_2) generated anisotropy of substrate rigidity and that cells aligned preferentially in the stiffer direction (Hu, Humphrey, and Yeh 2009). On the other hand, Barocas and Tranquillo developed an anisotropic biphasic theory that the uniaxial constraint (x_1 constrained, x_2 left free) allowed cells to exert traction forces in the transverse direction, re-aligning collagen fibers towards the direction of the

constraint. The cells then aligned parallel to these remodeled collagen fibers (Barocas and Tranquillo 1997; Barocas and Tranquillo 1994). Studies conducted with cells aligning on top of microgrooves or within pre-aligned matrix further supported the concept that contact guidance could be the dominant factor guiding cell alignment in 3D (Vernon et al. 2005; Zhong et al. 2006).

Collagen Deposition and Alignment

Previous studies have pointed toward the importance of fibroblast alignment in guiding aligned deposition of collagen in healing scar tissue (Fomovsky, Rouillard, and Holmes 2012; Rouillard and Holmes 2012). While we know that the cells produce the collagen, several potential theories have emerged on how cells generate collagen fiber alignment. The Ruberti group has observed that flow could polymerize soluble collagen monomers into long, highly aligned collagen fibers and theorized that forces generated between cells *in vivo* could create flow and generate aligned collagen in the tendon (Paten et al. 2016). Others have observed that collagen monomers confined between aligned microgroove plates polymerize aligned with the grooves and theorized that the same “structural constraint” phenomena could occur *in vivo*, in which monomers may be constrained physically by existing collagen and other cells as they polymerize and align (Ruberti and Zieske 2008; Bhole et al. 2009; Giraud-Guille, Besseau, and Martin 2003). However, both of these theories originate from experiments performed in non-physiologic conditions and are hard to prove *in vivo*. The Kadler group has used electron microscopy to capture the existence of a structure they termed fibropositors, vesicles hypothesized to process procollagen

into collagen fibers within the cell and then protrude from the plasma membrane along the cell boundary to lay down collagen fibers (Canty et al. 2004; Canty and Kadler 2005). Picrosirius red, H&E staining, and immunostaining techniques have been commonly used to determine the alignment and amount of collagen, but have mostly been used to observe the overall collagen structure produced by entire populations of cells (Robinson et al. 2008; Sander, Barocas, and Tranquillo 2011; Nieponice et al. 2007). For instance, Breidenbach *et al.* demonstrated that fibroblasts cultured within fibrin gels can build aligned collagen matrices when subjected to uniaxial boundary conditions (Breidenbach et al. 2015). Second harmonic generation (SHG) microscopy has recently emerged as a non-invasive, non-destructive technique to observe collagen, as it relies on the triple helical configuration of collagen to generate natural fluorescence of the fibers (Hase et al. 2016). Mortati *et al.* recently demonstrated the potential of this technique by using it to observe co-localization of nano-scale collagen signals with individual cells, although their cells did not produce enough collagen to form actual fibers, even by 28 days. These studies demonstrate that observing how single cells specifically deposit individual collagen fibrils remains challenging and difficult to test experimentally. Cells must be cultured in conditions that stimulate enough proliferation and collagen synthesis to develop collagen fibers and maintain cell homeostasis, but not so much that cells become confluent and build entire tissue matrices.

Collagen Synthesis

In addition to guiding alignment of fibroblasts and subsequent alignment of collagen, the mechanical environment also guides the amount of collagen synthesized by fibroblasts. Within the heart, our group recently demonstrated this by sewing a patch to anisotropically unload the infarcted area in a rat heart (Caggiano, Lee, and Holmes 2018). They measured levels of carboxy-terminal propeptide of type I procollagen (PICP), a biomarker for collagen synthesis, using microdialysis to collect fluid within the infarct. Infarcts with patches, and consequently a decreased mechanical stimulus, produced much lower levels of procollagen I, especially during the first two weeks. Similar responses have been more extensively observed in the tendon, where the mechanical environment is much easier to modulate. Studies in humans have interestingly observed that after a bout of exercise, collagen levels initially drop within the first 24 hours (Sullivan et al. 2009; Langberg et al. 1999; Rennie and Tipton 1998), but then increase over 3-fold after 72 hours in healthy tendon. Kongsgaard *et al.* (Kongsgaard et al. 2005) also observed that the cross sectional area (normalized to body weight) of human Achilles tendon can vary significantly depending on different exercise modes, such as volleyball (intermittent loading of tendon), long-distance running (repetitive loading), and kayaking (minimal loading). More specific relationships between strain and collagen synthesis have been explored in a myriad of *in vitro* studies that culture fibroblasts on stretchable substrates, input specific amplitudes and frequencies of strain, and measure collagen production (A. A. Lee et al. 1999; Galatz et al. 2006; Magnusson, Langberg, and

Kjaer 2010; Sullivan et al. 2009; Miller et al. 2005; Carver et al. 1991; Leung et al. 2014; Screen et al. 2005; Yang, Crawford, and Wang 2004). Most of these studies find that increasing cyclic loading increases the amount of collagen produced. Once cells form the extracellular matrix around them, they can then exert traction forces on their surrounding environment as they migrate through and bind to the extracellular matrix (Checa et al. 2015; Krishnan et al. 2009).

Aims and Approaches

The overall objective of this dissertation is to develop predictive models of cellular alignment and scar formation in response to mechanical loading during wound healing. We approached this objective by developing both experimental and numerical methods applied to native and engineered tissues in the heart and tendon and according to two specific aims:

- 1) Test the hypothesis that strain avoidance of compaction and stretch explains how fibroblasts align in response to mechanical stimuli.
- 2) Develop a multiscale computational model and test its ability to predict collagen scar structures in the Achilles tendon healing under a range of loading conditions.

In Chapters 2 and 3, we tested the specific hypothesis that strain avoidance of compaction and stretch explains how fibroblasts align in response to mechanical stimuli. In Chapter 2, we explored and reviewed existing computational models of stress fiber alignment, implementing one that used the idea of strain avoidance to

predict alignment in both 2D and 3D stretch conditions. After verifying our implementation against previously published data, we utilized the model to design a set of novel test conditions that would directly challenge this hypothesis, specifically predicting that cells cultured under large, isotropic compaction strains should avoid those strains and randomly align. In Chapter 3, we developed a novel *in vitro* system to specifically test our computational predictions. We generated alignment data across a wide range of boundary conditions, cyclic stretching amplitudes and frequencies, and compaction strains, and showed that previous models could not account for our new data. In collaboration with another group, we used the results of our new experiments to generate an improved model of cell alignment that could accurately predict behaviors over a wide range of conditions and provide an attractive alternative hypothesis for how mechanical environment determines cell alignment responses reported in both 2D and 3D studies.

In Chapter 4, we developed experimental protocols to determine how the mechanical environment and cell alignment can affect cell-matrix interactions during scar formation. We tested ways to measure local, micro-scale strains around cells during stretching of collagen gels, giving us more information about how global strains can affect matrix and cell strains. We also developed a novel protocol to image individual fibroblasts synthesizing and depositing collagen fibers, demonstrating some of the first images to use SHG microscopy to capture this phenomena on a single cell level.

In Chapter 5, we developed a multiscale computational model and tested its ability to predict collagen scar structures in the Achilles tendon healing under various mechanical loading conditions. Using our improved model of cell alignment together with a model of rat hindlimb musculoskeletal kinematics implemented in OpenSim and an agent-based model of wound healing, this multiscale model integrated information about how local mechanics influences cellular alignment and collagen remodeling to predict the effects of various repair and loading protocols on tendon structure. We found that the multiscale model predicted the major observed trends in the evolution of tissue-level scar properties across a wide variety of published rat studies. Furthermore, the model simulations identified a potential mechanism underlying the apparently paradoxical finding that mechanical loading enhances collagen alignment in unrepaired Achilles tendons yet decreases it in repaired tendons.

Significance

The significance of this proposed research is that it will develop an experimental framework to uncover the principles governing cell alignment, improve current computational predictions of cell alignment, investigate how cells deposit collagen and form scar, and generate a computational model that predicts scar tissue structure during healing.

Alignment of cells in response to mechanical cues plays an important role in a wide range of physiologic processes. Multiple cell types orient perpendicular to

applied cyclic stretch in 2D culture but parallel to stretch in 3D culture, and the mechanisms underlying this behavior remain elusive. We tested a promising hypothesized mechanism called strain avoidance and showed that it cannot explain cell alignment across the conditions we examined. By contrast, a computational model of stress fiber kinetics incorporating the influence of traction boundary conditions and altered strain transmission in soft gels reproduced all of our experimental results as well as published 2D stretch experiments. These findings could improve understanding, modeling, and therapeutic modulation of tissue development, regeneration, and repair.

Tendons and ligaments transmit force between muscles and bones throughout the body and are comprised of highly aligned collagen fibers that help bear high loads. The Achilles tendon in particular is exposed to exceptionally high loads and is prone to rupture. When damaged Achilles tendons heal, they typically have reduced strength and stiffness, and while most believe that appropriate physical therapy can help improve these mechanical properties, both clinical and animal studies of mechanical loading following injury have produced highly variable and somewhat disappointing results. To help better understand the effects of mechanical loading on tendon healing and potentially guide future therapies, we developed a computational model of rat Achilles tendon healing and showed that we could predict the main effects of different mechanical loading and surgical repair conditions reported across a wide range of published studies. Our model offers potential explanations for some surprising findings of

prior studies and for the high variability observed in those studies and may prove useful in designing future therapies or experiments to test new therapies.

These findings will improve our understanding of cell alignment and scar formation within healing tissue. We can use this information to inform the design of interventions that modulate scar tissue formation, such as physical therapy protocols for tendon and ligament healing or mechanical reinforcement of myocardial infarcts, enhancing the speed and effectiveness of these healing regimens.

References

- Amin, Nirav H, Andrew B Old, Loni P Tabb, Rohit Garg, Nader Toossi, and Douglas L Cerynik. 2013. "Performance Outcomes after Repair of Complete Achilles Tendon Ruptures in National Basketball Association Players." *The American Journal of Sports Medicine* 41 (8): 1864–68. doi:10.1177/0363546513490659.
- Andersson, Therese, Pernilla Eliasson, and Per Aspenberg. 2009. "Tissue Memory in Healing Tendons: Short Loading Episodes Stimulate Healing." *Journal of Applied Physiology (Bethesda, Md.: 1985)* 107 (2): 417–21. doi:10.1152/jappphysiol.00414.2009.
- Andersson, Therese, Pernilla Eliasson, Malin Hammerman, Olof Sandberg, and Per Aspenberg. 2012. "Low-Level Mechanical Stimulation Is Sufficient to Improve Tendon Healing in Rats." *Journal of Applied Physiology* 113 (9): 1398–1402. doi:10.1152/jappphysiol.00491.2012.
- Årøen, A., D. Helgø, O. G. Granlund, and R. Bahr. 2004. "Contralateral Tendon Rupture Risk Is Increased in Individuals with a Previous Achilles Tendon Rupture." *Scandinavian Journal of Medicine and Science in Sports* 14 (1): 30–33. doi:10.1111/j.1600-0838.2004.00344.x.
- Barocas, V. H., and R. T. Tranquillo. 1994. "Biphasic Theory and In Vitro Assays of Cell-Fibril Mechanical Interactions in Tissue-Equivalent Gels." In *Cell Mechanics and Cellular Engineering*, 185–209. New York, NY: Springer New York. doi:10.1007/978-1-4613-8425-0_12.
- . 1997. "An Anisotropic Biphasic Theory of Tissue-Equivalent Mechanics: The Interplay Among Cell Traction, Fibrillar Network Deformation, Fibril Alignment, and Cell Contact Guidance." *Journal of Biomechanical Engineering* 119 (2). American Society of Mechanical Engineers: 137–45. doi:10.1115/1.2796072.
- Bellows, C G, A H Melcher, and J E Aubin. 1981. "Contraction and Organization of Collagen Gels by Cells Cultured from Periodontal Ligament, Gingiva and Bone Suggest Functional Differences between Cell Types." *J Cell Sci* 50: 299–314. <http://jcs.biologists.org/content/50/1/299.full.pdf>.
- . 1982. "Association between Tension and Orientation of Periodontal Ligament Fibroblasts and Exogenous Collagen Fibres in Collagen Gels in Vitro." *Journal of Cell Science* 58 (1): 125–38. <http://www.ncbi.nlm.nih.gov/pubmed/6820794>.
- Bhole, A P, B P Flynn, M Liles, N Saeidi, C A Dimarzio, and J W Ruberti. 2009. "Mechanical Strain Enhances Survivability of Collagen Micronetworks in the Presence of Collagenase: Implications for Load-Bearing Matrix Growth and Stability." *Philos Trans A Math Phys Eng Sci* 367 (1902): 3339–62. doi:10.1098/rsta.2009.0093.
- Breidenbach, Andrew P., Nathaniel A. Dymant, Yinhui Lu, Marepalli Rao, Jason T. Shearn, David W. Rowe, Karl E. Kadler, and David L. Butler. 2015. "Fibrin Gels Exhibit Improved Biological, Structural, and Mechanical Properties Compared with Collagen Gels in Cell-Based Tendon Tissue-Engineered Constructs." *Tissue Engineering Part A* 21 (3–4). Mary Ann Liebert, Inc. 140 Huguenot Street, 3rd Floor

New Rochelle, NY 10801 USA: 438–50. doi:10.1089/ten.tea.2013.0768.

Bring, Daniel K I, Carol Reno, Per Renstrom, Paul Salo, David A. Hart, and Paul W. Ackermann. 2009. “Joint Immobilization Reduces the Expression of Sensory Neuropeptide Receptors and Impairs Healing after Tendon Rupture in a Rat Model.” *Journal of Orthopaedic Research* 27 (2): 274–80. doi:10.1002/jor.20657.

Caggiano, Laura Rose, Jia-Jye Lee, and Jeffrey W. Holmes. 2018. “Surgical Reinforcement Alters Collagen Alignment and Turnover in Healing Myocardial Infarcts.” *American Journal of Physiology-Heart and Circulatory Physiology*, July. American Physiological Society Bethesda, MD , ajpheart.00088.2018. doi:10.1152/ajpheart.00088.2018.

Canty, Elizabeth G., Yinhui Lu, Roger S. Meadows, Michael K. Shaw, David F. Holmes, and Karl E. Kadler. 2004. “Coalignment of Plasma Membrane Channels and Protrusions (Fibropositors) Specifies the Parallelism of Tendon.” *Journal of Cell Biology* 165 (4): 553–63. doi:10.1083/jcb.200312071.

Canty, Elizabeth G, and Karl E Kadler. 2005. “Procollagen Trafficking, Processing and Fibrillogenesis.” *Journal of Cell Science* 118 (Pt 7). The Company of Biologists Ltd: 1341–53. doi:10.1242/jcs.01731.

Carver, W, M L Nagpal, M Nachtigal, T K Borg, and L Terracio. 1991. “Collagen Expression in Mechanically Stimulated Cardiac Fibroblasts.” *Circulation Research* 69 (1). American Heart Association, Inc.: 116–22. doi:10.1161/01.RES.69.1.116.

Checa, Sara, Manuel K. Rausch, Ansgar Petersen, Ellen Kuhl, and Georg N. Duda. 2015. “The Emergence of Extracellular Matrix Mechanics and Cell Traction Forces as Important Regulators of Cellular Self-Organization.” *Biomechanics and Modeling in Mechanobiology* 14 (1). Springer Verlag: 1–13. doi:10.1007/s10237-014-0581-9.

Costa, Kevin D., Eun Jung Lee, and Jeffrey W. Holmes. 2003. “Creating Alignment and Anisotropy in Engineered Heart Tissue: Role of Boundary Conditions in a Model Three-Dimensional Culture System.” *Tissue Engineering* 9 (4). Mary Ann Liebert, Inc. : 567–77. doi:10.1089/107632703768247278.

Costa, M. L., K. MacMillan, D. Halliday, R. Chester, L. Shepstone, A. H. N. Robinson, and S. T. Donell. 2006. “Randomised Controlled Trials of Immediate Weight-Bearing Mobilisation for Rupture of the Tendo Achillis.” *The Journal of Bone and Joint Surgery. British Volume* 88–B (1). The British Editorial Society of Bone and Joint Surgery: 69–77. doi:10.1302/0301-620X.88B1.16549.

De, Rumi, Assaf Zemel, and Samuel a. Safran. 2007. “Dynamics of Cell Orientation.” *Nature Physics* 3 (9): 655–59. doi:10.1038/nphys680.

Deshpande, Vikram S, Robert M McMeeking, and Anthony G Evans. 2006. “A Bio-Chemo-Mechanical Model for Cell Contractility.” *Proceedings of the National Academy of Sciences of the United States of America* 103 (38). National Academy of Sciences: 14015–20. doi:10.1073/pnas.0605837103.

Eliasson, Pernilla, Therese Andersson, and Per Aspenberg. 2009. “Rat Achilles Tendon Healing: Mechanical Loading and Gene Expression.” *Journal of Applied Physiology* 107 (2): 399–407. doi:10.1152/jappphysiol.91563.2008.

- . 2012. “Influence of a Single Loading Episode on Gene Expression in Healing Rat Achilles Tendons.” *Journal of Applied Physiology* 112 (2): 279–88. doi:10.1152/japplphysiol.00858.2011.
- Fomovsky, Gregory M., Samantha A. Clark, Katherine M. Parker, Gorav Ailawadi, and Jeffrey W. Holmes. 2012. “Anisotropic Reinforcement of Acute Anteroapical Infarcts Improves Pump Function.” *Circulation: Heart Failure* 5 (4): 515–22. doi:10.1161/CIRCHEARTFAILURE.111.965731.
- Fomovsky, Gregory M., Jesse R. MacAdangdang, Gorav Ailawadi, and Jeffrey W. Holmes. 2011. “Model-Based Design of Mechanical Therapies for Myocardial Infarction.” *Journal of Cardiovascular Translational Research* 4 (1): 82–91. doi:10.1007/s12265-010-9241-3.
- Fomovsky, Gregory M., Andrew D. Rouillard, and Jeffrey W. Holmes. 2012. “Regional Mechanics Determine Collagen Fiber Structure in Healing Myocardial Infarcts.” *Journal of Molecular and Cellular Cardiology* 52 (5). Elsevier Ltd: 1083–90. doi:10.1016/j.yjmcc.2012.02.012.
- Foolen, Jasper, Vikram S Deshpande, Frans M W Kanters, and Frank P T Baaijens. 2012. “The Influence of Matrix Integrity on Stress-Fiber Remodeling in 3D.” *Biomaterials* 33 (30): 7508–18. doi:10.1016/j.biomaterials.2012.06.103.
- Freedman, Benjamin R., Joshua A. Gordon, Pankti R. Bhatt, Adam M. Pardes, Stephen J. Thomas, Joseph J. Sarver, Corinne N. Riggan, et al. 2016. “Nonsurgical Treatment and Early Return to Activity Leads to Improved Achilles Tendon Fatigue Mechanics and Functional Outcomes during Early Healing in an Animal Model.” *Journal of Orthopaedic Research* 34 (12): 2172–80. doi:10.1002/jor.23253.
- Freedman, Benjamin R., Joshua A Gordon, and Louis J Soslowky. 2014. “The Achilles Tendon: Fundamental Properties and Mechanisms Governing Healing.” *Muscles, Ligaments and Tendons Journal* 4 (2): 245–55. doi:10.11138/mltj/2014.4.2.245.
- Freedman, Benjamin R., Joseph J Sarver, Mark R Buckley, Pramod B Voleti, and Louis J Soslowky. 2013. “Biomechanical and Structural Response of Healing Achilles Tendon to Fatigue Loading Following Acute Injury.” *Journal of Biomechanics*, November. doi:10.1016/j.jbiomech.2013.10.054.
- Galatz, Leesa M., Linda J. Sandell, Stefan Y. Rothermich, Rosalina Das, Ava Mastny, Necat Havlioglu, Matthew J. Silva, and Stavros Thomopoulos. 2006. “Characteristics of the Rat Supraspinatus Tendon during Tendon-to-Bone Healing after Acute Injury.” *Journal of Orthopaedic Research* 24 (3). Wiley Subscription Services, Inc., A Wiley Company: 541–50. doi:10.1002/jor.20067.
- Giraud-Guille, Marie Madeleine, Laurence Besseau, and Raquel Martin. 2003. “Liquid Crystalline Assemblies of Collagen in Bone and in Vitro Systems.” *Journal of Biomechanics* 36 (10): 1571–79. doi:10.1016/S0021-9290(03)00134-9.
- Glazebrook, Mark A., James R. Wright, Maxine Langman, William D. Stanish, and J. Michael Lee. 2008. “Histological Analysis of Achilles Tendons in an Overuse Rat Model.” *Journal of Orthopaedic Research* 26 (6): 840–46. doi:10.1002/jor.20546.
- Grinnell, Frederick. 1984. “Fibronectin and Wound Healing.” *Journal of Cellular*

Biochemistry. doi:10.1002/jcb.240260206.

- Gurtner, Geoffrey C., Sabine Werner, Yann Barrandon, and Michael T. Longaker. 2008. "Wound Repair and Regeneration." *Nature* 2008 453:7193, May. Nature Publishing Group.
- Hase, Eiji, Oki Matsubara, Takeo Minamikawa, Katsuya Sato, and Takeshi Yasui. 2016. "In Situ Time-Series Monitoring of Collagen Fibers Produced by Standing-Cultured Osteoblasts Using a Second-Harmonic-Generation Microscope." *Applied Optics* 55 (12). Optical Society of America: 3261. doi:10.1364/AO.55.003261.
- Heinemeier, K. M., D. Skovgaard, M. L. Bayer, K. Qvortrup, A. Kjaer, M. Kjaer, S. P. Magnusson, and M. Kongsgaard. 2012. "Uphill Running Improves Rat Achilles Tendon Tissue Mechanical Properties and Alters Gene Expression without Inducing Pathological Changes." *Journal of Applied Physiology* 113 (5): 827–36. doi:10.1152/japplphysiol.00401.2012.
- Holmes, Jeffrey W., Thomas K. Borg, and James W. Covell. 2005. "Structure and Mechanics of Healing Myocardial Infarcts." *Annual Review of Biomedical Engineering* 7 (1): 223–53. doi:10.1146/annurev.bioeng.7.060804.100453.
- Hsu, Hui-Ju, Chin-Fu Lee, and Roland Kaunas. 2009. "A Dynamic Stochastic Model of Frequency-Dependent Stress Fiber Alignment Induced by Cyclic Stretch." Edited by Johannes Jaeger. *PLoS ONE* 4 (3): e4853. doi:10.1371/journal.pone.0004853.
- Hu, Jin-Jia, Jay D Humphrey, and Alvin T Yeh. 2009. "Characterization of Engineered Tissue Development under Biaxial Stretch Using Nonlinear Optical Microscopy." *Tissue Engineering. Part A* 15 (7). Mary Ann Liebert, Inc. 140 Huguenot Street, 3rd Floor New Rochelle, NY 10801 USA: 1553–64. doi:10.1089/ten.tea.2008.0287.
- Huang, Chenyu, Kunio Miyazaki, Satoshi Akaishi, Atsushi Watanabe, Hiko Hyakusoku, and Rei Ogawa. 2013. "Biological Effects of Cellular Stretch on Human Dermal Fibroblasts." *Journal of Plastic, Reconstructive and Aesthetic Surgery* 66 (12). Elsevier: e351-61. doi:10.1016/j.bjps.2013.08.002.
- Huang, Tung Fu, Stephanie M. Perry, and Louis J. Soslowsky. 2004. "The Effect of Overuse Activity on Achilles Tendon in an Animal Model: A Biomechanical Study." *Annals of Biomedical Engineering* 32 (3): 336–41. doi:10.1023/B:ABME.0000017537.26426.76.
- Ikoma, Kazuya, Masamitsu Kido, Masateru Nagae, Takumi Ikeda, Toshiharu Shirai, Keiichiro Ueshima, Yuji Arai, Ryo Oda, Hiroyoshi Fujiwara, and Toshikazu Kubo. 2013. "Effects of Stress-Shielding on the Dynamic Viscoelasticity and Ordering of the Collagen Fibers in Rabbit Achilles Tendon." *Journal of Orthopaedic Research* 31 (11): 1708–12. doi:10.1002/jor.22424.
- Ives, C. L., S. G. Eskin, and L. V. McIntire. 1986. "Mechanical Effects on Endothelial Cell Morphology: In Vitro Assessment." *In Vitro Cellular & Developmental Biology* 22 (9). Springer-Verlag: 500–507. doi:10.1007/BF02621134.
- Jozsa, L, M Kvist, BJ Balint, A Reffy, M Jarvinen, M. Lehto, and M. Barzo. 1989. "The Role of Recreational Sport Activity in Achilles Tendon Rupture." *The American Journal of Sports Medicine* 17 (3): 338–43. doi:10.1177/036354658901700305.

- Jungbauer, Simon, Huajian Gao, Joachim P. Spatz, and Ralf Kemkemer. 2008. "Two Characteristic Regimes in Frequency-Dependent Dynamic Reorientation of Fibroblasts on Cyclically Stretched Substrates." *Biophysical Journal* 95 (7): 3470–78. doi:10.1529/biophysj.107.128611.
- Karlon, William J., Pin-Pin Hsu, Song Li, Shu Chien, Andrew D. McCulloch, and Jeffrey H. Omens. 1999. "Measurement of Orientation and Distribution of Cellular Alignment and Cytoskeletal Organization." *Annals of Biomedical Engineering* 27 (6). Kluwer Academic Publishers-Plenum Publishers: 712–20. doi:10.1114/1.226.
- Kaunas, Roland, and Hui Ju Hsu. 2009. "A Kinematic Model of Stretch-Induced Stress Fiber Turnover and Reorientation." *Journal of Theoretical Biology* 257 (2): 320–30. doi:10.1016/j.jtbi.2008.11.024.
- Kaunas, Roland, Phu Nguyen, Shunichi Usami, and Shu Chien. 2005. "Cooperative Effects of Rho and Mechanical Stretch on Stress Fiber Organization." *Proceedings of the National Academy of Sciences of the United States of America* 102 (44). National Academy of Sciences: 15895–900. doi:10.1073/pnas.0506041102.
- Knezevic, V, a J Sim, T K Borg, and J W Holmes. 2002. "Isotonic Biaxial Loading of Fibroblast-Populated Collagen Gels: A Versatile, Low-Cost System for the Study of Mechanobiology." *Biomechanics and Modeling in Mechanobiology* 1 (1): 59–67. doi:10.1007/s10237-002-0005-0.
- Kongsgaard, M, P Aagaard, M Kjaer, and S P Magnusson. 2005. "Structural Achilles Tendon Properties in Athletes Subjected to Different Exercise Modes and in Achilles Tendon Rupture Patients." *Journal of Applied Physiology* 99 (5): 1965–71. doi:10.1152/jappphysiol.00384.2005.
- Krishnan, Ramaswamy, Chan Young Park, Yu-Chun Lin, Jere Mead, Richard T Jaspers, Xavier Trepate, Guillaume Lenormand, et al. 2009. "Reinforcement versus Fluidization in Cytoskeletal Mechanoresponsiveness." *PloS One* 4 (5). Public Library of Science: e5486. doi:10.1371/journal.pone.0005486.
- Langberg, Henning, Dorthe Skovgaard, Lars J Petersen, J Bulow, and M Kjaer. 1999. "Type I Collagen Synthesis and Degradation in Peritendinous Tissue after Exercise Determined by Microdialysis in Humans." *The Journal of Physiology* 521 Pt 1: 299–306. doi:10.1111/j.1469-7793.1999.00299.x.
- Layman, D L, E B McGoodwin, and G R Martin. 1971. "The Nature of the Collagen Synthesized by Cultured Human Fibroblasts." *Proceedings of the National Academy of Sciences of the United States of America* 68 (2): 454–58. doi:10.1073/pnas.68.2.454.
- Lee, A A, T Delhaas, A D McCulloch, and F J Villarreal. 1999. "Differential Responses of Adult Cardiac Fibroblasts to in Vitro Biaxial Strain Patterns." *Journal of Molecular and Cellular Cardiology* 31 (10). Elsevier: 1833–43. doi:10.1006/jmcc.1999.1017.
- Lee, Eun Jung, Jeffrey W. Holmes, and Kevin D. Costa. 2008. "Remodeling of Engineered Tissue Anisotropy in Response to Altered Loading Conditions." *Annals of Biomedical Engineering* 36 (8): 1322–34. doi:10.1007/s10439-008-9509-9.
- Leppilahti, J, J Puranen, and S Orava. 1996. "Incidence of Achilles Tendon Rupture."

- Acta Orthopaedica Scandinavica* 67 (3): 277–79. doi:10.3109/17453679608994688.
- Leung, Donald Y M, Seymour Glagov, Martin B Mathews, Stable Url, and Laura V O Brient. 2014. “Cyclic Stretching Stimulates Synthesis of Matrix Components by Arterial Smooth Muscle Cells in Vitro” 191 (4226): 475–77.
- Livne, Ariel, Eran Bouchbinder, and Benjamin Geiger. 2014. “Cell Reorientation under Cyclic Stretching.” *Nature Communications* 5 (1). Nature Publishing Group: 3938. doi:10.1038/ncomms4938.
- Lloyd-Jones, Donald, Robert J. Adams, Todd M. Brown, Mercedes Carnethon, Shifan Dai, Giovanni De Simone, T. Bruce Ferguson, et al. 2010. “Executive Summary: Heart Disease and Stroke Statistics-2010 Update: A Report from the American Heart Association.” *Circulation* 121 (7). doi:10.1161/CIRCULATIONAHA.109.192667.
- Magnusson, S. Peter, Henning Langberg, and Michael Kjaer. 2010. “The Pathogenesis of Tendinopathy: Balancing the Response to Loading.” *Nature Reviews Rheumatology* 6 (5). Nature Publishing Group: 262–68. doi:10.1038/nrrheum.2010.43.
- Matsumoto, Takuya, Jun-Ichi Sasaki, Eben Alsberg, Hiroshi Egusa, Hirofumi Yatani, and Taiji Sohmlura. 2007. “Three-Dimensional Cell and Tissue Patterning in a Strained Fibrin Gel System.” Edited by Mark Isalan. *PLoS ONE* 2 (11). Public Library of Science: e1211. doi:10.1371/journal.pone.0001211.
- McCormack, R, and J Bovard. 2015. “Early Functional Rehabilitation or Cast Immobilisation for the Postoperative Management of Acute Achilles Tendon Rupture? A Systematic Review and Meta-Analysis of Randomised Controlled Trials.” *British Journal of Sports Medicine* 49 (20): 1329–35. doi:10.1136/bjsports-2015-094935.
- Meier Bürgisser, Gabriella, Maurizio Calcagni, Elias Bachmann, Gion Fessel, Jess G Snedeker, Pietro Giovanoli, and Johanna Buschmann. 2016. “Rabbit Achilles Tendon Full Transection Model – Wound Healing, Adhesion Formation and Biomechanics at 3, 6 and 12 Weeks Post-Surgery.” *Biology Open* 5 (9): 1324–33. doi:10.1242/bio.020644.
- Metz, Roderick, Egbert-Jan M. M. Verleisdonk, Geert J.-M.-G. van der Heijden, Geert-Jan Clevers, Erik R. Hammacher, Michiel H. J. Verhofstad, and Christiaan van der Werken. 2008. “Acute Achilles Tendon Rupture.” *The American Journal of Sports Medicine* 36 (9). SAGE PublicationsSage CA: Los Angeles, CA: 1688–94. doi:10.1177/0363546508319312.
- Miller, Benjamin F, Jens L Olesen, Mette Hansen, Simon Døssing, Regina M Cramer, Rasmus J Welling, Henning Langberg, et al. 2005. “Coordinated Collagen and Muscle Protein Synthesis in Human Patella Tendon and Quadriceps Muscle after Exercise.” *J Physiol* 567 (3): 1021–33. doi:10.1113/jphysiol.2005.093690.
- Min, YM, JH Seo, YB Kwon, and MH Lee. 2013. “Effect of the Position of Immobilization upon the Tensile Properties in Injured Achilles Tendon of Rat.” *Annals of Rehabilitation Medicine* 73 (3): 253–57.

- Moller, Anders, M Astron, and N Westlin. 1996. "Increasing Incidence of Achilles Tendon Rupture." *Acta Orthop Scand* 67 (5): 479–81. doi:10.3109/17453679608996672.
- Moretti, M., A. Prina-Mello, A. J. Reid, V. Barron, and P. J. Prendergast. 2004. "Endothelial Cell Alignment on Cyclically-Stretched Silicone Surfaces." *Journal of Materials Science: Materials in Medicine* 15 (10). Kluwer Academic Publishers: 1159–64. doi:10.1023/B:JMSM.0000046400.18607.72.
- Müller, Sebastian A., Christopher H. Evans, Patricia E. Heisterbach, and Martin Majewski. 2018. "The Role of the Paratenon in Achilles Tendon Healing: A Study in Rats." *The American Journal of Sports Medicine* 46 (5). SAGE PublicationsSage CA: Los Angeles, CA: 1214–19. doi:10.1177/0363546518756093.
- Murrell, G A, E G Lilly, R D Goldner, A V Seaber, and T M Best. 1994. "Effects of Immobilization on Achilles Tendon Healing in a Rat Model." *Journal of Orthopaedic Research : Official Publication of the Orthopaedic Research Society* 12 (4): 582–91. doi:10.1002/jor.1100120415.
- Nieponice, Alejandro, Timothy M. Maul, Joy M. Cumer, Lorenzo Soletti, and David A. Vorp. 2007. "Mechanical Stimulation Induces Morphological and Phenotypic Changes in Bone Marrow-Derived Progenitor Cells within a Three-Dimensional Fibrin Matrix." *Journal of Biomedical Materials Research - Part A* 81 (3): 523–30. doi:10.1002/jbm.a.31041.
- Obbink-Huizer, Christine, Cees W J Oomens, Sandra Loerakker, Jasper Foolen, Carlijn V C Bouten, and Frank P T Baaijens. 2014. "Computational Model Predicts Cell Orientation in Response to a Range of Mechanical Stimuli." *Biomechanics and Modeling in Mechanobiology* 13 (1): 227–36. doi:10.1007/s10237-013-0501-4.
- Olsson, N., K. Gravare Silbernagel, Bengt Eriksson, M. Sansone, A. Brorsson, K. Nilsson-Helander, and J. Karlsson. 2013. "Stable Surgical Repair with Accelerated Rehabilitation versus Nonsurgical Treatment for Acute Achilles Tendon Ruptures: A Randomized Controlled Study." *The American Journal of Sports Medicine* 41 (12): 2867–76. doi:10.1177/0363546513503282.
- Palmes, D, H U Spiegel, T O Schneider, M Langer, U Stratmann, T Budny, and A Probst. 2002. "Achilles Tendon Healing: Long-Term Biomechanical Effects of Postoperative Mobilization and Immobilization in a New Mouse Model." *Journal of Orthopaedic Research : Official Publication of the Orthopaedic Research Society* 20 (5): 939–46. doi:10.1016/S0736-0266(02)00032-3.
- Pang, Yonggang, Xiaoli Wang, Dongkeun Lee, and Howard P Greisler. 2011. "Dynamic Quantitative Visualization of Single Cell Alignment and Migration and Matrix Remodeling in 3-D Collagen Hydrogels under Mechanical Force." *Biomaterials* 32 (15): 3776–83. doi:10.1016/j.biomaterials.2011.02.003.
- Parekh, Selene G, Walter H Wray, Olubusola Brimmo, Brian J Sennett, Keith L Wapner, W H Wray 3rd, Olubusola Brimmo, Brian J Sennett, and Keith L Wapner. 2009. "Epidemiology and Outcomes of Achilles Tendon Ruptures in the National Football League." *Foot & Ankle Specialist* 2 (6): 283–86. doi:10.1177/1938640009351138.
- Paten, Jeffrey A., Seyed Mohammad Siadat, Monica E. Susilo, Ebraheim N. Ismail, Jayson L. Stoner, Jonathan P. Rothstein, and Jeffrey W. Ruberti. 2016. "Flow-

- Induced Crystallization of Collagen: A Potentially Critical Mechanism in Early Tissue Formation." *ACS Nano* 10 (5). American Chemical Society: 5027–40. doi:10.1021/acsnano.5b07756.
- Rennie, Michael J., and Kevin D. Tipton. 1998. "Protein and Amino Acid Metabolism During and After Exercise and the Effects of Nutrition." *Annual Review of Nutrition*, no. July 2000. doi:0199-9885/00/0715-0457.
- Richardson, William J., Samantha A. Clarke, T. Alexander Quinn, and Jeffrey W. Holmes. 2015. "Physiological Implications of Myocardial Scar Structure." *Comprehensive Physiology* 5 (4): 1877–1909. doi:10.1002/cphy.c140067.
- Richardson, William J., and Jeffrey W. Holmes. 2015. "Why Is Infarct Expansion Such an Elusive Therapeutic Target?" *Journal of Cardiovascular Translational Research* 8 (7). Springer US: 421–30. doi:10.1007/s12265-015-9652-2.
- Riggin, Corinne N, Joseph J Sarver, Benjamin R Freedman, Stephen J Thomas, and Louis J Soslowsky. 2014. "Analysis of Collagen Organization in Mouse Achilles Tendon Using High-Frequency Ultrasound Imaging." *Journal of Biomechanical Engineering* 136 (2): 0210291-6. doi:10.1115/1.4026285.
- Robinson, Paul S., Sandra L. Johnson, Michael C. Evans, Victor H. Barocas, and Robert T. Tranquillo. 2008. "Functional Tissue-Engineered Valves from Cell-Remodeled Fibrin with Commissural Alignment of Cell-Produced Collagen." *Tissue Engineering Part A* 14 (1). Mary Ann Liebert, Inc. 140 Huguenot Street, 3rd Floor New Rochelle, NY 10801 USA : 83–95. doi:10.1089/ten.a.2007.0148.
- Roby, Tiffany, Shawn Olsen, and Jiro Nagatomi. 2008. "Effect of Sustained Tension on Bladder Smooth Muscle Cells in Three-Dimensional Culture." *Annals of Biomedical Engineering* 36 (10). Springer US: 1744–51. doi:10.1007/s10439-008-9545-5.
- Rouillard, Andrew D, and Jeffrey W Holmes. 2012. "Mechanical Regulation of Fibroblast Migration and Collagen Remodelling in Healing Myocardial Infarcts." *The Journal of Physiology* 590 (Pt 18): 4585–4602. doi:10.1113/jphysiol.2012.229484.
- Ruberti, Jeffrey W., and James D. Zieske. 2008. "Prelude to Corneal Tissue Engineering - Gaining Control of Collagen Organization." *Progress in Retinal and Eye Research* 27 (5). Elsevier Ltd: 549–77. doi:10.1016/j.preteyeres.2008.08.001.
- Sander, E. A., V. H. Barocas, and R. T. Tranquillo. 2011. "Initial Fiber Alignment Pattern Alters Extracellular Matrix Synthesis in Fibroblast-Populated Fibrin Gel Cruciforms and Correlates with Predicted Tension." *Annals of Biomedical Engineering* 39 (2): 714–29. doi:10.1007/s10439-010-0192-2.
- Schizas, Nikos, Jian Li, Therese Andersson, Anna Fahlgren, Per Aspenberg, Mahmood Ahmed, and Paul W Ackermann. 2010. "Compression Therapy Promotes Proliferative Repair during Rat Achilles Tendon Immobilization." *Journal of Orthopaedic Research : Official Publication of the Orthopaedic Research Society* 28 (7): 852–58. doi:10.1002/jor.21066.
- Screen, H. R C, Julia C. Shelton, Dan L. Bader, and David A. Lee. 2005. "Cyclic Tensile Strain Upregulates Collagen Synthesis in Isolated Tendon Fascicles." *Biochemical and Biophysical Research Communications* 336 (2): 424–29.

doi:10.1016/j.bbrc.2005.08.102.

- Soslowsky, L.J., S. Thomopoulos, S. Tun, C.L. Flanagan, C.C. Keefer, J. Mastaw, and J.E. Carpenter. 2000. "Neer Award 1999: Overuse Activity Injures the Supraspinatus Tendon in an Animal Model: A Histologic and Biomechanical Study." *Journal of Shoulder and Elbow Surgery* 9 (2): 79–84. doi:10.1067/mse.2000.101962.
- Sullivan, Bridget E, Chad C Carroll, Bozena Jemiolo, Scott W Trappe, S Peter Magnusson, Simon Døssing, Michael Kjaer, and Todd A Trappe. 2009. "Effect of Acute Resistance Exercise and Sex on Human Patellar Tendon Structural and Regulatory mRNA Expression." *Journal of Applied Physiology (Bethesda, Md. : 1985)* 106 (2): 468–75. doi:10.1152/jappphysiol.91341.2008.
- Thomopoulos, S., G. R. Williams, and L. J. Soslowsky. 2003. "Tendon to Bone Healing: Differences in Biomechanical, Structural, and Compositional Properties Due to a Range of Activity Levels." *Journal of Biomechanical Engineering* 125 (1). American Society of Mechanical Engineers: 106–13. doi:10.1115/1.1536660.
- Tuzuner, Serdar, Ozlenen Ozkan, Nuray Erin, Sibel Ozkaynak, An Cinpolat, and Omer Ozkan. 2013. "Effects of Botulinum Toxin-A Injection on Healing and Tensile Strength of Ruptured Rabbit Achilles Tendons." *Annals of Plastic Surgery* 00 (00): 1–5. doi:10.1097/SAP.0b013e31829aa2e1.
- Twaddle, B. C., and P. Poon. 2007. "Early Motion for Achilles Tendon Ruptures: Is Surgery Important?: A Randomized, Prospective Study." *The American Journal of Sports Medicine* 35 (12): 2033–38. doi:10.1177/0363546507307503.
- Vernon, Robert B., Michel D. Gooden, Stephanie L. Lara, and Thomas N. Wight. 2005. "Microgrooved Fibrillar Collagen Membranes as Scaffolds for Cell Support and Alignment." *Biomaterials* 26 (16): 3131–40. doi:10.1016/j.biomaterials.2004.08.011.
- Vigliotti, A., W. Ronan, F. P. T. Baaijens, and V. S. Deshpande. 2016. "A Thermodynamically Motivated Model for Stress-Fiber Reorganization." *Biomechanics and Modeling in Mechanobiology* 15 (4). Springer Berlin Heidelberg: 761–89. doi:10.1007/s10237-015-0722-9.
- Weber, Martin, Marco Niemann, Renate Lanz, and Thorsten Müller. 2003. "Nonoperative Treatment of Acute Rupture of the Achilles Tendon: Results of a New Protocol and Comparison with Operative Treatment." *The American Journal of Sports Medicine* 31 (5). SAGE PublicationsSage CA: Los Angeles, CA: 685–91. doi:10.1177/03635465030310050901.
- Wehrens, Xander H T, and Pieter A. Doevendans. 2004. "Cardiac Rupture Complicating Myocardial Infarction." *International Journal of Cardiology* 95 (2–3): 285–92. doi:10.1016/j.ijcard.2003.06.006.
- Wei, Zhensong, Vikram S. Deshpande, Robert M. McMeeking, and Anthony G. Evans. 2008. "Analysis and Interpretation of Stress Fiber Organization in Cells Subject to Cyclic Stretch." *Journal of Biomechanical Engineering* 130 (3). American Society of Mechanical Engineers: 0310091-9. doi:10.1115/1.2907745.
- Weisman, Harlan F., and Bernadine Healy. 1987. "Myocardial Infarct Expansion, Infarct

- Extension, and Reinfarction: Pathophysiologic Concepts." *Progress in Cardiovascular Diseases* 30 (2): 73–110. doi:10.1016/0033-0620(87)90004-1.
- White, L. D. W., J. C. Wenke, M. D. S. Mosely, S. B. Mountcastle, and C. J. Basamania. 2007. "Incidence of Major Tendon Ruptures and Anterior Cruciate Ligament Tears in US Army Soldiers." *The American Journal of Sports Medicine* 35 (8): 1308–14. doi:10.1177/0363546507301256.
- Wills, CA, S Washburn, V Caiozzo, and CA Prietto. 1986. "Achilles Tendon Rupture." *Clinical Orthopaedics and Related Research*.
- Yang, Guoguang, Richard C. Crawford, and James H C Wang. 2004. "Proliferation and Collagen Production of Human Patellar Tendon Fibroblasts in Response to Cyclic Uniaxial Stretching in Serum-Free Conditions." *Journal of Biomechanics* 37 (10): 1543–50. doi:10.1016/j.jbiomech.2004.01.005.
- Zhong, Shaoping, Wee Eong Teo, Xiao Zhu, Roger W. Beuerman, Seeram Ramakrishna, and Lin Yue Lanry Yung. 2006. "An Aligned Nanofibrous Collagen Scaffold by Electrospinning and Its Effects on in Vitro Fibroblast Culture." *Journal of Biomedical Materials* 79A (3). Wiley Subscription Services, Inc., A Wiley Company: 456–63. doi:10.1002/jbm.a.

Chapter 2

Computational Modeling of Stress Fiber Alignment

*The primary findings and conclusions of this chapter
set up the experimental hypothesis in Chapter 3.*

2.1 Introduction:

Stress, Strain, and Substrate Stiffness: Effects on Cellular Alignment and Stress Fiber Formation

The ability of cells to orient in response to mechanical stimuli is essential to embryonic development, cell migration, mechanotransduction, and other critical physiologic functions in a range of organs. Endothelial cells, fibroblasts, mesenchymal stem cells, and osteoblasts all orient perpendicular to an applied cyclic stretch when plated on stretchable elastic substrates, suggesting a common underlying mechanism. However, many of these same cells orient parallel to stretch in vivo and in 3D culture (See Chapter 1). A number of published computational models have attempted to address the effects of mechanical stretch on cell orientation (Obbink-Huizer et al. 2014; Vigliotti et al. 2016; Kaunas and Hsu 2009; Deshpande, McMeeking, and Evans 2006; Wei et al. 2008; De, Zemel, and Safran 2007), with some addressing the different orientation responses in 2D and 3D more than others. Several of these are conceptually similar: they use a set of differential equations to track the assembly and disassembly of stress fiber (SF) families or subsets oriented in different directions and then introduce experimentally-motivated phenomenologic terms and equations that drive the assembly (lengthening) or disassembly (shortening) rates. We reviewed and implemented several of these SF computational models, identified the one that seemed to be able to predict alignment responses in both

2D and 3D, and used it to generate novel test conditions that could be tested experimentally.

Kaunas and Hsu developed a model assuming that stretch or shortening of a SF relative to its preferred homeostatic length promotes disassembly (Kaunas and Hsu 2009). In this model, cyclic stretching induces cell alignment perpendicular to the stretch direction by forcing SF disassembly in that direction. This model could capture alignment behavior in traditional 2D and equibiaxial conditions, but could not accurately predict cellular responses for any conditions of static stretch or for cyclic uniaxial stretch cases in 3D. Specifically, the model predicted that a singular static stretch on 2D substrates would also generate increased disassembly in the stretch direction and subsequent perpendicular cell alignment. Experimentally, however, cells align parallel to the direction of a singular static stretch in both 2D and 3D conditions.

Deshpande et al. assumed that stress within the SFs reduces the disassembly rate, so that cells develop more SFs on stiffer substrates and along the local direction of greatest resistance to cell contraction (Deshpande, McMeeking, and Evans 2006); in their model, uniaxial cyclic stretch reduces stress in SFs parallel to the stretch direction through the force-velocity behavior of the actomyosin subunits, resulting in increasing disassembly of parallel SFs and net cell orientation perpendicular to the stretch as shortening rates increase. Their incorporation of force-velocity behavior allowed their model to accurately capture

parallel alignment of cells in static uniaxial stretch cases that could not be captured by Kaunas and Hsu.

Obbink-Huizer et al. (Obbink-Huizer et al. 2014) proposed an attractive hypothesis that could reproduce observed alignments on 2D or in 3D culture. They postulated that the dominant cellular response in both situations is strain avoidance, in which net disassembly of stress fibers parallel to an applied strain produces cytoskeletal alignment perpendicular to that strain. According to this hypothesis, cells in 3D gels align parallel to applied cyclic stretch because they are able to compact these gels perpendicular to the stretch direction, producing compaction strains that are much larger than the applied cyclic strains; in other words, cells in gels align with applied stretch only because they are avoiding much larger transverse compaction strains. In order to better understand this promising hypothesis, we implemented the model to specifically test the full range of available data for cells cultured on 2D and in 3D. Then, we used the model to generate a set of novel experimental conditions that would specifically test the strain avoidance hypothesis.

2.2 Methods

Obbink-Huizer et al. constructed a computational SF model similar to that of Deshpande et al. However, they assumed that higher SF tension promotes SF assembly rather than inhibiting disassembly. They included not only force-velocity but also force-length behavior of the SFs, such that active stress

generation by the SFs decreased with either stretch or shortening (Obbink-Huizer et al. 2014); as a consequence, cells in their model turn perpendicular to an applied cyclic stretch or to a cell-induced compaction strain, with the larger strain dominating when both are present, matching a broad range of known experimental cell alignment data both on 2D and in 3D conditions.

2.2.1 Stress Fiber Alignment Model Description

The computational model developed by Obbink-Huizer et al. describes a cell as an array of stress fibers (SFs) in 20 angular bins. The assembly or disassembly of stress fibers at each angle is determined by:

$$\frac{d\Phi_{\theta}^p}{dt} = (k_0^f + k_1^f \sigma_{max} f_{\varepsilon,a} f_{\dot{\varepsilon}}) \Phi^m - k_d \Phi_{\theta}^p ; \quad (1)$$

$$\Phi^m = \Phi^{total} - \sum_i^{\theta} \Phi_{\theta}^p \quad (2)$$

$$f_{\varepsilon,a}(\varepsilon_{\theta}) = \exp^{-\left(\frac{\varepsilon_{\theta}}{\varepsilon_0}\right)^2} \quad (3)$$

$$f_{\dot{\varepsilon}}(\dot{\varepsilon}_{\theta}) = \frac{1}{1+\frac{2}{\sqrt{5}}} \left(1 + \frac{k_v \dot{\varepsilon} + 2}{\sqrt{(k_v \dot{\varepsilon} + 2)^2 + 1}} \right) \quad (4)$$

Here, Φ_{θ}^p describes the current stress fiber concentration in each bin. The change in stress fiber concentration at each time is governed by stress fiber assembly and disassembly. The disassembly ($-k_d \Phi_{\theta}^p$) is governed by a uniform ($k_d = 1.0e^{-3} \text{ sec}^{-1}$) fractional degradation rate of the stress fibers in all directions. The assembly of stress fibers is determined by the cell's available free-floating actin monomer concentration (Φ^m), strain ($f_{\varepsilon,a}$) and strain rate ($f_{\dot{\varepsilon}}$) terms, and constants ($k_0^f, k_1^f, \sigma_{max}$). Φ^m is calculated through equation 2, where Φ^{total} is a constant value 0.005. $f_{\varepsilon,a}$ represents the length-tension relationship of the

actomyosin subunits and is guided by the strain (ϵ_θ) using equation 3, with ϵ_0 as a constant value. As the stress fiber is strained away from zero, it loses active contractile force (Fig 2.1A), meaning that *higher strain magnitudes promote stress fiber disassembly*. Positive strains are applied through applied cyclic stretch protocols. As the cell exerts its own tension on its environment, it can compact the substrate and generate negative compaction strains. $f_{\dot{\epsilon}}$ describes the velocity-tension relationship as a Hill-type function dependent on strain rate ($\dot{\epsilon}$) using equation 4, with $f_{\dot{\epsilon}} \rightarrow 0$ as $\dot{\epsilon} \rightarrow -\infty$, $f_{\dot{\epsilon}} \rightarrow 2$ as $\dot{\epsilon} \rightarrow \infty$, and $f_{\dot{\epsilon}}(0) = 1$ (Fig 2.1B).

2.2.2 Description of Test Conditions

As mentioned previously, SF assembly and disassembly in the Obbink-Huizer model depend on strain and strain rate, which change over time based on compaction (negative strains) and cyclic stretching (positive strains). We initially explored the effects of both compaction and stretching on alignment using three test conditions: no compaction, transverse compaction, or isotropic compaction (Fig 2.2), using the tensor \mathbf{F}^C to denote the remodeling compaction of the gel and λ_1 to denote the imposed cyclic stretch amplitudes in the x_1 directions. First, we simulated a case where the cell could not compact its environment while being exposed to a strip uniaxial cyclic stretch (stretch applied in the x_1 direction, x_2 direction held fixed) (Fig. 2.2A). Second, we tested uniaxial cyclic stretching conditions (x_1 direction constrained, x_2 direction left free to compact), in which the

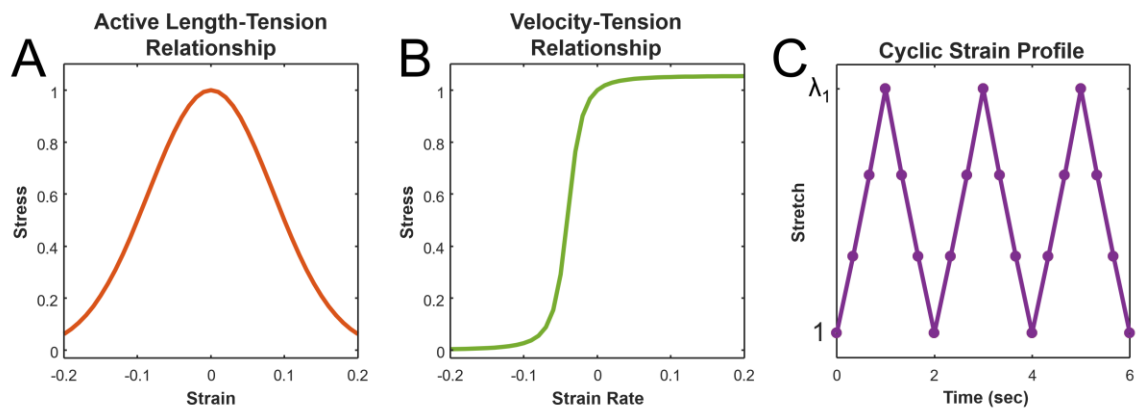


Figure 2.1

A) Active length-tension relationship of stress fibers to show range of values for equation 2. **B)** Velocity-tension relationship depicting equation 3. **C)** Prescribed cyclic strain profile. Cycle was discretized into 6 time points, depicted by each point on the graph.

cell could not compact in the x_1 direction ($F_{11}^C = 1$) but experienced a range of prescribed magnitudes of transverse compaction, $F_{22}^C = [0.5, 0.625, 0.75, 0.875]$ (Fig. 2.2B). Finally, we tested a condition in which the cell generated isotropic compaction strains before being stretched uniaxially, considering a range of compaction strains $F_{11}^C = F_{22}^C = [0.5, 0.625, 0.75, 0.875]$ (Fig 2.2C). In all conditions, we simulated cyclic stretch amplitudes ranging from $\lambda_1 = [1, 1.025, 1.05, 1.1, 1.2]$ applied in the x_1 direction. We used a constant frequency of 0.5 Hz, matching the frequency used by Obbink-Huizer et al.

2.2.3 Implementation of Model

We initialized cells with no SFs in any of the 20 9° angular bins. We prescribed each of our compaction strain profiles (Fig 2.2) at $t=0$ and then simulated cyclic stretching for 6 hours. We discretized our cyclic strain patterns into 6 incremental step changes up to our strain magnitude λ_1 and frequency of 0.5Hz (Fig 2.1C). Combining our stretch amplitude $\lambda_1(t)$ and compaction strains F_{11}^C and F_{22}^C , we determined a total deformation tensor \mathbf{F}^{tot} :

$$F^{tot}(t) = \begin{bmatrix} \lambda_1(t) * F_{11}^C & 0 \\ 0 & F_{22}^C [1 - \nu(\lambda_1(t) - 1)] \end{bmatrix} \quad (5)$$

At each time point, we calculated the current strain and strain rate for each of the angular bins and used equation 1 to determine the change in stress fiber concentration in each direction. Since we applied the λ_1 stretch in the x_1 (0°) direction, we determined the stretch in the other angular directions, $\lambda^\theta(t)$ using the following:

$$\lambda^\theta(t)^2 = [F^{tot}(t) \cdot M^\theta]^T \cdot [F^{tot}(t) \cdot M^\theta] \quad (6)$$

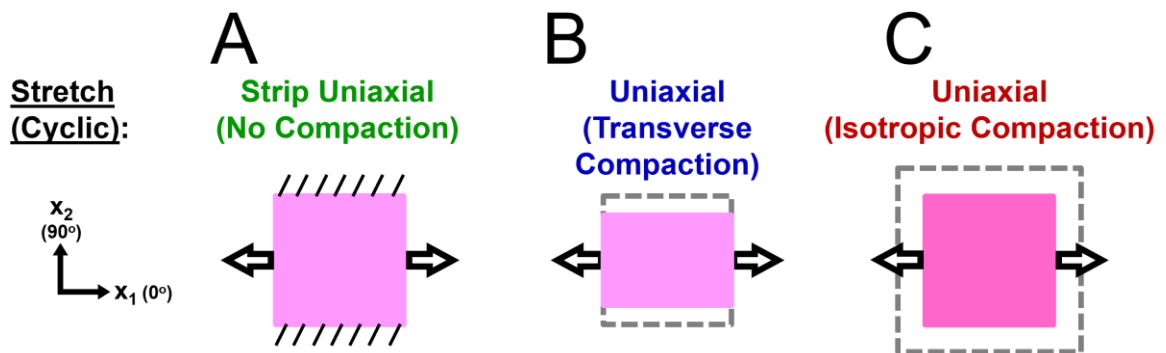


Figure 2.2

Experimental Setup and Test Conditions. **A)** Strip uniaxial stretching in x_1 (x_2 held fixed), where no compaction strains are prescribed. **B)** Uniaxial stretching in the x_1 direction (x_2 left free), so transverse (x_2) compaction occurs. **C)** Uniaxial stretching in the x_1 direction (x_2 left free), after isotropic compaction strains are prescribed. Diagonal lines indicate constraint; arrows indicate direction of cyclic stretch; dashed boxes indicate original substrate size before compaction.

$$\varepsilon_{\theta}(t) = \frac{1}{2}(\lambda_1^{\theta}(t)^2 - 1) \quad (7)$$

where M^{θ} is the unit vector:

$$M^{\theta} = \begin{bmatrix} \cos \theta \\ \sin \theta \end{bmatrix} \quad (8)$$

We plotted angular and circular histograms to show the distribution of SFs in the 20 angular bins. Both histograms were plotted as a fraction of the total actin available (ϕ^{total}).

To further quantify the alignment of the SFs, we also calculated the orientation and strength of alignment of the SFs using mean vectors calculated using equations 10-12, consistent with circular statistics theory for the analysis of angular data (Batschelet 1981):

$$Y = \frac{\sum(L_j * \sin(2\theta_j))}{N} \quad X = \frac{\sum(L_j * \cos(2\theta_j))}{N} \quad (10)$$

$$MVL = \sqrt{(Y)^2 + (X)^2} \quad (11)$$

$$MA = \frac{1}{2} \arctan\left(\frac{Y}{X}\right) \quad (12)$$

For each cell, we used the lengths and angles of each stress fiber (L_j and θ_j , with $j = 1, 2, \dots, N$ and $N = 19$ angular bins) to compute a vector whose length, MVL, indicated strength of alignment (ranging from MVL = 0 for a circular cell to MVL = 1 for a highly aligned, spindly cell), and mean angle, MA, indicated orientation. The 2θ terms in equations 10 and $\frac{1}{2}$ term in equation 12 account for the fact that the full range of possible angles is only 180° , since a cell oriented horizontally could be correctly described as oriented at 0° or at 180° (Batschelet 1981).

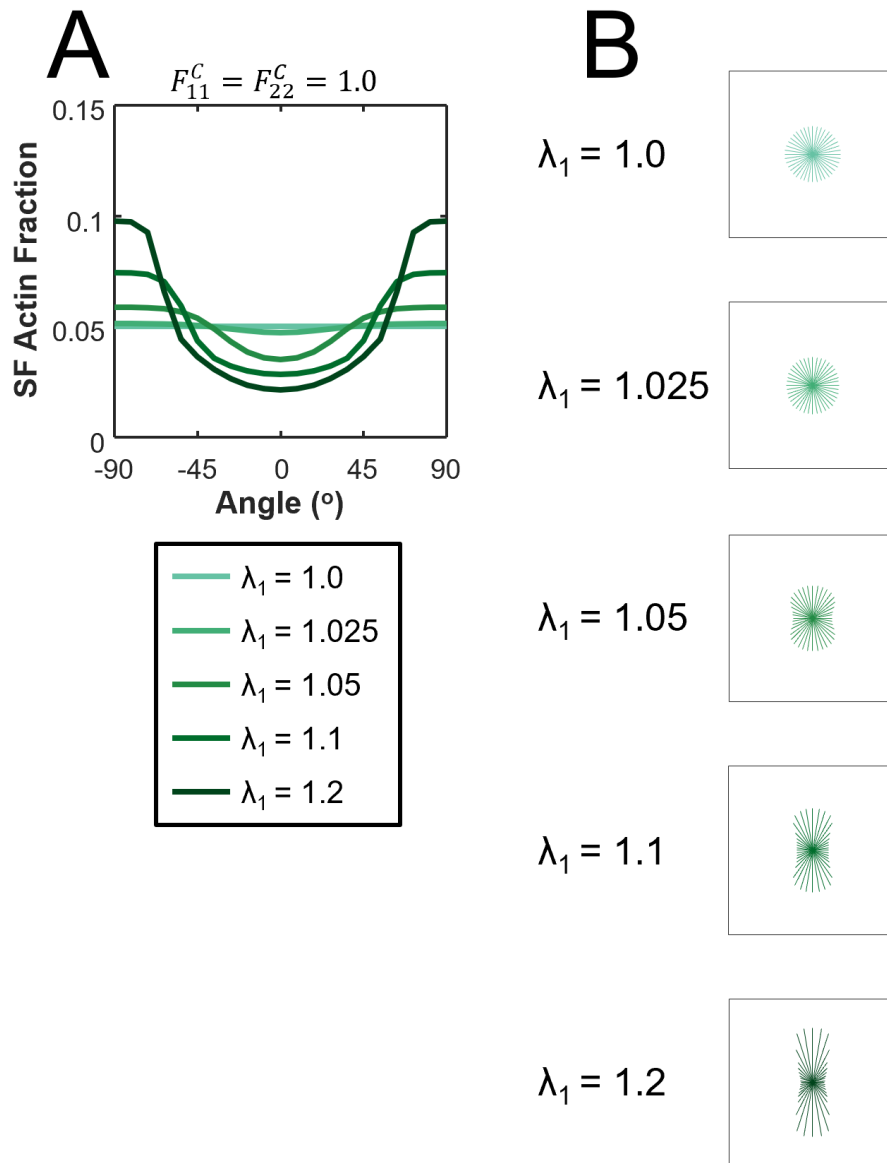
2.3 Results and Discussion

2.3.1 Stress Fiber Alignment in the Absence of Compaction

Cells experiencing no compaction and no cyclic stretching feel no strains in any directions, leading to equal predicted assembly of stress fibers in all angular directions (Fig 2.3). As cyclic stretching magnitude increases along the x_1 direction, SF assembly slows down, leading to increased perpendicular alignment of stress fibers (mean angle = 90°). Angular histograms (Fig 2.3A) and circular histograms (Fig. 2.3B) demonstrate this evolution of alignment. This experiment replicates the classic 2D results described previously by multiple groups, wherein cells on 2D substrates align perpendicular to imposed cyclic stretch (Foolen et al. 2012; Costa, Lee, and Holmes 2003; Lee, Holmes, and Costa 2008).

2.3.2 Stress Fiber Alignment in the Presence of Transverse Compaction

The model predicted strain avoidance of large x_2 compaction (F_{22}^C) resulting in stress fiber alignment in the x_1 direction (parallel to stretch), with alignment increasing as x_2 strains increased in magnitude (Fig. 2.4). Cyclic stretching at high enough amplitudes could generate a bimodal distribution of SFs, but cells still oriented primarily in the x_1 direction (mean angle = 0°) for most combinations of compaction and stretch amplitude explored here. Angular histograms (Fig 2.4A-D) and circular histograms (Fig. 2.4E-H) demonstrate this evolution of alignment. This experiment replicates the classic 3D results described previously

**Figure 2.3**

SF alignment with no compaction strains in response to strip uniaxial cyclic stretching. **A)** Angular histogram of actin distribution in each angular bin. Amount of actin in each bin represents the amount of formed stress fibers in that direction. Light green to dark green signifies progression from a strip uniaxial stretch of 1.0 to 1.2. **B)** Circular histogram depiction of the same conditions.

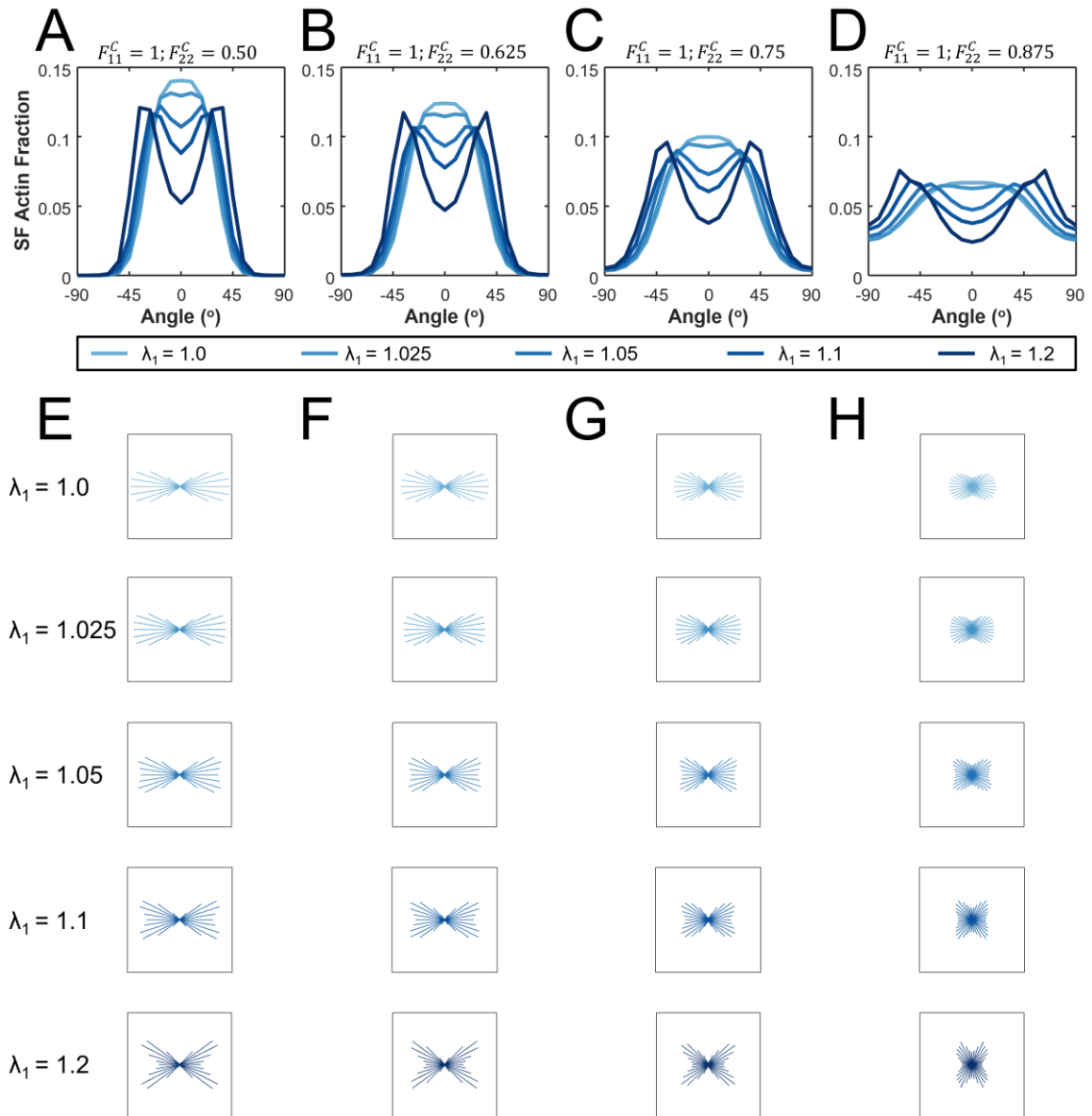


Figure 2.4

SF alignment with transverse (x_2) compaction strains in response to uniaxial cyclic stretching. **A-D)** Angular histogram of actin distribution in each angular bin. Amount of actin in each bin represents the amount of formed stress fibers in that direction. Light blue to dark blue signifies progression from a uniaxial cyclic stretch of 1.0 to 1.2. **E-H)** Circular histogram depiction of the same conditions.

by multiple groups, wherein cells in 3D culture align parallel to an imposed uniaxial stretch (Foolen et al. 2012; Costa, Lee, and Holmes 2003; Lee, Holmes, and Costa 2008).

2.3.3 Stress Fiber Alignment in the Presence of Isotropic Compaction

Simulations of cells experiencing large isotropic compaction strains ($F_{11}^C = F_{22}^C = 0.5$) predicted random alignment due to strain avoidance of the large isotropic strains. These strains were so large that they essentially prevented assembly of stress fibers (Fig. 2.5A,E). At lower isotropic strains of 0.625 or 0.75, we observed that increasing cyclic stretch amplitude λ_1 resulted in increasing alignment parallel to the direction of stretch (Figs. 2.5B,C,F,G; 2.6A), since stretching pulled the net strain in the x_1 direction closer to $\varepsilon_\theta = 0$ and therefore promoted assembly (Figs. 2.1A; 2.6B). Interestingly, this behavior did not occur with isotropic strains of 0.875 (Figs. 2.5D,H; 2.6A), since increasing stretch would cause the net strain to overshoot $\varepsilon_\theta = 0$ and become positive, promoting disassembly (Figs. 2.1A; 2.6B). This set of simulations represented an entirely novel set of experimental conditions that had not been previously tested in the literature, and the interesting predictions encouraged us to conduct these experiments to fully test the strain avoidance hypothesis.

2.3.4 Conclusions and Future Directions and Limitations

The Obbink-Huizer model utilizes the theory of strain avoidance to predict and explain cellular alignment responses to various mechanical loading conditions.

One of the models main underlying assumptions is that cells “remember” all strains from the time they are first seeded in a collagen gel or on a stretchable 2D substrate, integrate that entire strain history, and respond accordingly. Using this assumption, it could predict alignment responses currently available within the literature. We wanted to further interrogate this idea of the cell’s “memory” to its strain history, and this study motivated our experiments presented in Chapter 3. We used the simulations from Chapter 2 to design a set of novel experimental conditions (the isotropic compaction culturing condition) that would test the strain avoidance hypothesis more comprehensively than previously published work. As part of those studies, we could also use our implementation of the Obbink-Huizer model to make experiment-specific predictions of stress fiber alignment using experimentally measured deformations.

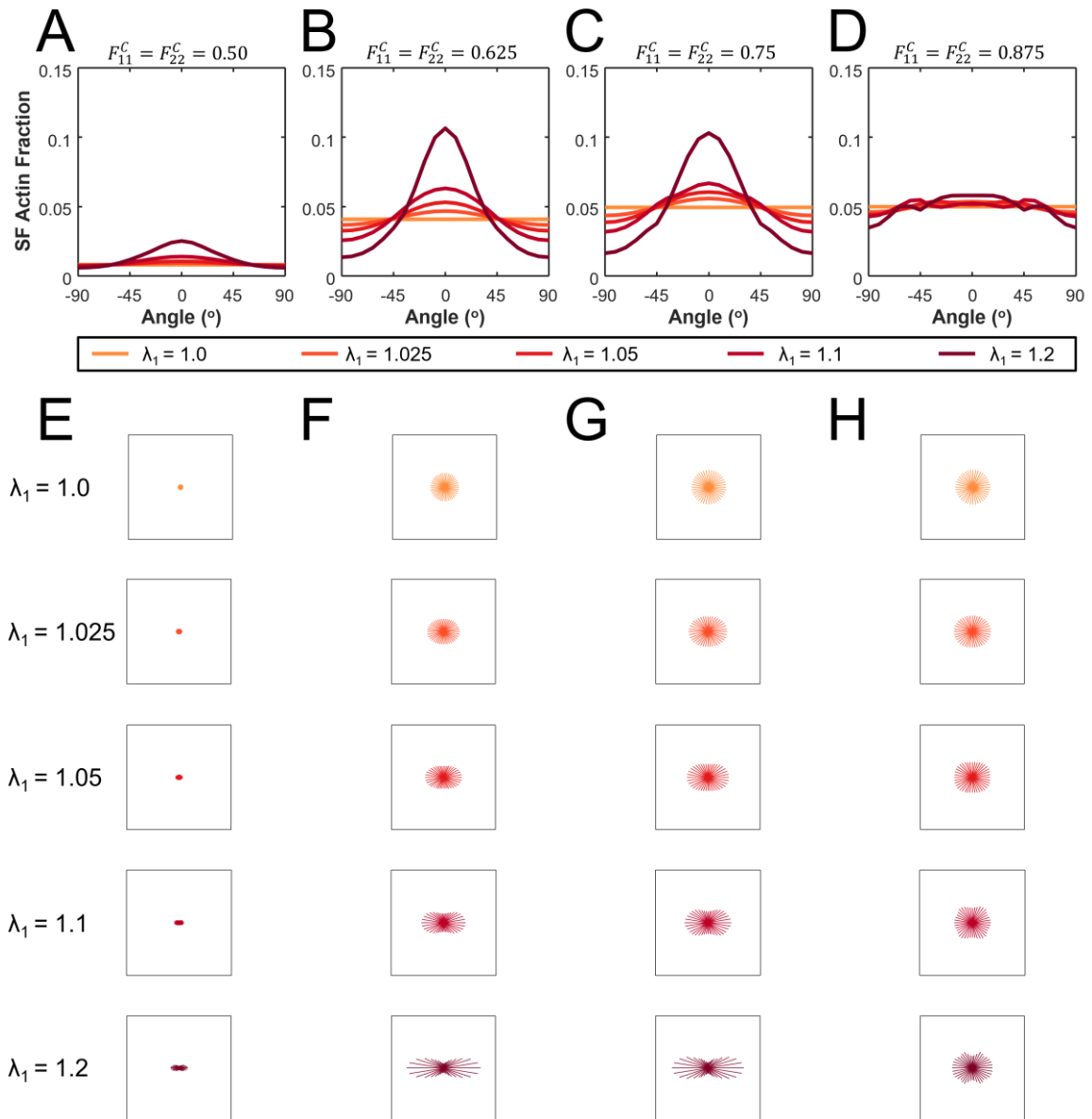
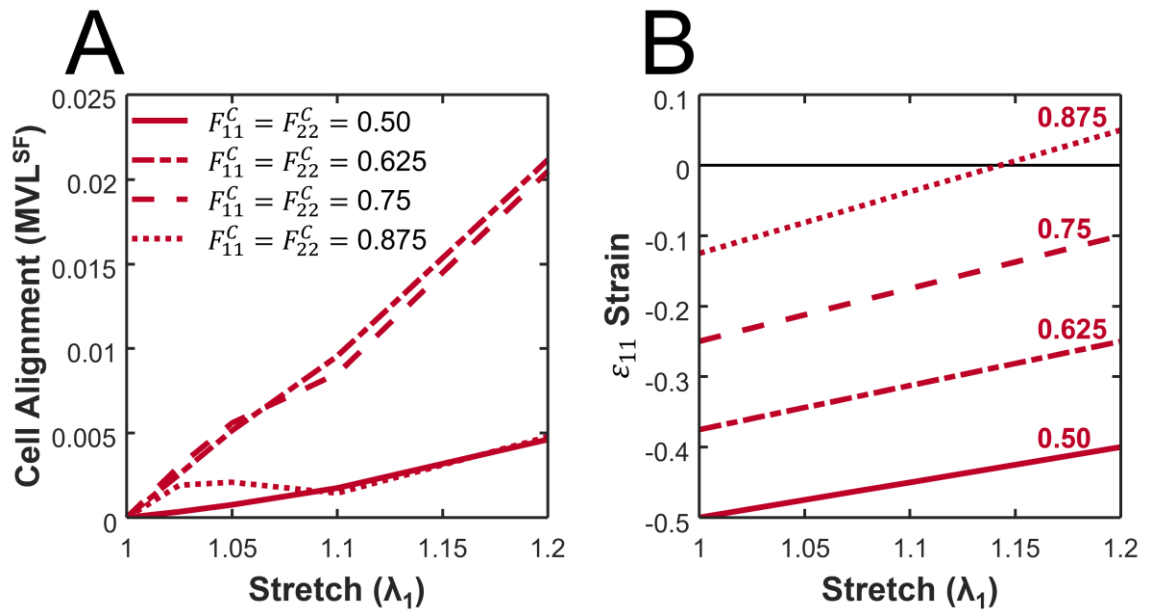


Figure 2.5

SF alignment in response to uniaxial cyclic stretching superimposed on isotropic compaction. **A-D)** Angular histogram of actin distribution in each angular bin. Amount of actin in each bin represents the amount of formed stress fibers in that direction. Light red to dark red signifies progression from a uniaxial cyclic stretch of 1.0 to 1.2. **E-H)** Circular histogram depiction of the same conditions.

**Figure 2.6**

Effect of increasing cyclic stretch amplitudes on **A**) Cell alignment (Mean Vector Length of SFs, MVL) and **B**) net peak ϵ_{11} strain over a range of simulated combinations of isotropic compaction strains and uniaxial cyclic stretch.

2.4 References

- Batschelet, Edward. 1981. *Circular Statistics in Biology*. London: Academic Press, London.
- Costa, Kevin D., Eun Jung Lee, and Jeffrey W. Holmes. 2003. "Creating Alignment and Anisotropy in Engineered Heart Tissue: Role of Boundary Conditions in a Model Three-Dimensional Culture System." *Tissue Engineering* 9 (4). Mary Ann Liebert, Inc. : 567–77. doi:10.1089/107632703768247278.
- De, Rumi, Assaf Zemel, and Samuel a. Safran. 2007. "Dynamics of Cell Orientation." *Nature Physics* 3 (9): 655–59. doi:10.1038/nphys680.
- Deshpande, Vikram S, Robert M McMeeking, and Anthony G Evans. 2006. "A Bio-Chemo-Mechanical Model for Cell Contractility." *Proceedings of the National Academy of Sciences of the United States of America* 103 (38). National Academy of Sciences: 14015–20. doi:10.1073/pnas.0605837103.
- Foolen, Jasper, Vikram S Deshpande, Frans M W Kanters, and Frank P T Baaijens. 2012. "The Influence of Matrix Integrity on Stress-Fiber Remodeling in 3D." *Biomaterials* 33 (30): 7508–18. doi:10.1016/j.biomaterials.2012.06.103.
- Kaunas, Roland, and Hui Ju Hsu. 2009. "A Kinematic Model of Stretch-Induced Stress Fiber Turnover and Reorientation." *Journal of Theoretical Biology* 257 (2): 320–30. doi:10.1016/j.jtbi.2008.11.024.
- Lee, Eun Jung, Jeffrey W. Holmes, and Kevin D. Costa. 2008. "Remodeling of Engineered Tissue Anisotropy in Response to Altered Loading Conditions." *Annals of Biomedical Engineering* 36 (8): 1322–34. doi:10.1007/s10439-008-9509-9.
- Obbink-Huizer, Christine, Cees W J Oomens, Sandra Loerakker, Jasper Foolen, Carlijn V C Bouten, and Frank P T Baaijens. 2014. "Computational Model Predicts Cell Orientation in Response to a Range of Mechanical Stimuli." *Biomechanics and Modeling in Mechanobiology* 13 (1): 227–36. doi:10.1007/s10237-013-0501-4.
- Vigliotti, A., W. Ronan, F. P. T. Baaijens, and V. S. Deshpande. 2016. "A Thermodynamically Motivated Model for Stress-Fiber Reorganization." *Biomechanics and Modeling in Mechanobiology* 15 (4). Springer Berlin Heidelberg: 761–89. doi:10.1007/s10237-015-0722-9.
- Wei, Zhensong, Vikram S. Deshpande, Robert M. McMeeking, and Anthony G. Evans. 2008. "Analysis and Interpretation of Stress Fiber Organization in Cells Subject to Cyclic Stretch." *Journal of Biomechanical Engineering* 130 (3). American Society of Mechanical Engineers: 0310091-9. doi:10.1115/1.2907745.

Chapter 3

Role of Boundary Conditions in Determining Cell Alignment in Response to Stretch

The primary findings and conclusions of this chapter are published:

Chen, K., Vigliotti, A., Bacca, M., McMeeking, R.M., Deshpande, V.S., Holmes, J.W. (2018) "Role of Boundary Conditions in Determining Cell Alignment in Response to Stretch." Proceedings of the National Academy of Sciences. 115 (5), 986-991. doi:10.1073/pnas.1715059115

3.1 Introduction

Alignment of cells in response to mechanical cues plays an important role in a wide range of physiologic responses, from sensing of shear stress by endothelial cells to production of aligned collagen in developing tendons. One of the most intriguing observations to emerge from studying these responses is that cells plated on a flexible 2D substrate orient perpendicular to an applied uniaxial cyclic stretch (Huang et al. 2013; Moretti et al. 2004; Kaunas et al. 2005; Ives, Eskin, and McIntire 1986; Karlon et al. 1999; Hsu, Lee, and Kaunas 2009), while cells embedded in a 3D gel orient parallel to that stretch (Lee, Holmes, and Costa 2008; Foolen et al. 2012; Matsumoto et al. 2007; Roby, Olsen, and Nagatomi 2008; Bellows, Melcher, and Aubin 1982; Hu, Humphrey, and Yeh 2009; Pang et al. 2011). Recently, Obbink-Huizer et al. proposed an attractive hypothesis to explain this discrepancy (Obbink-Huizer et al. 2014). They postulated that the dominant cellular response in both situations is strain avoidance, in which net disassembly of stress fibers parallel to an applied strain produces cytoskeletal alignment perpendicular to that strain. According to this hypothesis, in most 2D experiments there is little compaction, so the applied cyclic strains dominate and cells align perpendicular to an applied (uniaxial) stretch. By contrast, cells in 3D gels align parallel to applied cyclic stretch because they are able to compact these gels perpendicular to the stretch direction, producing compaction strains that are much larger than the applied cyclic strains; in other words, cells in gels align with applied stretch only because they are avoiding much larger transverse compaction strains.

To date, only limited experimental data are available to assess this hypothesis. Foolen et al. designed a collagen gel loading system that allowed them to perform either uniaxial cyclic stretching (in the x_1 direction with x_2 left free to compact) or strip uniaxial cyclic stretching (in the x_1 direction with x_2 constrained) (Foolen et al. 2012). However, this experimental system simultaneously varied both compaction and boundary conditions in the x_2 direction. In order to more specifically test the hypothesis that transverse compaction explains cell alignment parallel to stretch in 3D culture, we implemented a computational model of stress fiber (SF) alignment by Obbink-Huizer *et al.* (Obbink-Huizer et al. 2014) and used it to specifically design experiments that would challenge the strain avoidance model. We then developed a system that allows us to independently control compaction in the stretch and transverse directions, prior to and during the application of cyclic uniaxial stretch, in order to conduct the experiments we designed. We measured compaction and loading strains to make gel-specific simulations of alignment using the computational model and compared the models to the actual *in vitro* cell alignment distributions. Using the experimental compaction strains did not provide accurate computational SF predictions. Instead, our experiments with this new system suggested that traction boundary conditions – rather than compaction per se – govern the alignment of cardiac fibroblasts cultured in statically restrained collagen gels. Cyclic uniaxial stretch could modify this alignment, but only at frequencies an order of magnitude greater than required to induce perpendicular alignment in published 2D stretching experiments. We then modified a thermodynamic model

of stress fiber dynamics published recently by Vigliotti et al. (Vigliotti et al. 2016) and were able to reproduce these new experimental findings as well as previously published data from 2D cyclic stretching experiments. These experiments and model results suggest a new framework for understanding the apparently contradictory alignment responses of cells subjected to cyclic stretch on 2D membranes and in 3D gels.

3.2 Methods

3.2.1 Adult Cardiac Fibroblast Isolation and Culture

We euthanized Sprague-Dawley rats (6 weeks old, ~220 g), removed and minced their ventricles into ~1 mm³ pieces, and digested the pieces using Liberase TM Research Grade (Roche, Indianapolis, IN). We centrifuged successive digestions for 10 min at 400x *g*, resuspended the cells in culture medium containing Dulbecco's modified Eagle medium (Sigma-Aldrich, St. Louis, MO) with 10% fetal bovine serum (FBS, Atlanta Biologicals, Flowery Branch, GA), 100 U/mL penicillin, 100 µg/mL streptomycin, and 2 ng/mL amphotericin B (all Sigma-Aldrich), and transferred the cells into cell culture flasks incubated at 37°C and 5% CO₂. After 4h, we removed the culture media, rinsed the cells with phosphate-buffered saline (PBS, Sigma-Aldrich) to remove nonadherent cells, and resupplied with culture medium. We replaced media every 2-3 days and harvested cells for experiments at passage 1 (7 days after isolation) or 2 (10-11 days after isolation).

3.2.2 Fabrication of Fibroblast-Populated Collagen Hydrogels

We serum starved the fibroblasts for 18 hours before using 0.25% Trypsin-EDTA (Sigma-Aldrich) to dissociate them from their flasks and resuspending them in serum-free culture media. We created collagen solution at a 1:1:8 ratio of 0.2 M HEPES, 10X MEM (both Sigma-Aldrich), and 3.1 mg/mL type I Bovine Collagen Solution (PureCol, Advanced Biomatrix, San Diego, CA) and mixed it at a 4:1 ratio with the resuspended cells for a final cell concentration of 200k cells/mL and collagen concentration of ~2mg/mL. We placed this cell+collagen mixture on a rotator in an incubator for 20-30 min to initiate gelation before pouring it into 100mm x 15mm Petri dishes coated with polydimethylsiloxane (PDMS, Dow Corning, Sylgard 184 Silicone Elastomer Kit) to prevent adhesion and fitted with negative cruciform molds with small sponges at the arms (Fig. 3.1A). After the gels polymerized for 4h in an incubator, we left them for 1 day during a pre-culture period before transfer to the loading system (Fig. 3.1A). For the 1 day pre-culture period, we either isotropically constrained them for 1 day by pushing two small pins through each sponge into the PDMS layer, or we let them float freely in media and isotropically compact. The free-floating gels were cast from a larger total volume in larger molds to allow for compaction, so that dimensions of all gels would be matched after 1 day, prior to transfer to the loading system (Fig. 3.2).

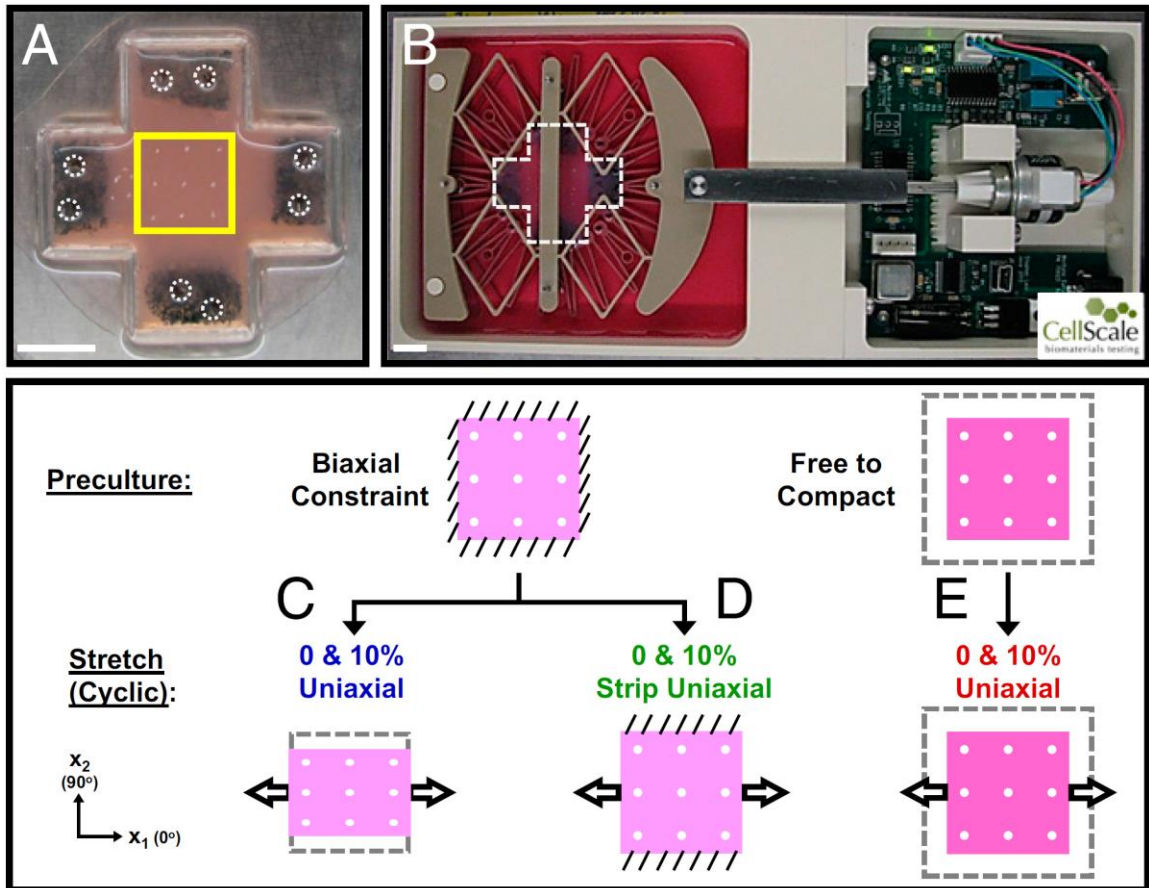


Figure 3.1

Experimental Setup and Test Conditions. **A)** Fibroblast-populated collagen gels with sponges embedded in the arms. During an initial pre-culture period, gel arms would either be biaxially constrained with pins (circled) or left to float freely in media and isotropically compact. Square box indicates region of interest painted with 9 TiO_2 dots to track gel deformations and later imaged to assess cell alignment. **B)** Collagen gel (cruciform shaped box) pinned in CellScale device. Scale bars=1cm. **C,D)** Collagen gels initially cultured under biaxial constraint before being subjected to **C)** 0 or 10% uniaxial stretch in the x_1 direction (x_2 left free) or **D)** 0 or 10% strip uniaxial stretch in x_1 (x_2 held fixed). **E)** Collagen gels initially allowed to compact isotropically before being subjected to either 0 or 10% uniaxial stretch in x_1 . All conditions tested for 24, 48, and 72h. Diagonal lines indicate constraint; arrows indicate direction of cyclic stretch; dashed boxes indicate original gel size before compaction.

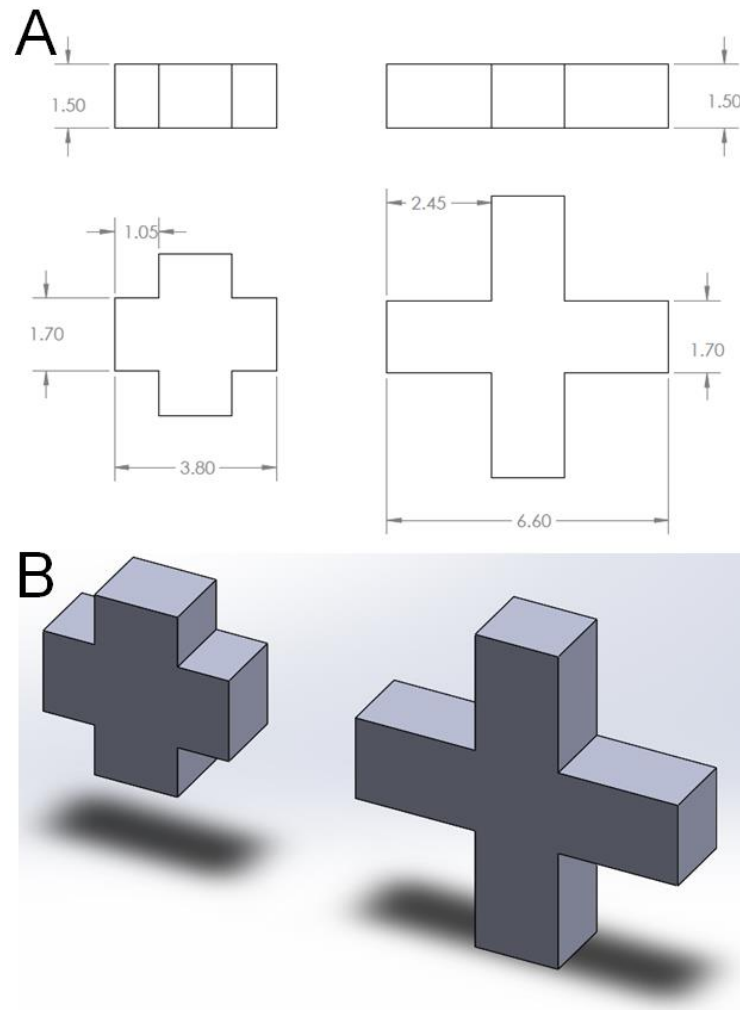


Figure 3.2

A) Size specifications of the positive molds used to generate the collagen gels. All values in cm. **B)** 3D isometric view. We either isotropically constrained collagen gels of a smaller size (**left**) or cast free-floating gels from a larger total volume in larger molds to allow for compaction (**right**), so that dimensions of all gels would be matched after 1 day, prior to transfer to the loading system.

3.2.3 Loading of Collagen Gels and Description of Test Conditions

We used CellScale MechanoCulture B1 devices (CellScale, Waterloo, ON, Canada) to either statically or dynamically load the cell-populated collagen hydrogels (Fig. 3.1B). These devices included a “dry” side, housing a circuit board and motor that could be programmed for a variety of amplitudes or frequencies of stretch (right side of Fig. 3.1B), connected by a stainless steel bridge to a “wet” side filled with 10% FBS containing media. Three interconnected deformable polyether ether ketone (PEEK) plastic layers transferred linear motion of the bridge into stretch of an inner circle (3.6cm diameter) of 24 pins. We pinned the arms of the collagen gels in the x_1 direction, and either pinned the arms in the x_2 direction to prevent compaction (strip uniaxial stretch) or cut them off to allow compaction (uniaxial stretch).

We transferred gels initially cultured under biaxial constraint to the B1 devices and subjected them to either 0% uniaxial stretch (x_1 direction constrained, x_2 direction left free to compact), 10% cyclic uniaxial stretch (stretch applied in the x_1 direction, x_2 direction left free to compact) (Fig. 3.1C), 0% strip uniaxial stretch (both directions constrained), or 10% cyclic strip uniaxial stretch (stretch applied in the x_1 direction, x_2 direction held fixed) (Fig. 3.1D). In this paper, we use “0% strip uniaxial stretch” and “0% uniaxial stretch” (synonymous to a biaxial and uniaxial constraint, respectively) in order to differentiate these loading conditions in the stretcher from the pre-culture conditions. We also transferred the gels that initially floated freely in media and compacted isotropically to CellScale devices

and subjected them to either 0% uniaxial stretch or 10% cyclic uniaxial stretch (Fig. 3.1E). We mapped the time course of the static (0%) and low-frequency (10%, 0.5 Hz) responses using 15 gels for each of these six conditions: five stretched for 24 h, five for 48 h, and five for 72 h. We explored the effect of higher frequencies by stretching gels for 72 h under each of the following conditions: 10% cyclic uniaxial stretch at 2 Hz (n=5), 10% cyclic uniaxial stretch at 4 Hz (n=4), 10% cyclic strip uniaxial stretch at 2 Hz (n=5), and 10% strip cyclic uniaxial stretch at 4 Hz (n=5). The five gels in any one experimental group contained cells from five separate rat fibroblast isolations. In addition to the 109 gels listed above, eight gels underwent the initial pre-culture step only (n=4 biaxial constraint, n=4 isotropic compaction).

3.2.4 Fabrication of Customized Stretching Frame

The CellScale MechanoCulture B1 device comes with three interconnecting deformable components that prescribe equibiaxial stretch, which we use for uniaxial stretch cases by only attaching the collagen gels in the x_1 direction and excising the arms in the x_2 direction (Fig. 3.1C,E). To generate our strip uniaxial stretch conditions (Fig. 3.1D), we used 3D Modeling Software (AutoCAD Inventor and SolidWorks) to design our own customized deformable component, with help and advice from Caleb Horst at CellScale (Figs. 3.1B, 3.3) (Waterloo, ON, N2L 5C6, Canada). Our design uses wide accordions to minimize flexion and fracture within the part and a central bar with mounting holes. Each piece was about

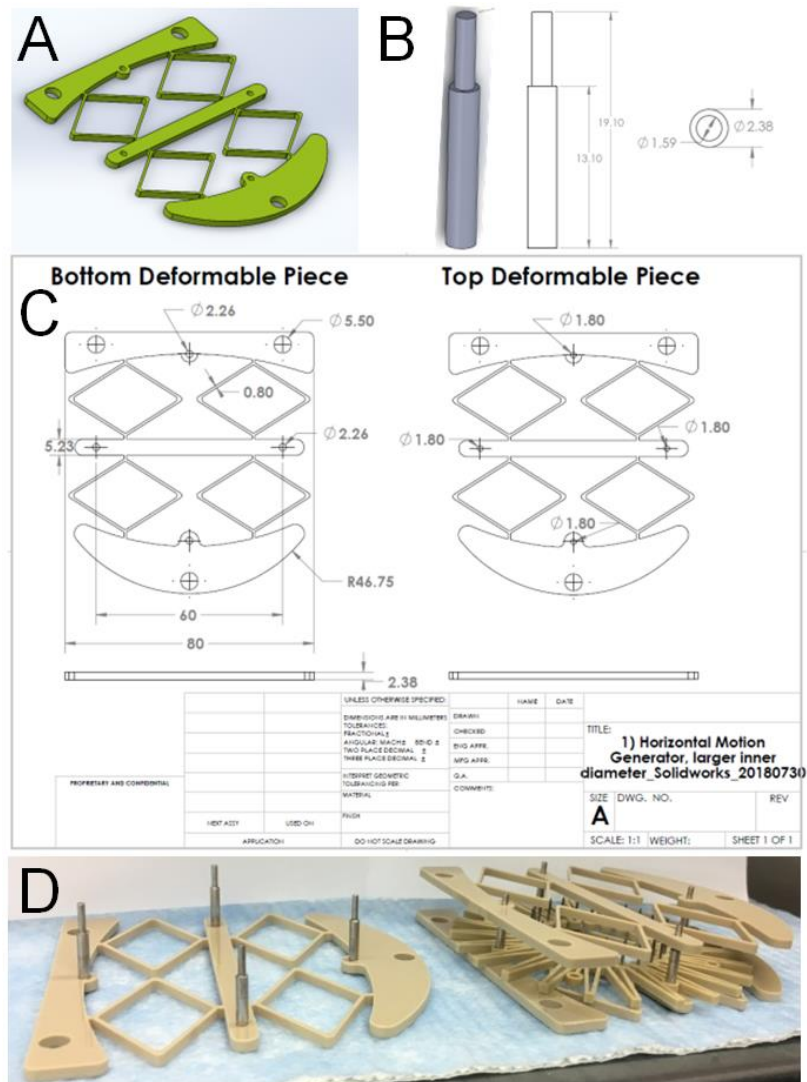


Figure 3.3

Design and fabrication of a customized, deformable stretching frame compatible with the CellScale MechanoCulture B1 devices. **A)** View of the part in SolidWorks. **B)** View of the mounting pins in SolidWorks (**left**) and a drawing of the pin (**right**) to show the length and diameter dimensions. All measurements in millimeters. **C)** Drawing of the bottom and top deformable pieces. The top piece is identical to the bottom, except for the 4 smaller diameter holes to allow for mounting on the pins. **D)** Final piece, showing just the bottom piece with the press fit mounting pins (**left**) or with the top piece mounted (**right**). The middle deformable piece maintains its original design.

80mm x 80mm, with full dimensions shown in Fig. 3.3C. We generated two versions of the piece for the device—a bottom piece with holes of diameter 2.26mm to accommodate the wider portion of each mounting pin, and a top piece with holes of diameter 1.8mm. We machined these mounting pins from a 3/32" 316 stainless steel rod (McMaster Carr) using a machine lathe at the University of Virginia Physics Department's machine shop to create mounting pins with a bottom diameter of 2.38mm and top diameter of 1.59mm (Fig. 3.3B) and press fit the mounting pins into the 2.26mm diameter holes in the bottom pieces. With the pins pressed into the bottom pieces, we could then easily slide on or remove the top pieces (Fig. 3.3D). Brian Pitts (bpitts@microwaterjet.com) at MicroWaterjet LLC (13420 Reese Blvd. West, Huntersville, NC 28078; Phone: (704) 948-1218; www.microwaterjet.com) cut the pieces from a 12" x 12" x 3/32" sheet of PEEK (PolyEther Ether Ketone, McMaster Carr) using a micron-precise high-pressure stream of water. One 12"x12" sheet, yielded 9 pieces (5 bottom pieces, 4 top) for \$857.

3.2.5 Quantification of Gel Compaction

We applied nine titanium oxide paint dots, consisting of 1 g/mL Titanium(IV) oxide powder (Sigma-Aldrich) mixed with PBS, on the surface of the central region of the gel (box in Fig. 3.1A) with a 7-0 nylon suture (Ethicon, 1647G) and used these markers to track compaction over the course of the experiment. We used a digital camera to image the markers before the pre-culture period, after the pre-culture period prior to the onset of loading, and at the end of each loading

protocol. All images were taken when the stretching devices were at the 0% strain position, so marker positions in these images reflected the deformations due to gel compaction. We used the markers to compute a single homogeneous deformation gradient tensor \mathbf{F} that provided the least-squares best fit mapping of the 9 marker positions from the undeformed (beginning of experiment) to deformed positions by solving the overdetermined matrix equation:

$$\mathbf{x} = \mathbf{F}\mathbf{X} + \mathbf{p} \quad (1),$$

where \mathbf{p} is an arbitrary vector included to account for translation between images.

3.2.6 Microscopy and Quantification of Cell Alignment

After the stretch protocols, we fixed the gels in 10% formalin, stained the F-actin with Alexa Fluor 488 Phalloidin (Thermo Fisher Scientific, A12379), and used a confocal microscope with a 10x objective to capture z-stacks consisting of one image every 2.5 μm through the gel thickness at three locations in the central region. Within each z-stack, we created 2D projections (Fig. 3.4A) by combining sets of 10 consecutive images separated by 25 μm , allowing for analysis of non-overlapping cells at different depths below the gel surface. Using MATLAB, we converted each 2D projection to binary (fluorescent pixels = white, dark pixels = black) and analyzed white pixel clusters above a size threshold of 15 μm x 15 μm (Fig. 3.4B).

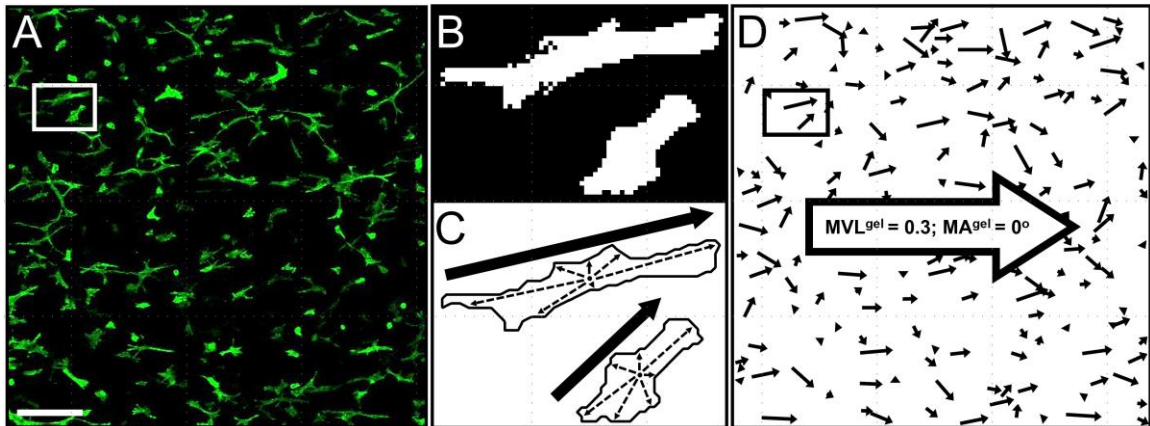


Figure 3.4

A) A representative 2D projection of F-actin stained adult rat cardiac fibroblasts taken from the core of the tissue at 10x. Scale bar, 200 μ m. **B)** Magnification of the boxed region in **(A)**, converted into a binary image. **C)** Vectors (dashed arrows represent subset of 400 vectors used) drawn from the centroid (dot) to the boundary of the cell were used to calculate the cell's strength of alignment (MVL^{cell} , ranging from 0, a circular cell, to 1, a highly aligned, spindly cell), and orientation (MA^{cell}) (black arrows). The top cell, which is longer and more highly aligned, has a higher MVL^{cell} . **D)** The mean vectors of all cells in **(A)** are saved and plotted. These vectors were used to calculate each gel's overall mean vector length (MVL^{gel} , ranging from 0, cells randomly aligned, to 1, all cells strongly aligned in the same direction) and mean angle (MA^{gel}). In this image, the cells are aligned in the 0° (x_1) direction with moderate strength.

We tracked the orientation and strength of alignment of fibroblasts using mean vectors calculated using equations 2-4, consistent with circular statistics theory for the analysis of angular data (Batschelet 1981):

$$Y = \frac{\sum(L_j \cdot \sin(2\theta_j))}{N} \quad X = \frac{\sum(L_j \cdot \cos(2\theta_j))}{N} \quad (2)$$

$$MVL = \sqrt{(Y)^2 + (X)^2} \quad (3)$$

$$MA = \frac{1}{2} \arctan\left(\frac{Y}{X}\right) \quad (4)$$

For each cell, we constructed 400 vectors from the centroid to equally spaced points around the cell boundary. We used the lengths and angles of these vectors (L_j and θ_j , with $j = 1, 2, \dots, N$ and $N = 400$) to compute a vector whose length, MVL^{cell} , indicated strength of alignment (ranging from $MVL^{\text{cell}} = 0$ for a circular cell to $MVL^{\text{cell}} = 1$ for a highly aligned, spindly cell), and mean angle, MA^{cell} indicated orientation (Fig. 3.4C). The 2θ terms in equations 2 and $\frac{1}{2}$ term in equation 4 account for the fact that the full range of possible angles is only 180° , since a cell oriented horizontally could be correctly described as oriented at 0° or at 180° (Batschelet 1981). We then combined the individual cell vectors for all cells in each gel and used equations 2-4 to compute a mean vector that reflected the mean strength of cell alignment within each gel (MVL^{gel} , ranging from $MVL^{\text{gel}} = 0$, all cells aligned randomly, to $MVL^{\text{gel}} = 1$, all cells aligned in the same direction) and direction (MA^{gel}) for the entire gel (Fig. 3.4D). Finally, we averaged MVL^{gel} values across the ($n=5$) gels for each experimental condition.

3.2.7 Quantifying Parallel vs. Perpendicular Alignment of Cells and Stress

Fibers

In order to quantitatively compare the alignment and directionality of experimentally measured cells and computationally simulated SFs at different frequencies, we used an order parameter (Hsu et al. 2010; Jungbauer et al. 2008):

$$S = \langle \cos 2\theta \rangle = \int h(\theta) \cos(2\theta) d\theta, \quad (5)$$

where $h(\theta)$ represents the probability distribution histogram of cells or SFs in each angular bin. S ranges from $S = 1$, all cells or stress fibers aligned completely parallel to the stretch (x_1) direction, to $S = -1$, all cells or fibers aligned completely perpendicular to stretch, with $S = 0$ representing completely random alignment.

3.2.8 Experimental Measurements of Cell Alignment in 2D

Jungbauer et al. (Jungbauer et al. 2008) explored the effects of various stretch amplitudes and frequencies on cells cultured on top of 2D silicone elastomer membranes and used the same $S = \langle \cos 2\theta \rangle$ order parameter (equation 5) to measure cell alignment. We digitized their figures for rat embryonic fibroblasts subjected to 30×10^3 s (8.33 h) of 8% uniaxial cyclic stretch at 0.01, 0.25, 2, and 15 Hz to obtain their mean \pm SD alignment values for 30-50 cells per tested frequency.

3.2.9 Statistics

We used a two-way ANOVA to assess whether transverse compaction (F_{22}) or alignment (MVL) varied significantly across the stretch amplitudes (0%, 10% 0.5 Hz) and durations (24, 48, 72h) tested (Prism, GraphPad Software, San Diego, CA). We used a one sample t-test to assess whether alignment (either parallel for $S>0$ or perpendicular for $S<0$) varied significantly from a hypothetical mean of $S=0$ (random alignment) at each of our experimentally tested frequencies. We did not run statistics on any of the measurements taken from Jungbauer (Jungbauer et al. 2008).

3.2.10 Improved Thermodynamic Computational Model of Stress Fiber

Alignment

We modified a previously published model by Vigliotti et al. (Vigliotti et al. 2016) and used it to simulate the experiments reported here. The model represents the thermodynamics of stress fiber assembly and disassembly and was previously shown to reproduce a number of experimentally observed cellular responses to a range of cyclic stretch waveforms applied to cells cultured on deformable 2D substrates. The model incorporates the fundamental observation that tension promotes stress fiber assembly by assuming that tension reduces the free energy of subunits in the bound state. It also incorporates force-length and force-velocity behavior for actomyosin, allowing it to capture phenomena such as the disassembly of stress fibers in response to rapid shortening (Vigliotti et al. 2016). The Vigliotti model was designed to simulate the response of a single cell to

known applied strains. However, cells embedded in collagen gels can locally remodel both the collagen fibers and their attachments to the collagen (Lee, Holmes, and Costa 2008; Moon and Tranquillo 1993; Pizzo et al. 2005; Kim, Lakshman, and Petroll 2006) over time scales of minutes to hours, so that the effective cell strain at any time point in our experiments likely differed from the gross compaction strains we measured using markers. We therefore introduced the additional assumption that over long time scales, the cell maintains an average stress state that minimizes its free energy. Furthermore, embedded cells and the surrounding gel are mechanically in series, so that in very soft gels the cells experience only a fraction of the applied cyclic strain (Ujihara et al. 2015). We therefore assumed that only a fraction of the applied cyclic strain was transmitted to cells when simulating 3D stretch, whereas the full applied cyclic strain was transmitted to cells when simulating 2D stretch. For more details, please consult both the main text and SI Appendix published by Chen et al. (Chen et al. 2018).

3.2.11 Comparison of Cell Alignment to In Vitro Stress Fiber Alignment

Our experiments quantified the orientation distribution of populations of cells, while most models (including the one employed here, see below) predict distributions of stress fibers (SFs) within a single hypothetical cell. In order to understand any differences between these two metrics that might confound interpretation, we imaged ten cells from each 72h, 0.5Hz loading condition (60 total) with a confocal microscope with a 60x objective, creating z-stacks

consisting of one image every $0.5\mu\text{m}$ through each cell's thickness. Within each z-stack, we created 2D grayscale projections by manually selecting images that most clearly showed the cell's SFs (Fig. 3.5). We measured stress fiber orientation using the custom software MatFiber, a MATLAB implementation of an intensity-gradient-detection algorithm originally developed by Karlon et al. (Karlon et al. 1998) and subsequently used by our group to quantify collagen fiber orientation in histologic sections (Fomovsky and Holmes 2010; Holmes 2015) and by others to quantify stress fiber alignment within stretched cells (Kaunas et al. 2005; Karlon et al. 1999). We used the orientations of structures within 6×6 pixel subregions to calculate the strength of alignment, MVL^{SF} (ranging from 0, all SFs randomly oriented, to 1, all SFs aligned) and mean angle, MA^{SF} (Fig. 3.5A; equations 2-4). Then, the boundaries of each cell were traced to calculate each cell's MA^{cell} and MVL^{cell} as described above for comparison (Figs. 3.4, 3.5B).

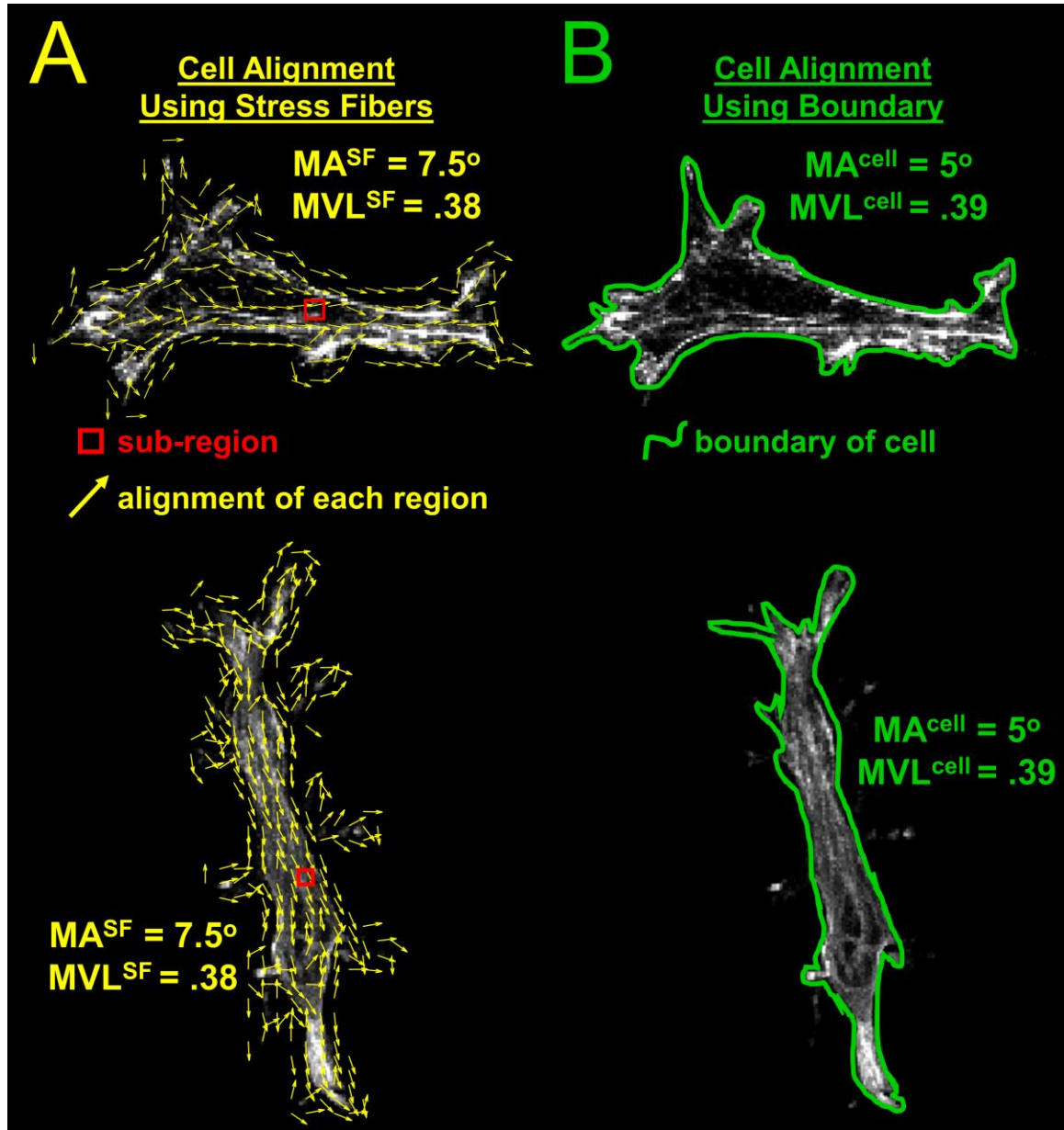


Figure 3.5

Two representative 2D projections of F-actin stained adult rat cardiac fibroblasts taken from the core of the tissue at 60x. **A)** Modified MatFiber software analyzes all sub-regions (red boxes) across the cell to determine the alignment at each location (yellow arrows denote orientation). The orientation and strength of alignment of these regions are combined to calculate an overall MA^{SF} and MVL^{SF} . **B)** MA^{cell} and MVL^{cell} calculated using the cell boundary (see Figure 3.4 and corresponding methods).

3.3 Results and Discussion

3.3.1 Cellular Alignment in the Presence of Transverse Compaction

In order to separate the effects of compaction and boundary conditions, we subjected collagen gels containing primary adult cardiac fibroblasts to different combinations of experimental conditions during a 24h pre-culture period and subsequent cyclic stretch periods (Fig. 3.1). In one group, we restrained gels during pre-culture, then left the x_2 direction free while we imposed low-frequency uniaxial stretch (10%, 0.5 Hz) or restraint (0% stretch) in the x_1 direction (Fig. 3.1C). Marker-based measurements of deformation in the central region of these gels confirmed the presence of substantial transverse compaction (Fig. 3.6B). Fibroblasts were randomly aligned after the pre-culture phase, but aligned strongly in the x_1 direction (parallel to stretch) during the stretching phase (Fig. 3.6C). The strength of cell alignment (average MVL^{gel}) varied with both time and stretch amplitude ($p < 0.001$) (Fig. 3.6C). Angular histograms of cell alignment at 24h (Fig. 3.7A,B) and 72h (Fig. 3.8A,B) show that cells aligned at 0° (in the stretch direction) and show that the strength of alignment (height of peak) increases over time. Cells also aligned at 0° at 48h (not shown).

Using the experimentally measured compaction and cyclic strains as inputs for the Obbink-Huizer computational model of strain avoidance we implemented in Chapter 2, we predicted strain avoidance of large x_2 compaction strains and alignment in the x_1 direction (parallel to stretch) at 24h for uniaxial constraint (Fig.

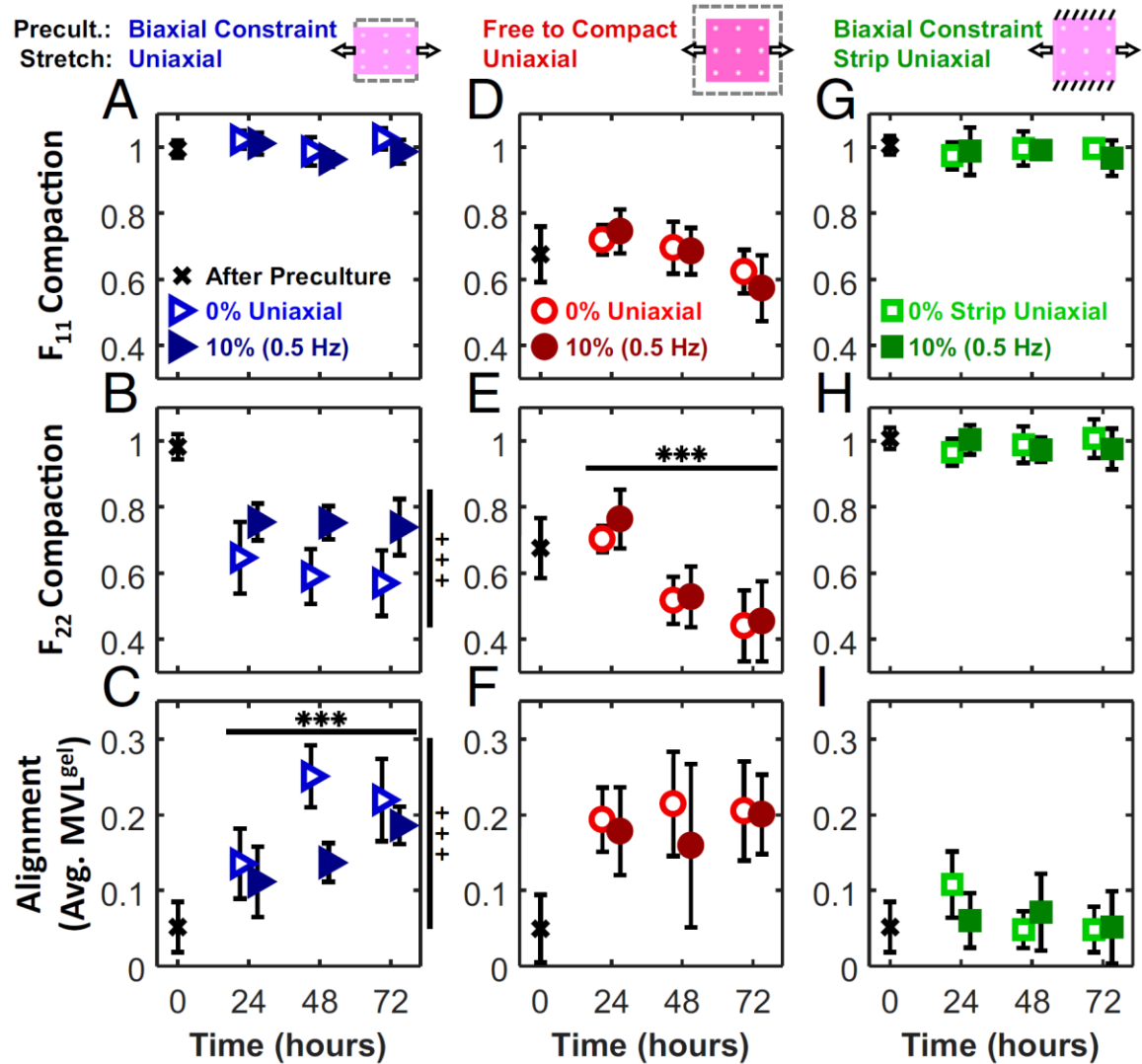


Figure 3.6

Time course of gel deformation and cell alignment at 24, 48, and 72h. After an initial pre-culture period (**black x**), collagen gels were subjected to either 0% stretch (**open symbols**) or 10% (0.5 Hz) stretch (**closed symbols**). Compaction deformations in the x_1 (F_{11} : **A,D,G**) and x_2 (F_{22} : **B,E,H**) directions were measured using titanium oxide markers. Average mean vector length (MVL^{gel} : **C,F,I**) describes the strength of cell alignment. Mean angle of all uniaxial cases was 0° . (***)ANOVA $p < 0.001$ difference over time, (***)ANOVA $p < 0.001$ difference between 0% and 10% groups). Each data point is representative of five independent experiments and expressed as the mean \pm SD.

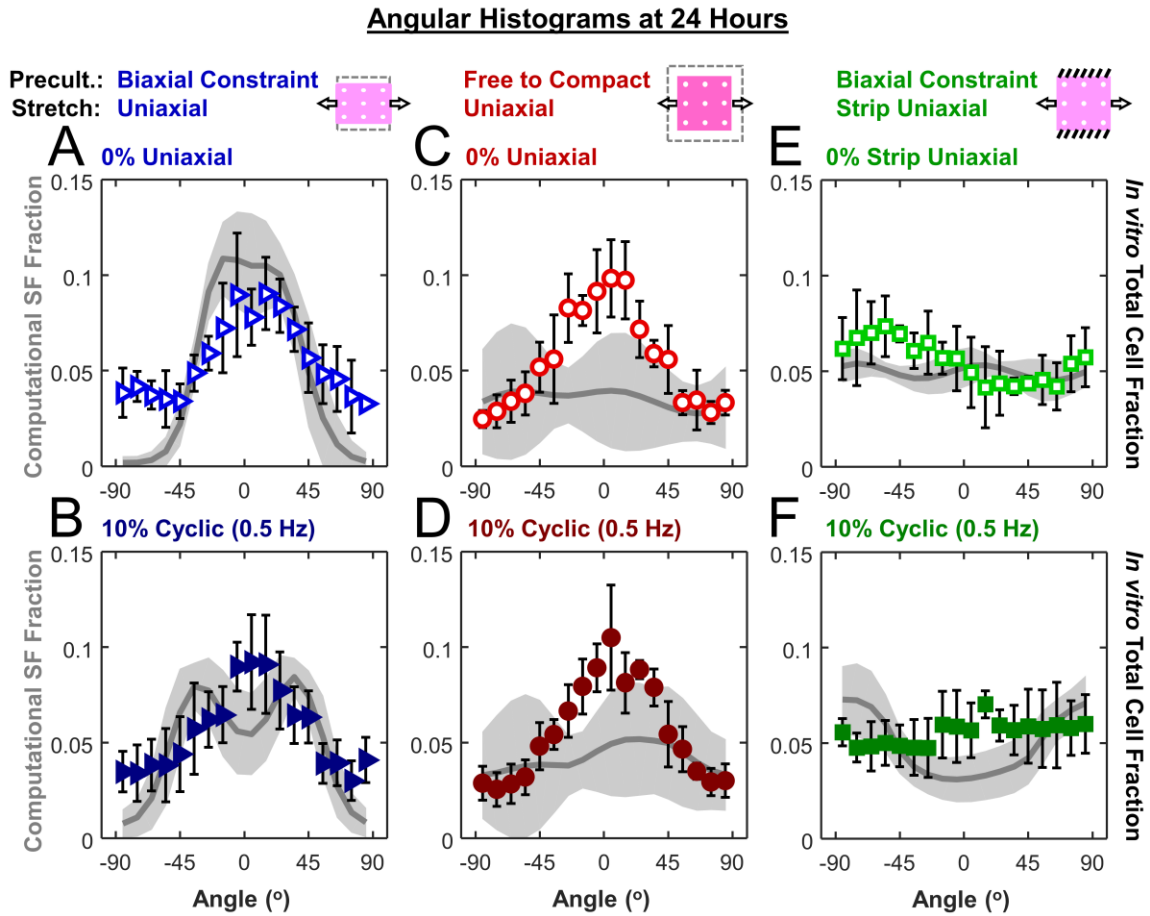


Figure 3.7

Angular histograms of computational stress fiber predictions (grey lines; light gray shading for standard deviations) and *in vitro* cell orientations for 0% stretch (**open symbols**, row 1: **A,C,E**) or 10% stretch (**closed symbols**, row 2: **B,D,F**) at 24 hour time points. Stress fiber alignment was modeled using experimentally measured strains from each condition. In all uniaxial cases, cells aligned with similar strength in the direction of stretch, regardless of the pattern of compaction (anisotropic vs. isotropic) or the presence of cyclic stretch.

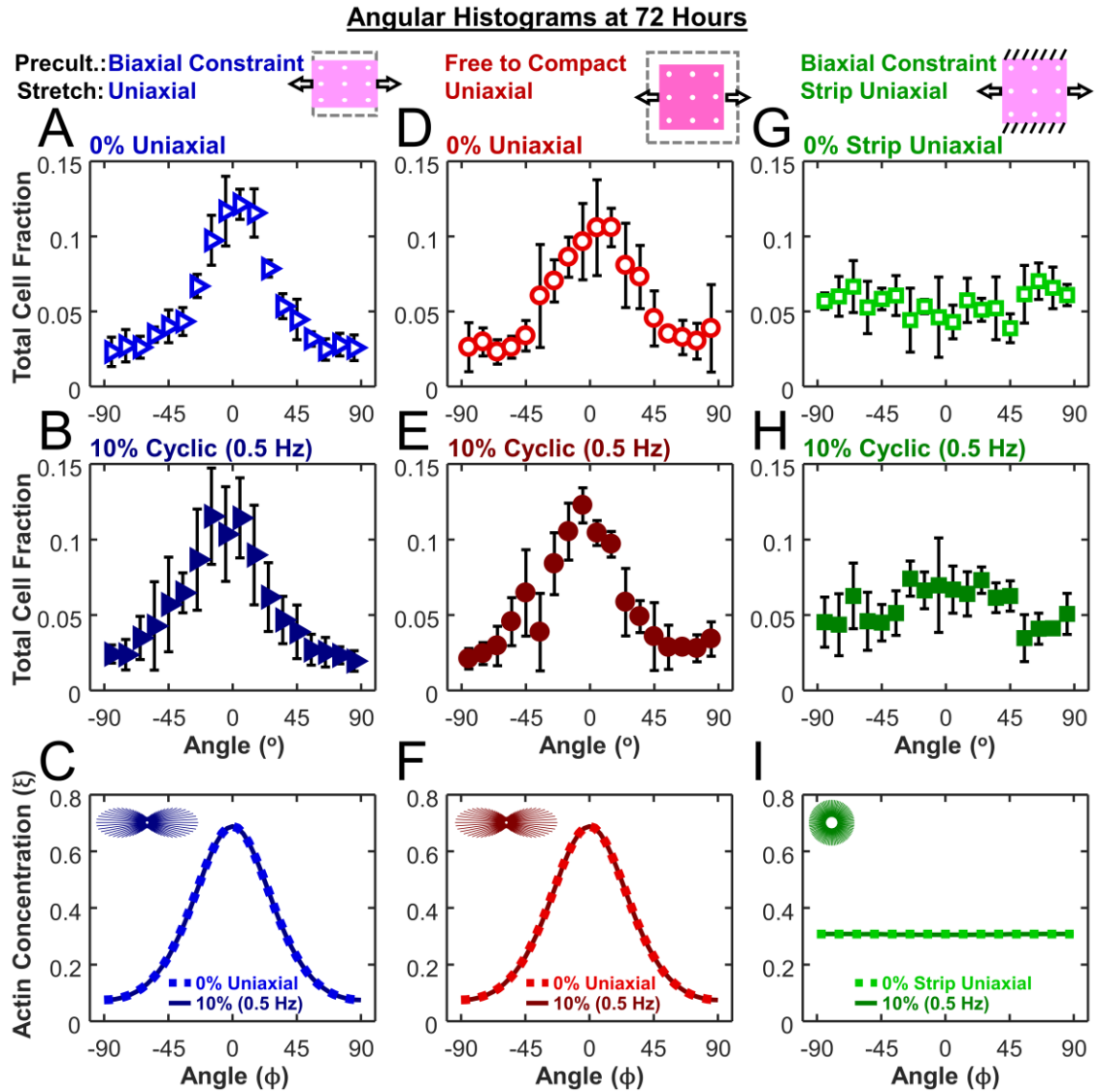


Figure 3.8

In all uniaxial cases, cells aligned with similar strength in the direction of stretch, regardless of the pattern of compaction (anisotropic vs. isotropic) or the presence of cyclic stretch. Angular histograms of cell orientation for 0% stretch (**open symbols**, row 1: **A,D,G**) or 10% (0.5 Hz) stretch (**closed symbols**, row 2: **B,E,H**) at 72 hour time points. Each data point is representative of five independent experiments and expressed as the mean \pm SD. Angular histograms of stress fiber orientation from computational simulations of our test conditions (row 3: **C,F,I**). In agreement with the experimental findings, the model predicted uniformly distributed stress fibers along the x_1 axis under uniaxial stretch (**C,F**) and uniformly distributed SFs under strip uniaxial stretch (**I**). Dotted lines indicate 0% stretch and solid lines indicate 10% cyclic (0.5 Hz) stretch. *Insets* show circular histogram representations of stress fibers for 0% cases.

3.7A) and 10% cyclic stretch (Fig. 3.7B), with a slight bimodal distribution observed in the latter due to some strain avoidance induced by cyclic stretching. Experimentally, angular histograms of cell orientations at 24h indicated that cells in both groups strongly aligned at 0° , parallel to the direction of stretch. The experimental curves showed good agreement with our *in silico* stress fiber alignment predictions for the static case and less good agreement for the 10% cyclic stretch case (Fig. 3.7A,B).

This experiment replicates the classic 3D results described previously by multiple groups, wherein cells in 3D culture align parallel to an imposed stretch (Foolen et al. 2012; Costa, Lee, and Holmes 2003; Lee, Holmes, and Costa 2008). Unfortunately, this experiment alone provides limited insight into the factors governing cell alignment because so many potential determinants co-vary. Cells could be aligning parallel to the imposed stretch or restraint or perpendicular to the compaction strains; furthermore, since transverse compaction generates collagen alignment parallel to a uniaxial restraint (Costa, Lee, and Holmes 2003; Lee, Holmes, and Costa 2008; Thomopoulos et al. 2007; Bellows, Melcher, and Aubin 1982), cells could also be aligning along the local collagen fiber direction.

3.3.2 Cellular Alignment in the Presence of Isotropic Compaction

In order to better separate these potentially confounding variables, we took advantage of the fact that collagen gel compaction is very rapid during the first few hours, then slows dramatically (Fig. 3.1E) (Knezevic et al. 2002). Thus, when

we left gels unconstrained in both directions for 24 hours, they compacted isotropically, inducing no net cell alignment (Fig. 3.6D,E,F). 24 hours of subsequent uniaxial restraint or low-frequency cyclic stretch (10%, 0.5 Hz) along the x_1 direction produced no additional transverse compaction in the x_2 direction, and the Obbink-Huizer model consequently predicted random alignment in both conditions at 24h due to strain avoidance of the large initial isotropic compaction strains (Fig. 3.7E,F). In contrast to these predictions, cells aligned strongly over that same time period (Fig. 3.7E,F) in both experimental groups; thus it seems clear that compaction strains could not be the primary driver of cell alignment in this experiment. The time course of experiments showed no further change in alignment over time (Figure 3.6I). We note that with longer culture periods in this experimental group, we did see some additional x_2 compaction. However, this compaction was not associated with higher levels of cell alignment (Fig. 3.6D,E,F; no change in peak height between Fig. 3.7C,D and Fig. 3.8D,E), again demonstrating a lack of correlation between the degree of transverse compaction and the degree of cell alignment.

3.3.3 Cellular Alignment in the Absence of Compaction

In other gels, we prevented transverse compaction by constraining gels biaxially during the pre-culture period and then applying “strip uniaxial” stretch conditions: stretching (10%, 0.5 Hz) or restraining (0% stretch) gels in the x_1 direction while preventing deformation in the x_2 direction (Fig. 3.1D). As expected, these gels displayed no transverse compaction (Fig. 3.6H). According to the strain

avoidance hypothesis, this experiment should produce similar results to those observed with cells cultured on 2D stretchable membranes: in the absence of transverse compaction, cells should avoid the imposed 10% cyclic strain and orient perpendicular to the loading direction. In contrast to this expectation, we found that average fibroblast alignment remained low at all time points in these gels (Fig. 3.6I), and histograms showed similar numbers of cells oriented in all directions at all times (24h: Fig. 3.7E,F; 72h: Fig. 3.8G,H).

These results are consistent with most previous reports employing 3D gels, but there are some inconsistencies. In agreement with our findings, Foolen et al. reported that vascular-derived cells cultured in collagen/matrigel gels developed random orientations during an initial biaxial constraint and that subsequent 10% strip uniaxial cyclic stretch at 0.5 Hz caused no change in the orientation within the core of the gel (Foolen et al. 2012). However, they also reported that cells on the top and bottom surfaces of their gels aligned perpendicular to the direction of stretch (Foolen et al. 2012); by contrast, cells at the surface and within the core of our gels showed similar alignment responses in all conditions. In another study, De Jonge et al. reported that myofibroblasts and collagen in 3D fibrin gels subjected to 5% strip uniaxial cyclic stretch at 1 Hz oriented perpendicular to the stretch direction (De Jonge et al. 2013), which appears to contradict both our data and that of Foolen.

3.3.4 Effect of Stretching Frequency on Cellular Alignment in 3D Gels

Published data suggest that cells on 2D elastic membranes subjected to cyclic uniaxial stretch align perpendicular to stretch only above a critical frequency of approximately 0.1 Hz (Terracio, Miller, and Borg 1988; Hsu et al. 2010; Jungbauer et al. 2008). We therefore tested the possibility that higher frequencies might induce perpendicular alignment in our strip uniaxial gels; for comparison we imposed the same stretch conditions on uniaxially stretched gels that were unconstrained in the x_2 direction. We plotted an order parameter that quantifies alignment (1 = parallel, -1 = perpendicular, 0 = random, see equation (5) in Materials and Methods) as a function of frequency alongside published 2D data (Jungbauer et al. 2008) from cyclically stretched rat embryonic fibroblasts (Fig. 3.9A). Cells in gels subjected to strip uniaxial stretch showed no alignment at 0.5 Hz, modest but statistically significant perpendicular alignment at 2 Hz, and clear perpendicular alignment at 4 Hz (orientation histograms for each case provided in Fig. 3.10E-G). Thus, under strip uniaxial conditions it was possible to induce perpendicular alignment similar to that commonly observed in 2D, but the transition frequency at which this occurred was an order of magnitude higher in our gel experiments than has been reported in 2D. Cells in gels subjected to uniaxial stretch with the x_2 direction left free showed clear parallel alignment at 0.5 Hz, modest but statistically significant alignment at 2 Hz, and no significant alignment at 4 Hz (Figs. 3.9A, 3.10A-C).

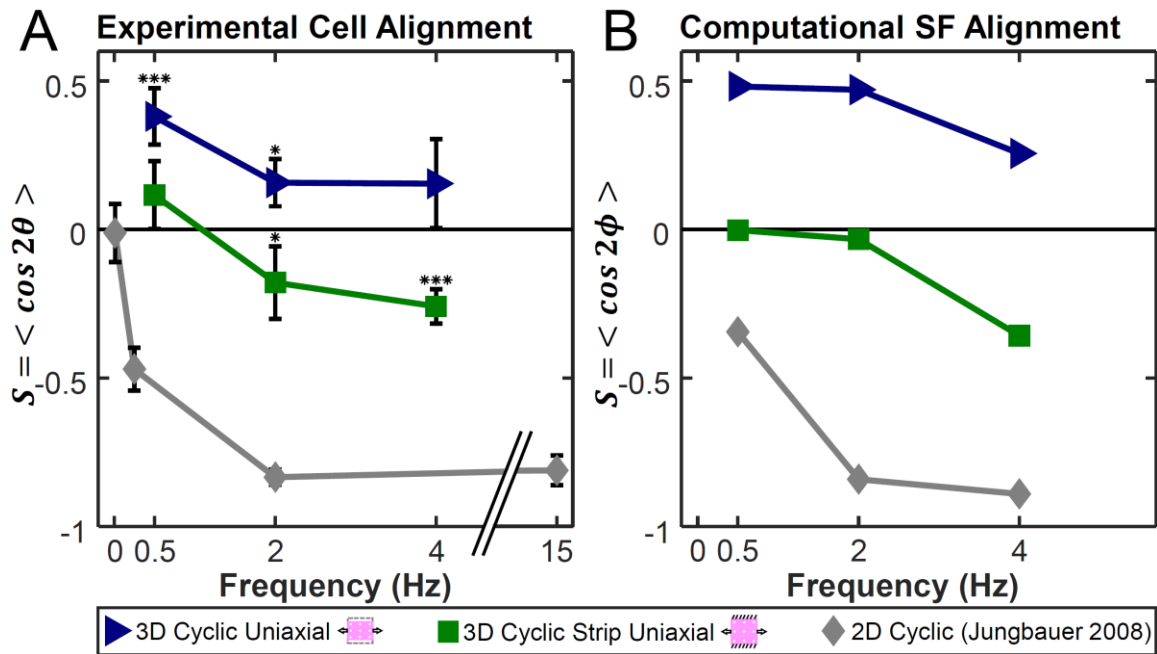


Figure 3.9

The model captures alignment trends across a range of frequencies and boundary conditions in both 3D and 2D culture conditions. We plotted the order parameter $S = \langle \cos 2\theta \rangle$ that quantifies alignment (1 = parallel, -1 = perpendicular, 0 = random) as a function of frequency in 3D uniaxial cyclic stretch (**blue triangles**), 3D strip uniaxial cyclic stretch (**green squares**), and 2D cyclic stretch on silicone elastomer membranes (**grey diamonds**) in experimentally measured cell orientations (**A**) and computationally predicted stress fiber orientations (**B**). Each data point for the experimental conditions is expressed as the mean \pm SD. 3D data points represent five independent experiments (except uniaxial 4 Hz, $n=4$) (** $p < 0.001$, * $p < 0.05$), while 2D data points represent 30-50 cells measured by Jungbauer et al. (Jungbauer et al. 2008) in rat embryonic fibroblasts at 8% cyclic stretch.

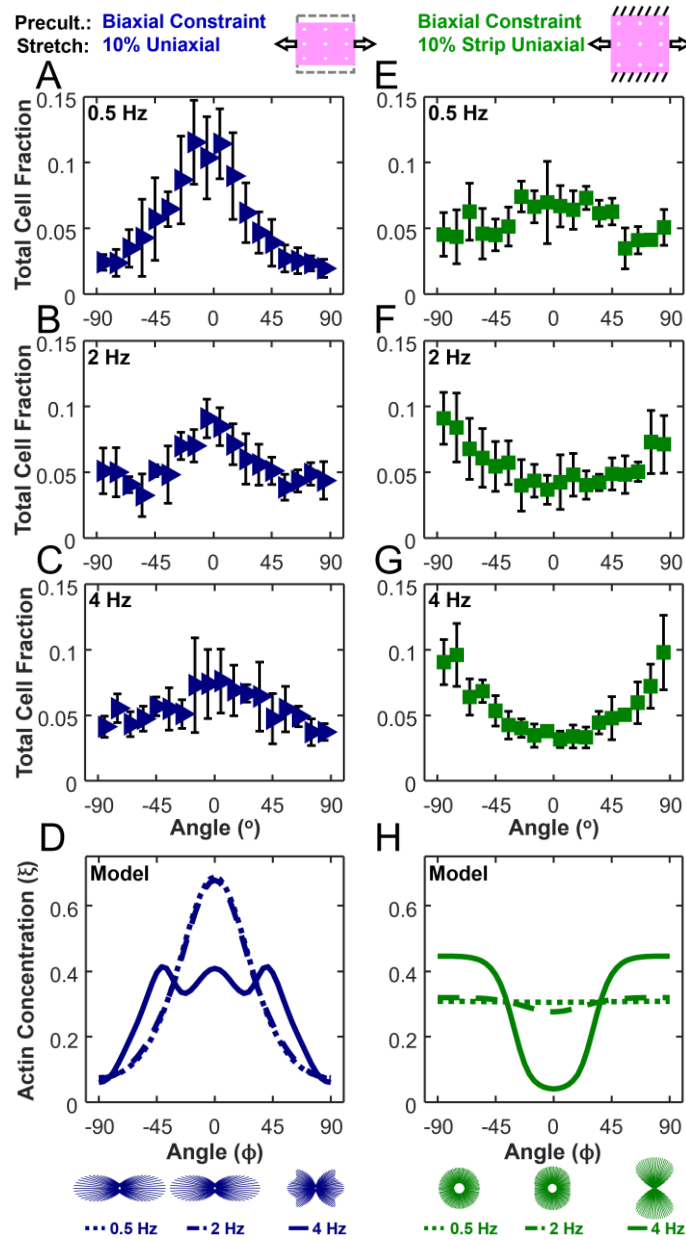


Figure 3.10

Angular histograms of cell orientation for 10% uniaxial cyclic stretch (**A-C**) and 10% strip uniaxial cyclic stretch (**E-G**) at 0.5, 2, and 4 Hz after 72 hours. Each data point is representative of five independent experiments (except uniaxial 4 Hz, $n=4$), and expressed as the mean \pm SD. Angular histograms of stress fiber orientation simulations for uniaxial (**D**) and strip uniaxial (**H**) conditions across our range of frequencies (**dotted** lines: 0.5 Hz, **dashed**: 2 Hz, **solid**: 4 Hz). *Insets* above the legend show circular histogram representations of these stress fibers.

3.3.5 Mechanical Determinants of Cell Alignment in 2D and 3D

Our experimental results suggest thinking about the mechanical factors that influence cell alignment on two different time scales. On the time scale of individual stretch and release cycles, sufficiently rapid or large strains do appear to modify cell alignment in 3D, inducing perpendicular alignment under conditions where static culture would produce randomly oriented cells and reducing parallel alignment under conditions where static culture would produce it. These observations are generally consistent with previous models (Obbink-Huizer et al. 2014; Deshpande, McMeeking, and Evans 2006) in which high strain rates either reduce stress fiber assembly or promote disassembly. However, any model that aims to simultaneously capture both 2D and 3D responses must explain why the transition frequency for perpendicular alignment appears to differ in these settings (Fig. 3.9A). We have incorporated one hypothesis to explain this discrepancy in the computational model presented below.

On the time scale of hours to days over which compaction of 3D gels occurs, we found that strain avoidance could not explain the alignment responses we observed. When cultured statically or at frequencies too low to induce reorientation, cells in gels restrained in the x_1 direction aligned just as strongly whether they compacted only in the x_2 direction or equally in both directions (Figs. 3.6, 3.7, 3.8). Thus, we believe the data presented here support the alternate hypothesis that cell alignment in these experiments was primarily determined by the presence or absence of a restraining boundary condition. This

alternate hypothesis fits better with prior observations that cells in collagen gels actively remodel the surrounding collagen as well as their attachments to it on a timescale of hours to days, making it difficult to imagine how cells would “remember” compaction strains over these longer times. The boundary condition hypothesis would also be consistent with a prior study by Lee et al., who allowed cell and collagen alignment to develop in uniaxially restrained collagen gels, then switched the direction of restraint from x_1 to x_2 (Lee, Holmes, and Costa 2008). Following the switch, cells re-oriented rapidly into the new direction of restraint (and away from the dominant collagen fiber direction), then gradually began reorienting collagen fibers towards the new preferred cell direction. This result suggested that the cells could sense and respond to a change in the direction of restraint independently of the alignment cues provided by surrounding collagen fibers, but did not directly address the role of compaction strains vs. restraint.

3.3.6 Modified Computational Predictions of Cell Alignment

In order to explore potential mechanisms that might explain the experimental results reported here, we collaborated with the authors of a previously published model (Vigliotti et al. 2016) that predicts the steady-state distribution of stress fibers (SFs) by accounting for the effects of imposed stretch and shortening on the kinetics of SF assembly and disassembly. The equations and details of the modified model are presented in the SI Appendix published by Chen et al. (Chen et al. 2018), but conceptually we made two modifications that reflect our proposed explanations for the novel findings presented above.

Our first modification to the original Vigliotti model was to assume that cells can remodel the surrounding collagen, their attachments to that collagen, and their cytoskeleton over time scales much longer than an individual loading cycle to achieve a state at which the increase in elastic energy due to stretching the cell beyond its reference configuration was balanced by the decrease in cytoskeletal free energy due to SF assembly (Fig. 3.12). As noted above, there is ample experimental evidence that cells embedded in collagen gels do remodel the surrounding collagen and their attachments (Moon and Tranquillo 1993; Pizzo et al. 2005; Kim, Lakshman, and Petroll 2006), but the hypothesis that this remodeling minimizes the free energy of the cell remains to be tested. When both the x_1 and x_2 directions were restrained as in our strip uniaxial stretching experiments, cells reached this minimum-energy state at stretches $F_{11} = 1.062$, $F_{22} = 1.062$ (Fig. 3.11). By contrast, when the x_1 direction was constrained and the x_2 direction left free as in our uniaxial stretching experiments, cells reached equilibrium at stretches $F_{11} = 1.075$, $F_{22} = 0.7893$ (Fig. 3.11B,C). Importantly, these stretches depended on the presence/absence of restraint in each direction, but not on the compaction history, because the cells in the model respond to compaction or stretch by shortening or lengthening individual SFs to hold the strain in each actomyosin subunit constant. Integrating these equilibrium stretches into the Vigliotti model resulted in nearly isotropic predicted stress fiber distributions for strip uniaxial stimulations of static and low-frequency stretch conditions (Fig. 3.8I). By contrast, in all uniaxial simulations where the x_2

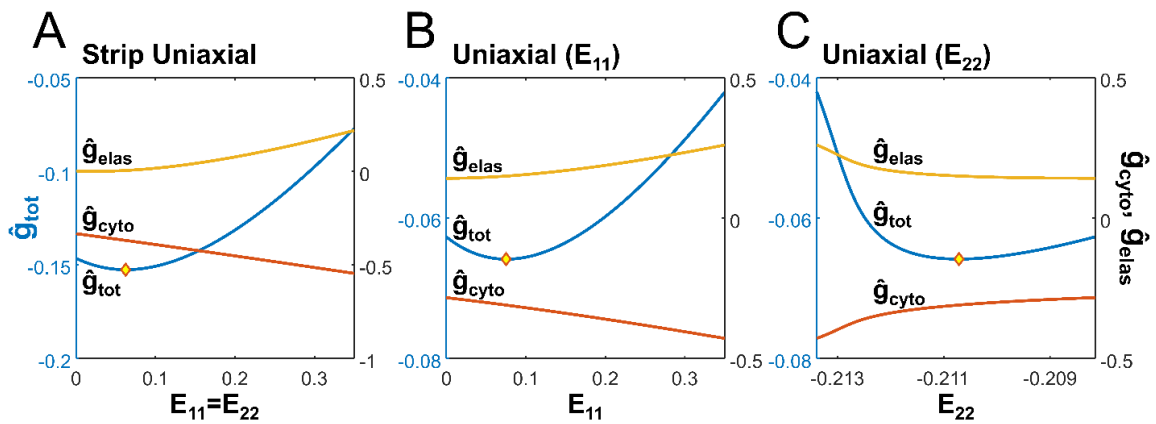


Figure 3.11

Modified computational model minimizes free energy ($\hat{g}_{tot} = \hat{g}_{cyto} + \hat{g}_{elas}$) based upon the boundary conditions to determine equilibrium cell strain. **A)** When the x_2 direction was constrained (strip uniaxial cases), stress fibers reached the same minimum free energy and cell strain in all directions ($E_{11}=E_{22}$). **B,C)** When the x_2 direction was free (uniaxial cases), stress fibers in x_2 (**C**) reached minimum free energy (**yellow diamond**) at a cell strain much lower than in x_1 (**B**).

boundary of the gels was left free, the model predicted strong SF alignment in the x_1 direction (Fig. 3.8C,F), consistent with the experimentally measured cell orientation distributions.

Our second modification accounts for the fact that when cells are embedded in very soft gels, the cells and gel act as springs in series, and the cells experience only a fraction of the stretch applied globally to the gel (Ujihara et al. 2015). In the Vigliotti model, large negative strain rates lead to lower SF forces due to the force-velocity behavior of myosin, discouraging parallel assembly and encouraging perpendicular assembly. Assuming that cells experience all of the global applied stretch in 2D but only a fraction of that stretch in a soft 3D gel, the model predicted that higher frequencies (or higher stretches) are required to modify SF distributions in 3D vs. 2D, in agreement with our 3D experiments and published 2D data (Fig. 3.9B; orientation histograms for 3D simulations in Fig. 3.10D,H). Together, these two modifications to the Vigliotti model allowed it to correctly predict not only the classic frequency-dependent perpendicular orientation response for 2D cyclic stretch experiments but also all of the key alignment responses reported here (Figs. 3.9, 3.10): 1) Under uniaxial restraint, cells in gels align parallel to the restraint regardless of the degree of transverse compaction; 2) Superimposing uniaxial cyclic stretch decreases the strength of that alignment in a frequency-dependent manner; 3) Under biaxial restraint, cells in gels align randomly; and 4) Superimposing uniaxial cyclic stretch promotes perpendicular alignment in a frequency-dependent manner.

A number of published models have addressed the effects of mechanical stretch on cell orientation (Obbink-Huizer et al. 2014; Vigliotti et al. 2016; Kaunas and Hsu 2009; Deshpande, McMeeking, and Evans 2006; De, Zemel, and Safran 2007), as discussed previously in Chapter 2. The Vigliotti model employed here incorporates some of the key components of previous models (such as force-length and force-velocity behavior of actomyosin) into a thermodynamically motivated framework, in which stresses or deformations influence SF assembly by altering the free energy of bound actomyosin subunits (Vigliotti et al. 2016). All of these models capture the experimental observation that cells on 2D substrates align parallel to a static restraint but perpendicular to an applied uniaxial cyclic stretch. Adding our assumption that only a fraction of the globally applied stretch is transferred to cells in soft gels would likely allow several of these models to also capture the difference in transition frequency between 2D and 3D experiments (Fig. 3.9). Of these models, only the Obbink-Huizer and Vigliotti models correctly predict that cells embedded in a 3D gel align parallel to uniaxial cyclic stretch, but both models rely on the magnitude of transverse compaction strains to make this prediction. In the Obbink-Huizer model, compaction strains perpendicular to the stretch direction reduce perpendicular SF assembly much more than the cyclic stretching reduces parallel SF assembly. In the Vigliotti model, SFs rapidly add or subtract actomyosin subunits along their length to hold the strain on individual subunits constant; large compaction strains perpendicular to stretch produce very short SFs in that direction, which are thermodynamically less stable than the longer SFs that persist in the stretch direction. Based on the

new experimental data presented here, our revised model proposes a slightly different mechanism: in the absence of external restraint, the minimum-energy equilibrium state for a cell embedded in a soft gel is one with very short, unstable SFs, while in the presence of restraint, equilibrium is achieved with longer, more stable SFs. In the presence of anisotropic boundary conditions, the SFs in different directions achieve a mix of these states, and perturbations due to cyclic stretch are then superimposed on this basal state. One conceptual advantage of this mechanism is that it does not assume that cells “remember” compaction strains that may have occurred days or weeks earlier, or even that changes induced in the cytoskeleton by compaction are maintained over long times; rather, it assumes only that the cell will continually remodel its cytoskeleton, surrounding ECM, and/or connections to that ECM to seek a minimum-energy state.

3.3.7 Comparison of Cell Alignment with In Vitro SF Alignment

Most models of the effects of stretch on cell orientation (including the one employed here) predict distributions of stress fibers within a single hypothetical cell. However, most experiments quantify the alignment of many cells subjected to a given experimental condition, in order to account for biologic variability and stochasticity that may not be represented in models. Thus, we do not expect model-predicted SF distributions to precisely match experimentally measured cell orientation distributions (Figs. 3.8, 3.10). Instead, we focused on features such as mean orientation and strength of alignment that we expected to be more

comparable. To test whether these features are in fact comparable between stress fiber (SF) and cell orientation distributions, we measured SF and cell orientations in the same subset of cells. The calculated orientation of the cell using its boundary, MA^{cell} , and its stress fibers, MA^{SF} , correlated closely across most of the 60 cells analyzed, with an overall regression equation $MA^{\text{cell}} = 0.88 \cdot MA^{\text{SF}} - 7.2$ and an R^2 value of 0.84 (Fig. 3.12A). This almost 1:1 correlation increased our confidence in comparisons between model-predicted mean stress fiber orientation and experimentally measured mean cell orientation (Fig. 3.12A). The strength of alignment computed from analyzing stress fibers (mean vector length, MVL^{SF}) also correlated on a cell-by-cell basis with that computed from the cell boundary (MVL^{cell}), although it was consistently lower, with an R^2 value of 0.65 (Fig. 3.12B). The relationship between these two measures ($MVL^{\text{cell}} = 1.25 \cdot MVL^{\text{SF}} + 0.08$) suggested that mean vector length computed from the cell boundary is generally higher than the mean vector length computed from stress fibers imaged in the same cell. On a cell-by-cell basis, this observation reflects the fact that even in cells that were clearly spindle-shaped and strongly aligned in a preferred direction, we frequently observed individual stress fibers oriented away from the primary cell axis.

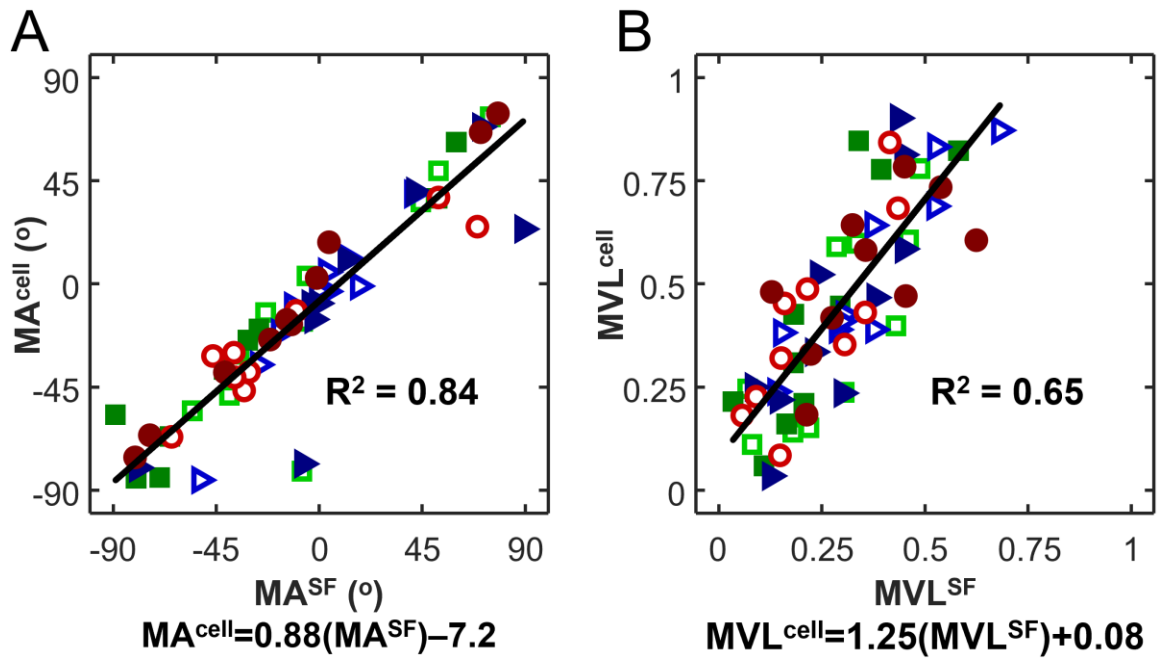


Figure 3.12

The orientation of stress fibers within ten cells from each stretch condition (sixty total; symbols correspond with Figs. 3.6, 3.7, 3.8) correlated strongly with the orientation of the entire cell. **A)** Orientation of the stress fibers (mean angle using stress fibers, MA^{SF}) versus tracing its boundary (MA^{cell}). **B)** Comparison of the strength of alignment of the cell using its stress fibers (mean vector length of stress fibers, MVL^{SF}) versus the alignment of the cell using its boundary (MVL^{cell}).

3.3.8 Limitations and Sources of Error

Limitations of the computational model presented here include the fact that we validated its predictions of cell alignment responses against experimental results for cyclic stretch at a range of frequencies from 0-4 Hz and amplitudes ranging from 0-10%, but predictions for other frequencies and amplitudes remain to be validated. In addition, although we expect that collagen gels that compacted more in the x_2 than in the x_1 direction in our experiments also developed some degree of collagen fiber alignment along the x_1 axis, we did not measure those collagen orientations or include them in our computational model of cell alignment. Our primary justification for this omission is that prior studies have clearly shown that isotropic compaction maintains random collagen orientation in the x_1 - x_2 plane in these gels (Bellows, Melcher, and Aubin 1982), yet some of our gels developed very strong cell alignment in the presence of isotropic compaction strains (i.e., 24h group in Fig. 3.6D,E,F). Thus, while contact guidance is certainly an important alignment cue in many settings, in our experiments it does not appear to be the dominant mechanism underlying cell alignment. Finally, the free-energy minimization approach used here to compute the equilibrium strain state of simulated cells ignored exchange of nutrients and heat with the surrounding bath and neglected the entropy and distribution of states observed in actual cell populations.

3.4 References

- Batschelet, Edward. 1981. *Circular Statistics in Biology*. London: Academic Press, London.
- Bellows, C G, A H Melcher, and J E Aubin. 1982. "Association between Tension and Orientation of Periodontal Ligament Fibroblasts and Exogenous Collagen Fibres in Collagen Gels in Vitro." *Journal of Cell Science* 58 (1): 125–38. <http://www.ncbi.nlm.nih.gov/pubmed/6820794>.
- Chen, Kellen, Andrea Vigliotti, Mattia Bacca, Robert M. McMeeking, Vikram S. Deshpande, and Jeffrey W. Holmes. 2018. "Role of Boundary Conditions in Determining Cell Alignment in Response to Stretch." *Proceedings of the National Academy of Sciences* 115 (5). National Academy of Sciences: 986–91. doi:10.1073/pnas.1715059115.
- Costa, Kevin D., Eun Jung Lee, and Jeffrey W. Holmes. 2003. "Creating Alignment and Anisotropy in Engineered Heart Tissue: Role of Boundary Conditions in a Model Three-Dimensional Culture System." *Tissue Engineering* 9 (4). Mary Ann Liebert, Inc. : 567–77. doi:10.1089/107632703768247278.
- De Jonge, Nicky, Frans M W Kanters, Frank P T Baaijens, and Carlijn V C Bouten. 2013. "Strain-Induced Collagen Organization at the Micro-Level in Fibrin-Based Engineered Tissue Constructs." *Annals of Biomedical Engineering* 41 (4): 763–74. doi:10.1007/s10439-012-0704-3.
- De, Rumi, Assaf Zemel, and Samuel a. Safran. 2007. "Dynamics of Cell Orientation." *Nature Physics* 3 (9): 655–59. doi:10.1038/nphys680.
- Deshpande, Vikram S, Robert M McMeeking, and Anthony G Evans. 2006. "A Bio-Chemo-Mechanical Model for Cell Contractility." *Proceedings of the National Academy of Sciences of the United States of America* 103 (38). National Academy of Sciences: 14015–20. doi:10.1073/pnas.0605837103.
- Fomovsky, Gregory M., and Jeffrey W. Holmes. 2010. "Evolution of Scar Structure, Mechanics, and Ventricular Function after Myocardial Infarction in the Rat." *American Journal of Physiology. Heart and Circulatory Physiology* 298 (1): H221-8. doi:10.1152/ajpheart.00495.2009.
- Foolen, Jasper, Vikram S Deshpande, Frans M W Kanters, and Frank P T Baaijens. 2012. "The Influence of Matrix Integrity on Stress-Fiber Remodeling in 3D." *Biomaterials* 33 (30): 7508–18. doi:10.1016/j.biomaterials.2012.06.103.
- Holmes, Jeffrey W. 2015. "Cardiac Biomechanics Group Downloads and Protocols." *University of Virginia Academic Web Pages*. <http://bme.virginia.edu/holmes/downloads/index.html>.

- Hsu, Hui-Ju, Chin-Fu Lee, and Roland Kaunas. 2009. "A Dynamic Stochastic Model of Frequency-Dependent Stress Fiber Alignment Induced by Cyclic Stretch." Edited by Johannes Jaeger. *PLoS ONE* 4 (3): e4853. doi:10.1371/journal.pone.0004853.
- Hsu, Hui-Ju, Chin-Fu Lee, Andrea Locke, Susan Q. Vanderzyl, and Roland Kaunas. 2010. "Stretch-Induced Stress Fiber Remodeling and the Activations of JNK and ERK Depend on Mechanical Strain Rate, but Not FAK." Edited by Marc Vooijs. *PLoS ONE* 5 (8). Public Library of Science: e12470. doi:10.1371/journal.pone.0012470.
- Hu, Jin-Jia, Jay D Humphrey, and Alvin T Yeh. 2009. "Characterization of Engineered Tissue Development under Biaxial Stretch Using Nonlinear Optical Microscopy." *Tissue Engineering. Part A* 15 (7). Mary Ann Liebert, Inc. 140 Huguenot Street, 3rd Floor New Rochelle, NY 10801 USA: 1553–64. doi:10.1089/ten.tea.2008.0287.
- Huang, Chenyu, Kunio Miyazaki, Satoshi Akaishi, Atsushi Watanabe, Hiko Hyakusoku, and Rei Ogawa. 2013. "Biological Effects of Cellular Stretch on Human Dermal Fibroblasts." *Journal of Plastic, Reconstructive and Aesthetic Surgery* 66 (12). Elsevier: e351-61. doi:10.1016/j.bjps.2013.08.002.
- Ives, C. L., S. G. Eskin, and L. V. McIntire. 1986. "Mechanical Effects on Endothelial Cell Morphology: In Vitro Assessment." *In Vitro Cellular & Developmental Biology* 22 (9). Springer-Verlag: 500–507. doi:10.1007/BF02621134.
- Jungbauer, Simon, Huajian Gao, Joachim P. Spatz, and Ralf Kemkemer. 2008. "Two Characteristic Regimes in Frequency-Dependent Dynamic Reorientation of Fibroblasts on Cyclically Stretched Substrates." *Biophysical Journal* 95 (7): 3470–78. doi:10.1529/biophysj.107.128611.
- Karlon, William J., James W. Covell, Andrew D. McCulloch, John J. Hunter, and Jeffrey H. Omens. 1998. "Automated Measurement of Myofiber Disarray in Transgenic Mice with Ventricular Expression of α -Sarcoplasmic Reticulum Calcium ATPase." *The Anatomical Record* 252 (4): 612–25. doi:10.1002/(SICI)1097-0185(199812)252:4<612::AID-AR12>3.0.CO;2-1.
- Karlon, William J., Pin-Pin Hsu, Song Li, Shu Chien, Andrew D. McCulloch, and Jeffrey H. Omens. 1999. "Measurement of Orientation and Distribution of Cellular Alignment and Cytoskeletal Organization." *Annals of Biomedical Engineering* 27 (6). Kluwer Academic Publishers-Plenum Publishers: 712–20. doi:10.1114/1.226.
- Kaunas, Roland, and Hui Ju Hsu. 2009. "A Kinematic Model of Stretch-Induced Stress Fiber Turnover and Reorientation." *Journal of Theoretical Biology* 257 (2): 320–30. doi:10.1016/j.jtbi.2008.11.024.
- Kaunas, Roland, Phu Nguyen, Shunichi Usami, and Shu Chien. 2005.

- “Cooperative Effects of Rho and Mechanical Stretch on Stress Fiber Organization.” *Proceedings of the National Academy of Sciences of the United States of America* 102 (44). National Academy of Sciences: 15895–900. doi:10.1073/pnas.0506041102.
- Kim, Areum, Neema Lakshman, and W. Matthew Petroll. 2006. “Quantitative Assessment of Local Collagen Matrix Remodeling in 3-D Culture: The Role of Rho Kinase.” *Experimental Cell Research* 312 (18): 3683–92. doi:10.1016/j.yexcr.2006.08.009.
- Knezevic, V, a J Sim, T K Borg, and J W Holmes. 2002. “Isotonic Biaxial Loading of Fibroblast-Populated Collagen Gels: A Versatile, Low-Cost System for the Study of Mechanobiology.” *Biomechanics and Modeling in Mechanobiology* 1 (1): 59–67. doi:10.1007/s10237-002-0005-0.
- Lee, Eun Jung, Jeffrey W. Holmes, and Kevin D. Costa. 2008. “Remodeling of Engineered Tissue Anisotropy in Response to Altered Loading Conditions.” *Annals of Biomedical Engineering* 36 (8): 1322–34. doi:10.1007/s10439-008-9509-9.
- Matsumoto, Takuya, Jun-Ichi Sasaki, Eben Alsberg, Hiroshi Egusa, Hirofumi Yatani, and Taiji Sohmura. 2007. “Three-Dimensional Cell and Tissue Patterning in a Strained Fibrin Gel System.” Edited by Mark Isalan. *PLoS ONE* 2 (11). Public Library of Science: e1211. doi:10.1371/journal.pone.0001211.
- Moon, Alice G., and Robert T. Tranquillo. 1993. “Fibroblast-populated Collagen Microsphere Assay of Cell Traction Force: Part 1. Continuum Model.” *AIChE Journal* 39 (1). American Institute of Chemical Engineers: 163–77. doi:10.1002/aic.690390116.
- Moretti, M., A. Prina-Mello, A. J. Reid, V. Barron, and P. J. Prendergast. 2004. “Endothelial Cell Alignment on Cyclically-Stretched Silicone Surfaces.” *Journal of Materials Science: Materials in Medicine* 15 (10). Kluwer Academic Publishers: 1159–64. doi:10.1023/B:JMSM.0000046400.18607.72.
- Obbink-Huizer, Christine, Cees W J Oomens, Sandra Loerakker, Jasper Foolen, Carlijn V C Bouten, and Frank P T Baaijens. 2014. “Computational Model Predicts Cell Orientation in Response to a Range of Mechanical Stimuli.” *Biomechanics and Modeling in Mechanobiology* 13 (1): 227–36. doi:10.1007/s10237-013-0501-4.
- Pang, Yonggang, Xiaoli Wang, Dongkeun Lee, and Howard P Greisler. 2011. “Dynamic Quantitative Visualization of Single Cell Alignment and Migration and Matrix Remodeling in 3-D Collagen Hydrogels under Mechanical Force.” *Biomaterials* 32 (15): 3776–83. doi:10.1016/j.biomaterials.2011.02.003.
- Pizzo, A M, K Kokini, L C Vaughn, B Z Waisner, and S L Voytik-Harbin. 2005.

- “Extracellular Matrix (ECM) Microstructural Composition Regulates Local Cell-ECM Biomechanics and Fundamental Fibroblast Behavior: A Multidimensional Perspective.” *Journal of Applied Physiology (Bethesda, Md. : 1985)* 98 (5): 1909–21. doi:10.1152/jappphysiol.01137.2004.
- Roby, Tiffany, Shawn Olsen, and Jiro Nagatomi. 2008. “Effect of Sustained Tension on Bladder Smooth Muscle Cells in Three-Dimensional Culture.” *Annals of Biomedical Engineering* 36 (10). Springer US: 1744–51. doi:10.1007/s10439-008-9545-5.
- Terracio, Louis, Bonnie Miller, and Thomas K Borg. 1988. “Effects of Cyclic Mechanical Stimulation of the Cellular Components of the Heart: In Vitro.” *In Vitro Cellular & Developmental Biology* 24 (1): 53–58. doi:10.1007/BF02623815.
- Thomopoulos, Stavros, Gregory M Fomovsky, Preethi L Chandran, and Jeffrey W Holmes. 2007. “Collagen Fiber Alignment Does Not Explain Mechanical Anisotropy in Fibroblast Populated Collagen Gels.” *Journal of Biomechanical Engineering* 129 (5). American Society of Mechanical Engineers: 642–50. doi:10.1115/1.2768104.
- Ujihara, Yoshihiro, Masanori Nakamura, Masatsugu Soga, Kenichiro Koshiyama, Hiroshi Miyazaki, and Shigeo Wada. 2015. “Computational Studies on Strain Transmission from a Collagen Gel Construct to a Cell and Its Internal Cytoskeletal Filaments.” *Computers in Biology and Medicine* 56. Elsevier: 20–29. doi:10.1016/j.combiomed.2014.10.015.
- Vigliotti, A., W. Ronan, F. P. T. Baaijens, and V. S. Deshpande. 2016. “A Thermodynamically Motivated Model for Stress-Fiber Reorganization.” *Biomechanics and Modeling in Mechanobiology* 15 (4). Springer Berlin Heidelberg: 761–89. doi:10.1007/s10237-015-0722-9.

Chapter 4

Development of Experimental Protocols to Study Fibroblast Alignment, Deformation, and Extracellular Matrix Synthesis

The primary findings and conclusions of this chapter developed experimental protocols found in the Appendix.

4.1 Introduction

In this chapter, we report a series of internal control and exploratory experiments related to aspects of fibroblast and extracellular matrix interactions during wound healing. In chapters 2 and 3, we developed a predictive model of cell alignment across a wide range of mechanical loading conditions. We made several key assumptions for this model, including that cells within collagen gels only experienced a fraction of the globally applied strains. The first half of this chapter develops an experimental setup to determine and compare the macro-scale global gel strains and micro-scale strains around the fibroblasts. We designed a custom rig to statically load the collagen gels and live stained the cells to observe cell deformations. To further explore differences in strains around the cells, we incorporated fluorescent microspheres within the gels, observing that groups of microspheres surrounding cells deformed less than groups of microspheres not near cells.

In the next part of this chapter, we began to experimentally explore the relationship between fibroblast alignment and the alignment of the collagen they deposit. First, we developed a protocol to use Second Harmonic Generation (SHG) microscopy to observe collagen fibers. Then, we employed culture conditions that encouraged fibroblast synthesis and deposition of collagen fibers and demonstrated some of the first images to use SHG microscopy to capture this phenomenon on a single cell level. The work described in this chapter helped

guide work described elsewhere in the thesis and established experimental protocols that could be utilized in the future to further explore these questions.

4.2 Methods

4.2.1 Utilizing Dil to Live Stain Fibroblasts in Collagen Gels

We used a highly lipophilic carbocyanine dye Dil Stain (1,1'-Dioctadecyl-3,3',3'-Tetramethylindocarbocyanine Perchlorate ('Dil'; DiIC₁₈(3))) (Invitrogen), which is weakly fluorescent until it binds with the cell membrane, to stain live adult rat cardiac fibroblasts. We created 9.338 $\mu\text{L}/\text{mL}$ Dil stock solution to serum starved media and mixed vigorously using a vortexer (Fisherbrand Analog Vortex Mixer) at the highest setting (setting level 10). Then, we re-suspended our cells at a concentration of 1×10^6 cells/mL in the Dil+media solution, rotated the solution in an incubator for 30 minutes, and centrifuged at $400 \times g$ to obtain a cell pellet. We used the cells to create collagen gels using methods mentioned previously (See Chapter 3 Methods 3.2.1-3), either allowing them to float freely in media or subjecting them to a 24h uniaxial constraint. We then imaged the gels under a confocal microscope with a 10x objective to capture z-stacks of the live cells. For gels under uniaxial restraint, we released the tension by cutting the arms of the gels and continued to image the live cells in 5 minutes increments.

4.2.2 Using Fluorescent Microspheres to Quantify ECM and Cell Strains

We mixed 1:200 Fluoresbrite YG microspheres (Polysciences, Inc.) in our Dil labeled cells + collagen solution before allowing the gels to polymerize as usual.

We biaxially restrained the gels during a 1-day pre-culture period (Methods 3.2.1-3; Figs. 3.1, 3.2) before using confocal microscopy to live image the gels. Using a Dremel tool and petri dish, we created a custom-made transparent rig that would allow us to statically load and fluorescently image the collagen gels (Fig. 4.1A). We statically stretched the gel by pulling on the arms and pushing pins through the sponges into the bottom holes of the rig, specifically testing strip uniaxial static stretch conditions (Fig. 4.1B). We took pictures at undeformed and multiple deformed configurations. For each configuration, we took a camera image to track TiO_2 markers and a confocal z-stack using 550 and 660 emission wavelengths for the microspheres and Dil-labeled cells, respectively. We used these images to track strains at multiple levels: global gel strains using the TiO_2 markers (Methods 3.2.5), cell strains using the Dil labeled cells, and strains near and away from cells using the microspheres (Fig 4.1C). We calculated cell strains by measuring the change in length of the cells in the x_1 (stretch) direction. We calculated strains near and away from cells by taking the coordinates of groups of microspheres at deformed and undeformed configurations and computing a single homogeneous deformation gradient tensor \mathbf{F} that provided the least-squares best fit mapping of the 9 marker positions from the undeformed (beginning of experiment) to deformed positions by solving the overdetermined matrix equation:

$$\mathbf{x} = \mathbf{F}\mathbf{X} + \mathbf{p} \quad (1),$$

where \mathbf{p} is an arbitrary vector included to account for translation between images.

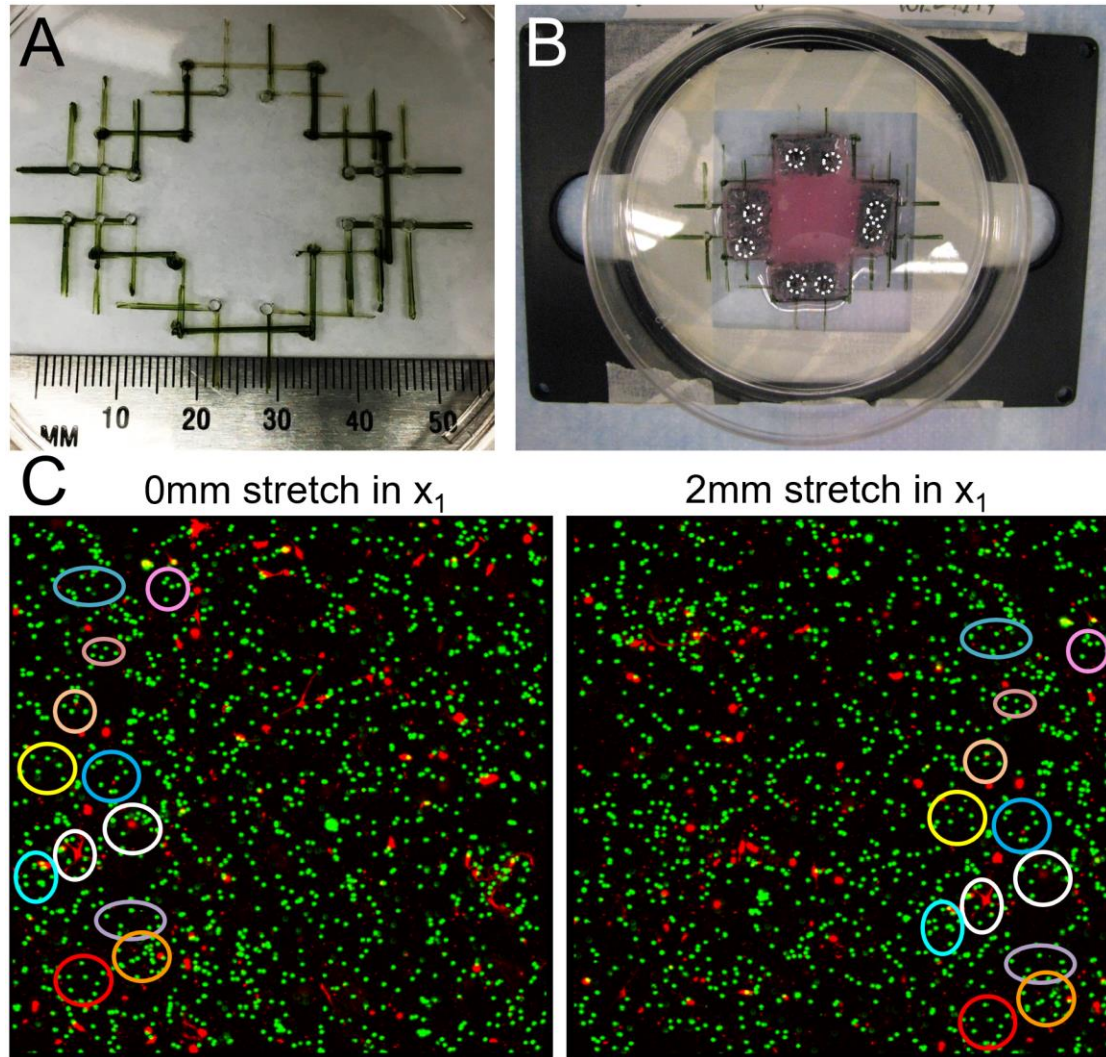


Figure 4.1

Methods for stretching cell-populated collagen gels and measuring local and global deformation. **A)** We used a Dremel tool to create holes within the dish at pre-determined locations. **B)** Loaded collagen gel on top of rig with stainless steel pins pushed through the sponge arms and through the holes (**grey dashed circles**). We taped the dish to a black dish holder, which we mounted on the confocal microscope stage for steady imaging (screw holes in corners of the holder). **C)** We tracked strains near and away from cells (**red**) using the coordinates of fluorescent microspheres (**green**) in undeformed and deformed conditions. Colored **circles** correspond to the different microsphere groups used. **White** circles correspond to sets of microspheres near cells, while all other circles correspond with sets of spheres away from cells.

We converted the deformation to a strain tensor \mathbf{E} using:

$$E = \frac{1}{2}([F^T F]^2 - I) \quad (2)$$

We categorized groups of microspheres as “near cells” if the spheres surrounded a cell (see white circles in Fig. 4.1C).

4.2.3 Second Harmonic Generation Microscopy of Collagen

We used second harmonic generation (SHG) microscopy to image collagen. First, we employed a 900-nm wavelength at 7% power to image collagen remodeling within our fibroblast-populated collagen gels cultured for 24h while either constrained biaxially or allowed to isotropically compact (Methods 3.2.1-3, Fig. 3.1). We imaged the fibroblasts by staining the F-actin with Alexa Fluor 488 Phalloidin (Thermo Fisher Scientific, A12379) (Methods 3.2.6). For cells cultured in a dish (discussed in the next section Methods 4.2.4) we used the laser at a 30% power to image the collagen produced by the fibroblasts and also capture the natural fluorescing intracellular components of the fibroblasts, such as NAD(P)H (Zipfel et al. 2003).

4.2.4 Stimulating Synthesis of Collagen and Fibronectin by Fibroblasts

We cultured fibroblasts in 24 well plates with glass bottoms (VWR) at a range of densities and different ascorbic acid concentrations (Fig. 4.2). During daily cell passaging, we will initially plate the cells at a density of 2.5 million cells/175cm², hereby referred to as 1.0x cell density, so we tested cell densities of 0.5x, 1.0x,

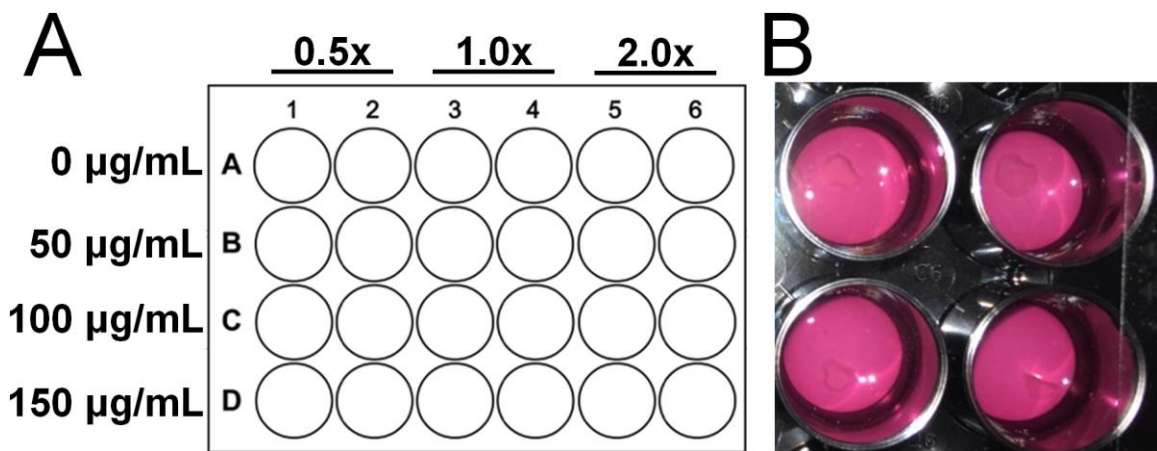


Figure 4.2

Setup of test conditions ranges to determine cell seeding density and ascorbic acid concentrations to best image collagen deposition. **A)** Ranges between 0.5x, 1.0x, and 2.0x normal cell seeding densities and 0, 50, 100, and 150 $\mu\text{g/mL}$ ascorbic acid tested in a 24 well plate. **B)** Camera image of the seeded wells after 9 days show formation of collagen tissue matrices created by the fibroblasts.

and 2.0x cell density. Previous studies reported that an ascorbic acid concentration of about 50 $\mu\text{g}/\text{mL}$ would promote collagen synthesis (Robinson et al. 2008), so we tested a range of 0, 50, 100, and 150 $\mu\text{g}/\text{mL}$ ascorbic acid.

We plated cells at day 0 in normal media with 10% Fetal Bovine Serum (FBS). At day 3, we rinsed and refed cells with media containing 10% FBS and ascorbic acid. On days 5 and 7, we rinsed and refed cells with serum-free media containing ascorbic acid. We fixed cells at day 9 in 10% formalin and stained the F-actin with Alexa Fluor 488 Phalloidin (Thermo Fisher Scientific, A12379) and fibronectin using a primary anti-fibronectin antibody (100 μg EMD Millipore AB2040) and a secondary goat anti-rabbit antibody (IgG (H-L) Cross-Absorbed Secondary Antibody, ThermoFisher A-11010, see Appendix 4.5.3).

4.3 Results and Discussion

4.3.1 Observing Fibroblast Alignment After Tension Release

Cells in free floating collagen gels qualitatively exhibited circular shapes (Fig. 4.3A), while those under uniaxial constraint elongated and aligned in the constraint direction (Fig. 4.3B). To determine if the DiI stain could capture live remodeling of the cell cytoskeleton, we released tension in the uniaxially constrained gels and observed some cells becoming less aligned and more circular on the time scale of 45 minutes or longer (Fig. 4.4). This observation

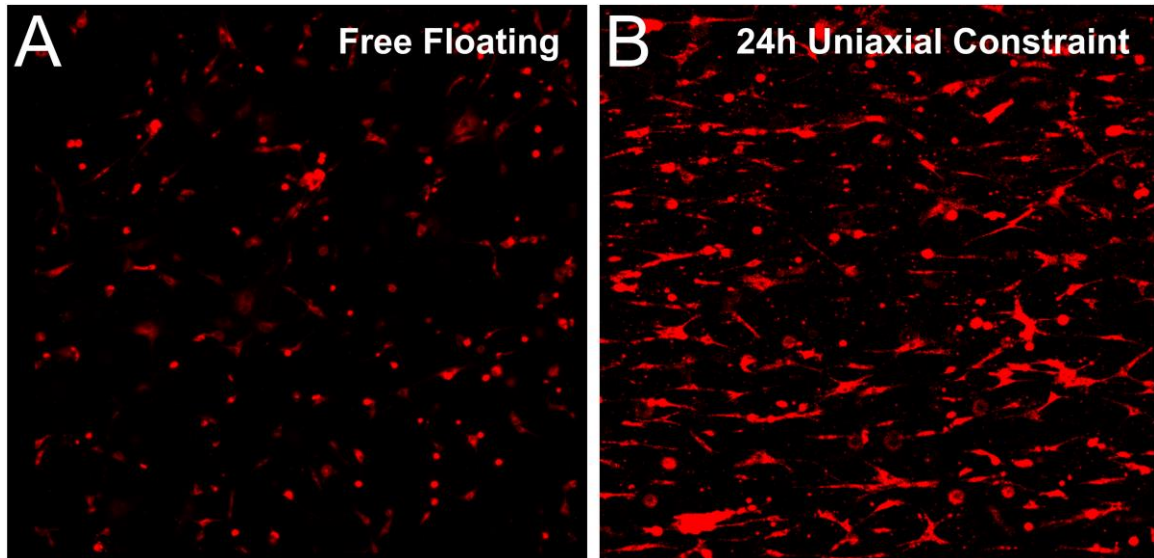


Figure 4.3

Live fluorescent microscopy of fibroblasts in collagen gels. **A)** Cells in free floating gels. **B)** Cells subjected to a 24h uniaxial constraint.

Release Experiments

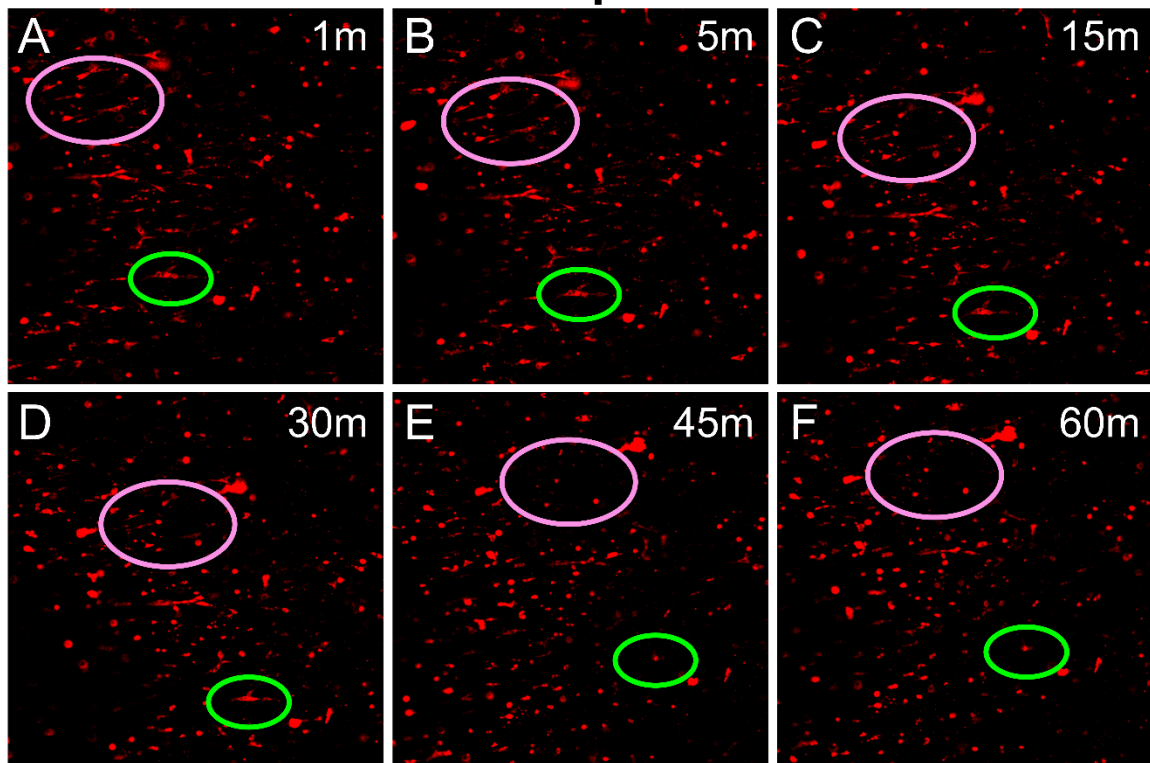


Figure 4.4

Live imaging time courses show aligned cells under uniaxial tension lose alignment and become circular on the scale of hours when tension is released.

Pink circle highlights a group of elongated cells and **green circle** highlights one specific elongated cell that all that become circular by 45min.

certainly supports the ideas embedded in our computational model from Chapter 3 that cell alignment was primarily determined by the presence or absence of a restraining boundary condition and that cells can remodel their connections to surrounding matrix and/or the matrix itself on a timescale of minutes, at least within collagen gels. These findings are also consistent with a prior study by Lee et al., who allowed cell alignment to develop in uniaxially restrained collagen gels, then switched the direction of restraint from x_1 to x_2 (Lee, Holmes, and Costa 2008). Following the switch, cells re-oriented rapidly into the new direction of restraint. Bayer et al. (Bayer et al. 2014) also demonstrated this phenomenon with their uniaxially loaded engineered tendon constructs. After removing the load by cutting one of the arms, similar to our protocol, they observed changes in integrin expression, which could indicate remodeling of cellular connections to the surrounding matrix. Overall, these experiments and observations give us confidence in one of our major assumptions from the previous chapter and our publication (Chen et al. 2018). Future work could be done to repeat these observations and rule out other explanations, such as the possibility that the cells migrated out of frame (in the z direction) as opposed to losing their alignment.

4.3.2 Global Gel Strains versus Strains Near and Away from Cells

We observed that cells deformed significantly less than the global gel strains in the x_1 stretch direction under a static strip uniaxial stretch (Fig. 4.5). Cell strains calculated using both the cell boundary and microbead methods resulted in significantly less deformation than the calculated global gel strains. Groups of microbeads not near cells did not demonstrate any difference in strain from the

global gel strain. In the x_2 direction (data not shown), deformations were much lower (strains close to 0), due to the strip uniaxial stretch condition, resulting in cell strains also being nearly zero. When we compared calculated cell strains to the global strains, we found that cells only experienced about 10-30% of the total gel strains, matching our damping parameter values used in Chapter 3. These results give us confidence and experimental evidence for another of our key assumptions for our model in Chapter 3: the fact that when cells are embedded in very soft gels, the cells and gel act as springs in series, and the cells experience only a fraction of the stretch applied globally to the gel. Assuming that cells experience all of the global applied stretch in 2D but only a fraction of that stretch in a soft 3D gel allowed us to correctly predict a different orientation-vs-frequency response curves for cells cultured on elastic 2D substrates vs. cells cultured in soft gels. Ujihara et al. (Ujihara et al. 2015) demonstrated this effect in a computer model simulating the material properties of cells within soft gels, and Screen et al. (Screen et al. 2003) also demonstrated that cells experienced lower strains with ex vivo tendon studies. Here, we have demonstrated preliminary experimental evidence that cells cultured in soft collagen gels experience strains substantially lower than the global macroscopic strain applied to the gel.

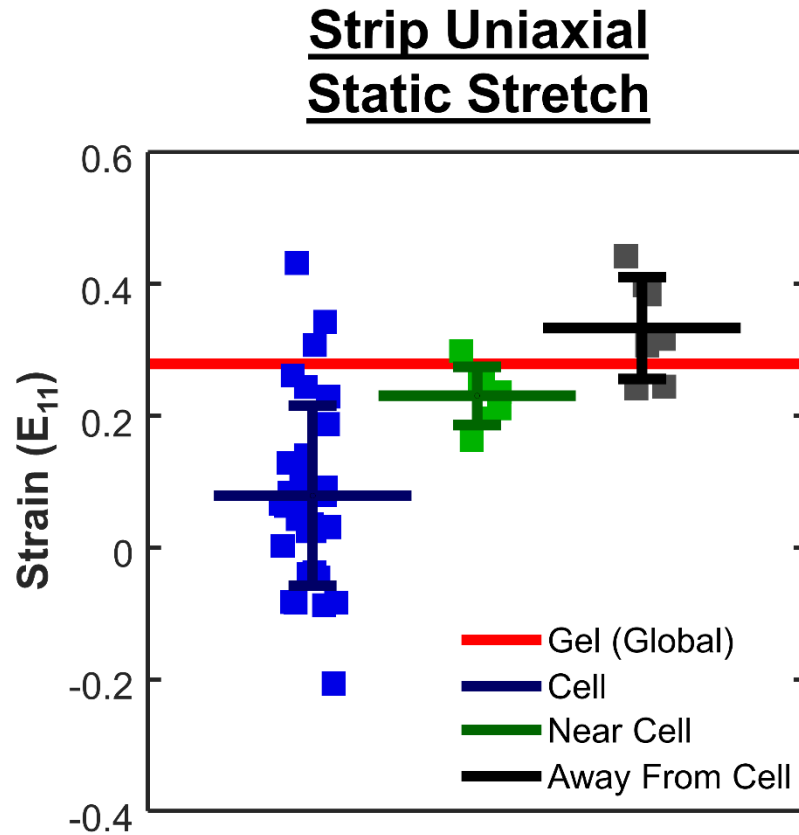


Figure 4.5

Comparison of global to micro-scale strains in collagen gel stretch experiments for a strip uniaxial static stretch. We calculated global gel deformation (**orange line**) using TiO_2 marker tracking on the surface of the gels, cell strain from the length change of Dil live imaged cells (**blue**), and micro-scale gel strains near using groups of fluorescent microspheres that surrounded nearby cells (**green**) or away from cells (**black**). Square markers represent each individually calculated strain, and the colored lines show the mean + std of each group.

4.3.3 SHG Microscopy of Fibroblasts Remodeling Collagen Gels

In biaxial constraint conditions, cells collected relatively little collagen around them and collagen was relatively homogeneously distributed throughout the depth of the gel (Fig. 4.6A). When cultured in free floating gels and allowed to isotropically compact the gels, the cells collected and concentrated fibers, resulting in higher intensities of collagen signal around the cell (Fig 4.6B). This remodeling also produced some areas that were relatively devoid of collagen, as multiple nearby cells pulled the collagen in different directions. Our images support observations made in the literature that have also shown similar local remodeling (Pizzo et al. 2005; Kim, Lakshman, and Petroll 2006; Moon and Tranquillo 1993; Vader et al. 2009) and provide additional support for the model premise in Chapter 3 and our manuscript (Chen et al. 2018) that cells can remodel the local matrix and/or their attachments to it. One interesting point here is that the degree to which the cells can remodel the collagen locally depends on the boundary conditions and initial culturing conditions. This could serve as an area of future investigation since the cells in our current cell model do not remodel differently depending on the initial culturing conditions (either biaxial restraint or isotropic compaction). Finally, these images also served as a validation that we could use SHG microscopy to image fixed collagen fibers.

4.3.4 Deposition of Collagen by Fibroblasts

Culturing cells at 1.0x cell density with 100 or 150 µg/mL ascorbic acid yielded enough fibrillar collagen around the cells to produce a strong signal under SHG

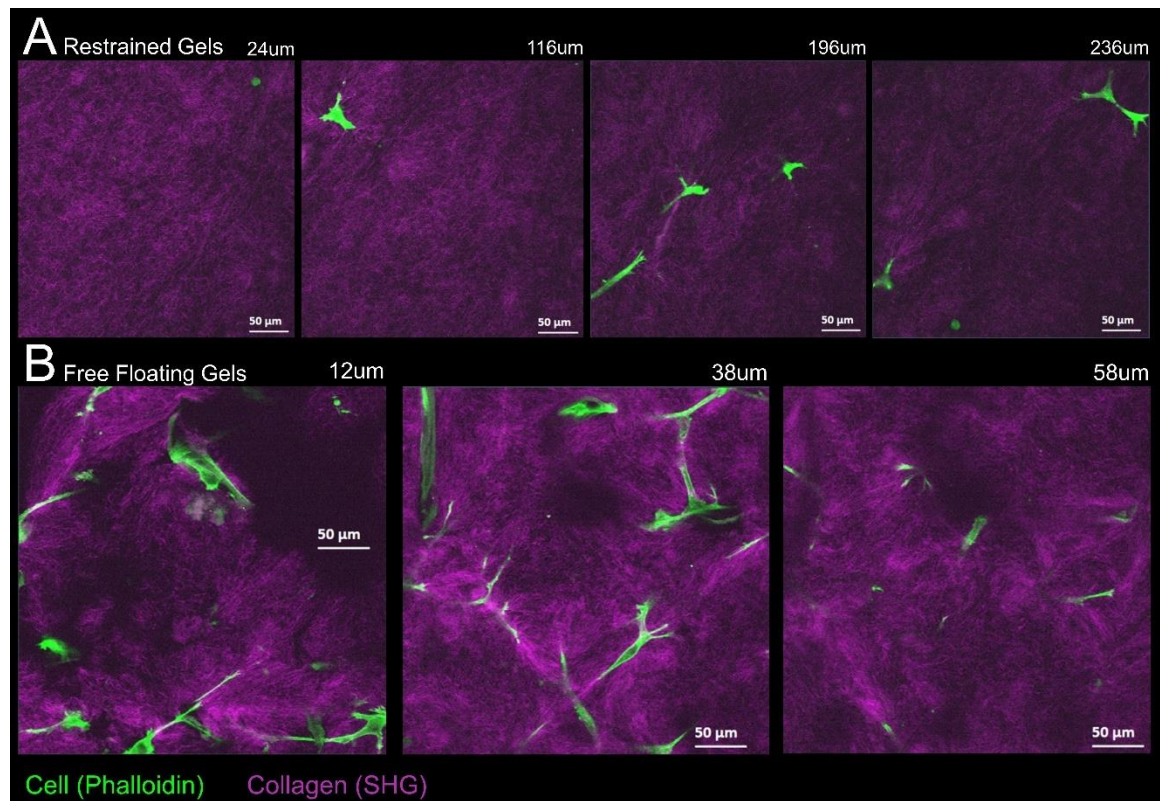


Figure 4.6

We used SHG microscopy to observe interactions between collagen (**purple**) and fibroblasts (**green**) within biaxially constrained and free-floating gels. **A)** Collagen within biaxially restrained gels demonstrated relatively homogenous distributions. **B)** By contrast, cellular remodeling produced uneven collagen distributions in free-floating gels.

microscopy. SHG microscopy also captured cell morphologies, enabling us to generate images of small clusters of cells depositing collagen fibrils between them (Fig. 4.7). Using this optimized culturing protocol (Appendix 4.5.2), we have demonstrated the ability to capture the thin layer of collagen fibers produced by a monolayer of rat cardiac fibroblasts. Previous studies using SHG microscopy to capture collagen deposition usually capture bulk numbers of cells producing bulk amounts of tissues (Hase et al. 2016) or individual cells producing small amounts of intracellular collagen co-localized with the cell cytoskeleton (Mortati, Divieto, and Sassi 2012). In the future, our culturing protocol might be further refined in order to capture single cells depositing their own singular collagen fibrils (Fig. 4.8). Cell densities too low make it difficult to locate any cells at high imaging magnifications, while higher cell densities caused a confluence of cells. Lower ascorbic acid concentrations did not encourage enough collagen production. If cultured at the right initial cell density and given enough FBS to encourage growth but not enough to create cell confluency, we could capture individual cells producing collagen fibers and interacting with them, demonstrated with Figure 4.8. We could then analyze the alignment of the cells and the newly produced collagen fibers to test the extent to which those new fibers are aligned with the cell. The cells could be traced to determine their own orientation and strength of alignment (Fig. 4.8B), and the collagen alignment (Fig. 4.8C) could be calculated using our custom MatFiber software (see Methods 3.2.11). In Chapter 5, we utilized an agent-based model of wound healing, in which aligned cells deposit

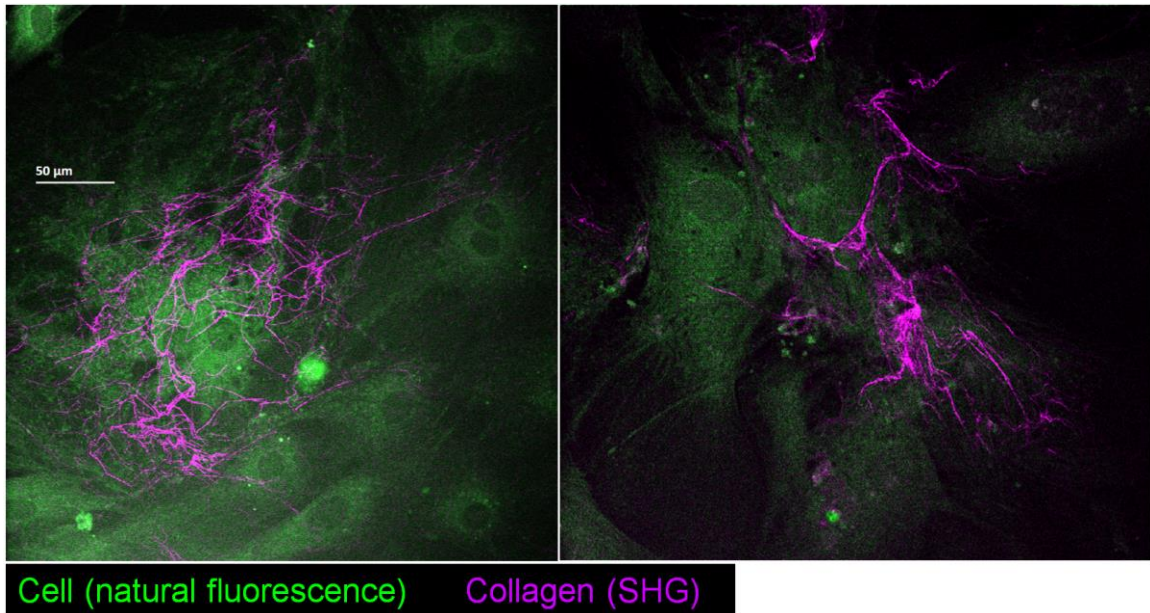


Figure 4.7

Fibroblasts cultured at a 1.0x cell density with 100 or 150 $\mu\text{g}/\text{mL}$ ascorbic acid yielded enough fibrillar collagen around some of the cells to produce a strong signal under SHG microscopy.

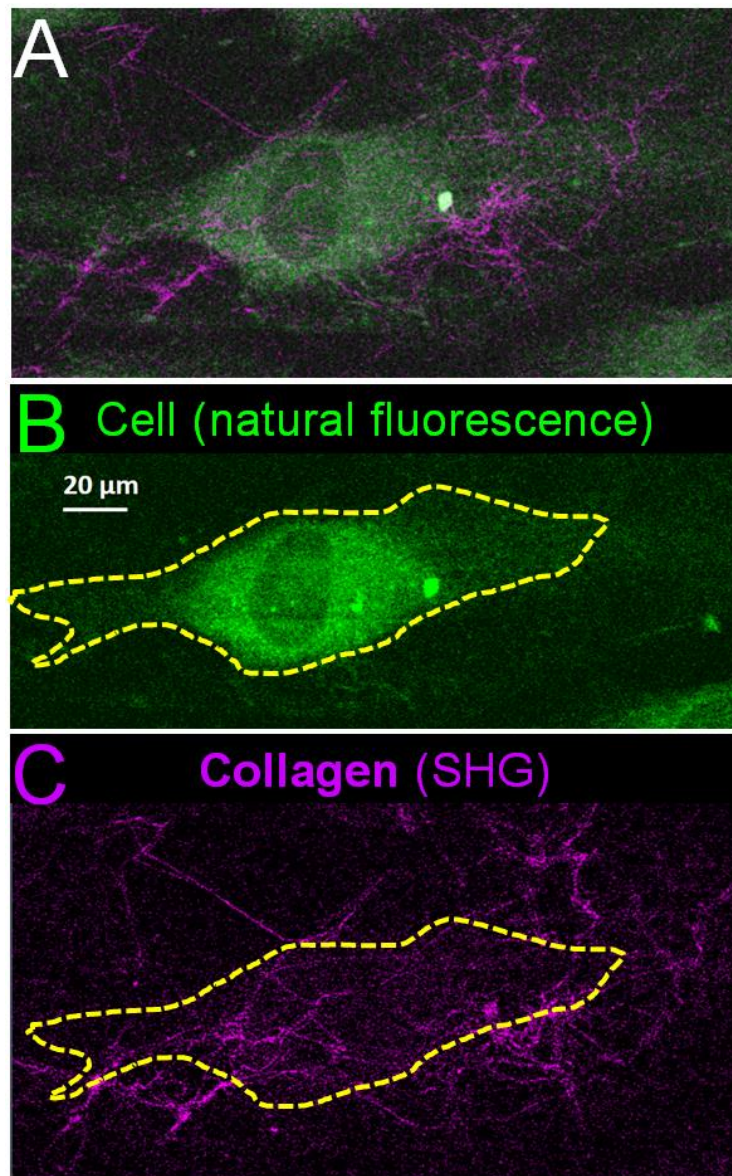


Figure 4.8

Potential proposed method to determine collagen deposition by cells using SHG microscopy. **A)** Overlay of a naturally fluorescing cell on top of deposited collagen. **B)** Cells could be traced to determine their individual orientations (**yellow dashed line**). **C)** Collagen orientation around the cell could be quantified to determine alignment of collagen deposited by the cell.

aligned collagen. We can use these experimental measurements to validate and refine this model and verify one of our assumptions.

4.3.5 Deposition of Fibronectin by Fibroblasts

While we know that cells produce preliminary matrix such as fibronectin before laying down collagen, we wanted to observe potential relationships between cell alignment, fibronectin alignment, and collagen alignment. We stained both fibroblasts and fibronectin and observed them co-localizing (Fig. 4.9). Unfortunately, we were unable to develop refine our protocol to allow both SHG microscopy and visualization of immunolabeled fibronectin in the same sample. Our current culturing protocol only stimulated some of the cells to produce individual collagen fibers around them and higher concentrations of ascorbic acid caused collagen to be produced everywhere. Thus, we first used the SHG laser at high power levels to locate and image the small amounts of collagen produced by individual cells. However, doing this photobleached the fluorescent label on the fibronectin (Figure 4.10 demonstrates a square field of view in which the fibronectin staining signal was eliminated by prior SHG). When we tried to first image the fibronectin to prevent photobleaching, the process became time expensive and generated many images of fibroblasts and fibronectin that did not contain any synthesized collagen fibers. Eventually, this process would also photobleach too many fields of view.

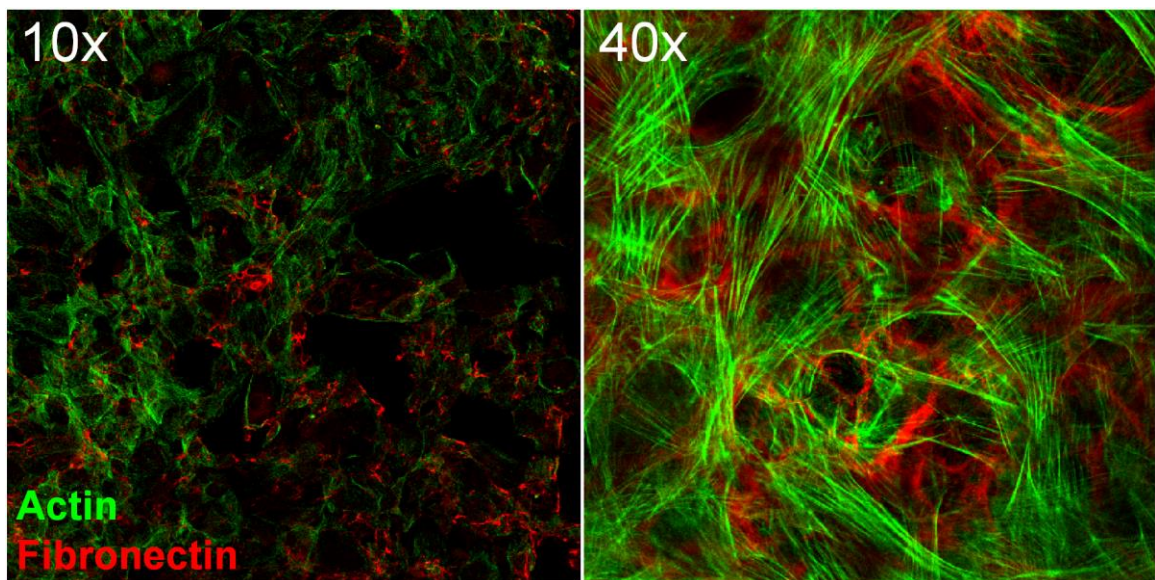


Figure 4.9

Fibroblasts interact with surrounding fibronectin during culture. Images showing our F-actin stained fibroblasts (**green**) interacting with nearby fibronectin (**red**) at 10x and 40x objectives.

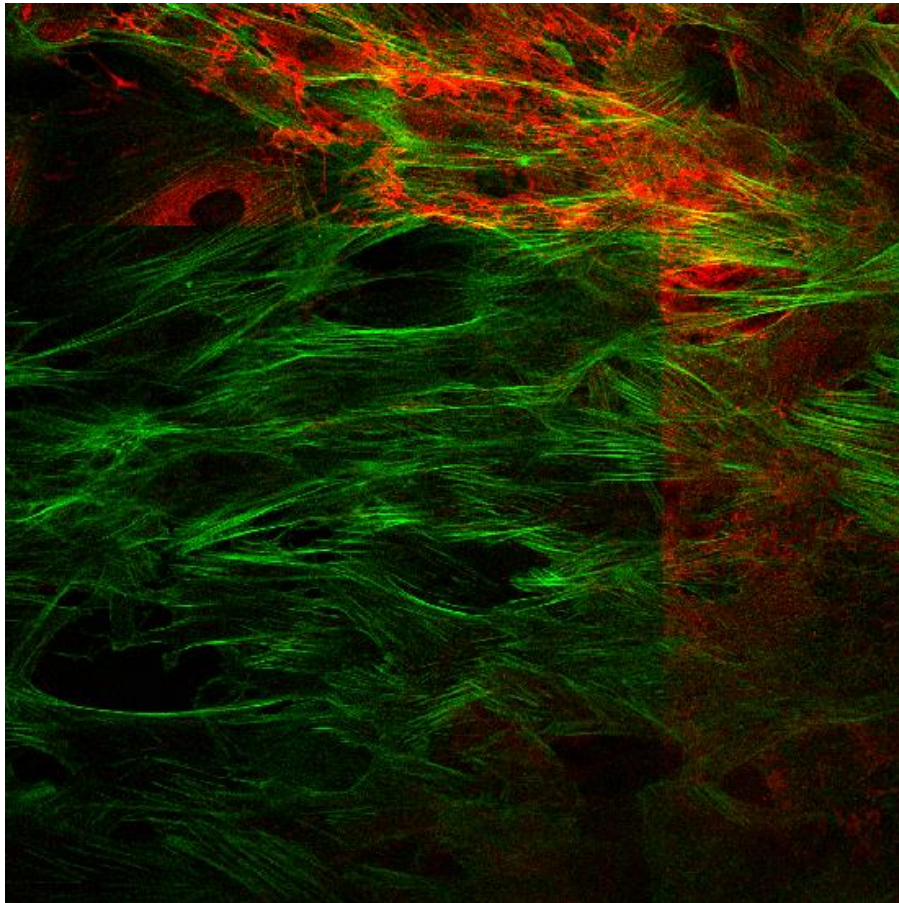


Figure 4.10

SHG microscopy and immunofluorescent staining could not be used in conjunction with each other to capture fibroblasts, fibronectin, and collagen. Using the SHG laser at high power levels photobleached the fluorescent label on the fibronectin antibody. This image clearly demonstrates a square field of view being eliminated of all fibronectin staining signal.

4.5 References

- Bayer, Monika L., Peter Schjerling, Andreas Herchenhan, Cedric Zeltz, Katja M. Heinemeier, Lise Christensen, Michael Krogsgaard, Donald Gullberg, and Michael Kjaer. 2014. "Release of Tensile Strain on Engineered Human Tendon Tissue Disturbs Cell Adhesions, Changes Matrix Architecture, and Induces an Inflammatory Phenotype." Edited by Christophe Egles. *PLoS ONE* 9 (1). Public Library of Science: e86078. doi:10.1371/journal.pone.0086078.
- Chen, Kellen, Andrea Vigliotti, Mattia Bacca, Robert M. McMeeking, Vikram S. Deshpande, and Jeffrey W. Holmes. 2018. "Role of Boundary Conditions in Determining Cell Alignment in Response to Stretch." *Proceedings of the National Academy of Sciences* 115 (5). National Academy of Sciences: 986–91. doi:10.1073/pnas.1715059115.
- Hase, Eiji, Oki Matsubara, Takeo Minamikawa, Katsuya Sato, and Takeshi Yasui. 2016. "In Situ Time-Series Monitoring of Collagen Fibers Produced by Standing-Cultured Osteoblasts Using a Second-Harmonic-Generation Microscope." *Applied Optics* 55 (12). Optical Society of America: 3261. doi:10.1364/AO.55.003261.
- Kim, Areum, Neema Lakshman, and W. Matthew Petroll. 2006. "Quantitative Assessment of Local Collagen Matrix Remodeling in 3-D Culture: The Role of Rho Kinase." *Experimental Cell Research* 312 (18): 3683–92. doi:10.1016/j.yexcr.2006.08.009.
- Lee, Eun Jung, Jeffrey W. Holmes, and Kevin D. Costa. 2008. "Remodeling of Engineered Tissue Anisotropy in Response to Altered Loading Conditions." *Annals of Biomedical Engineering* 36 (8): 1322–34. doi:10.1007/s10439-008-9509-9.
- Moon, Alice G., and Robert T. Tranquillo. 1993. "Fibroblast-populated Collagen Microsphere Assay of Cell Traction Force: Part 1. Continuum Model." *AIChE Journal* 39 (1). American Institute of Chemical Engineers: 163–77. doi:10.1002/aic.690390116.
- Mortati, L., C. Divieto, and M. P. Sassi. 2012. "CARS and SHG Microscopy to Follow Collagen Production in Living Human Corneal Fibroblasts and Mesenchymal Stem Cells in Fibrin Hydrogel 3D Cultures." *Journal of Raman Spectroscopy* 43 (5): 675–80. doi:10.1002/jrs.3171.
- Pizzo, A M, K Kokini, L C Vaughn, B Z Waisner, and S L Voytik-Harbin. 2005. "Extracellular Matrix (ECM) Microstructural Composition Regulates Local Cell-ECM Biomechanics and Fundamental Fibroblast Behavior: A Multidimensional Perspective." *Journal of Applied Physiology* 98 (5): 1909–21. doi:10.1152/jappphysiol.01137.2004.

- Robinson, Paul S., Sandra L. Johnson, Michael C. Evans, Victor H. Barocas, and Robert T. Tranquillo. 2008. "Functional Tissue-Engineered Valves from Cell-Remodeled Fibrin with Commissural Alignment of Cell-Produced Collagen." *Tissue Engineering Part A* 14 (1). Mary Ann Liebert, Inc. 140 Huguenot Street, 3rd Floor New Rochelle, NY 10801 USA : 83–95. doi:10.1089/ten.a.2007.0148.
- Screen, H R, D A Lee, D L Bader, and J C Shelton. 2003. "Development of a Technique to Determine Strains in Tendons Using the Cell Nuclei." *Biorheology* 40 (1–3). IOS Press: 361–68. doi:10.1007/978-0-387-73906-9_8.
- Ujihara, Yoshihiro, Masanori Nakamura, Masatsugu Soga, Kenichiro Koshiyama, Hiroshi Miyazaki, and Shigeo Wada. 2015. "Computational Studies on Strain Transmission from a Collagen Gel Construct to a Cell and Its Internal Cytoskeletal Filaments." *Computers in Biology and Medicine* 56. Elsevier: 20–29. doi:10.1016/j.combiomed.2014.10.015.
- Vader, David, Alexandre Kabla, David Weitz, and Lakshminarayana Mahadevan. 2009. "Strain-Induced Alignment in Collagen Gels." *PloS One* 4 (6). Public Library of Science: e5902. doi:10.1371/journal.pone.0005902.
- Zipfel, Warren R, Rebecca M Williams, Richard Christie, Alexander Yu Nikitin, Bradley T Hyman, and Watt W Webb. 2003. "Live Tissue Intrinsic Emission Microscopy Using Multiphoton-Excited Native Fluorescence and Second Harmonic Generation." *Proceedings of the National Academy of Sciences of the United States of America* 100 (12). National Academy of Sciences: 7075–80. doi:10.1073/pnas.0832308100.

4.6 Appendix

Appendix 4.5.1

Staining Cells with Dil (live cell stain)

Materials

- Cell Pellet
- Dil Stain (1,1'-Diocadecyl-3,3,3',3'-Tetramethylindocarbocyanine Perchlorate ('Dil'; DilC₁₈(3))) (Invitrogen D282)
- Vortex mixer (Fisherbrand Analog Vortex Mixer)
- Serum Starving Media (Protocol at <http://bme.virginia.edu/holmes/downloads/index.html>)
- Fibroblast-populated collagen gel solution (Collagen Gel and Cyclic Stretching Protocol at <http://bme.virginia.edu/holmes/downloads/index.html>)

Protocol

- 1) Count the number of cells you have, and then re-spin them down into a pellet (example: you want to make 20 mL stained collagen solution, so you need 4mL of cells in Dil. To be safe, you'll make 5mL of cells in Dil)
- 2) Re-spin your desired number of cells (example 5 million) into a pellet
- 3) Resuspend the cells in half the necessary media to give 2million cells/mL (example 2.5 mL serum free media)
- 4) Add 46.69 uL Dil to 2.5 mL of new serum free media (18.676uL per mL of media) and wrap **tightly** in parafilm. Mix vigorously using the vortexer at the highest setting (setting level 10).
- 5) Combine 2.5mL of cells with 2.5mL of Dil media
- 6) Incubate on rotator for 30 minutes
- 7) Centrifuge solution. Make your collagen gel solution while you wait
- 8) Your cell pellet should be magenta colored. Resuspend it in 5mL of serum starved media
- 9) Use 4mL of your media with your collagen gel solution to reach your desired 20mL of collagen gel solution with cells in it

Last updated: Kellen Chen 11/15/2018

Appendix 4.5.2

Culturing Fibroblasts to Produce Collagen and Imaging

Materials

- 24 well plates with glass bottom
- L-Ascorbic Acid (Sigma A4544)
- 10% Neutral Buffered Formalin (VWR 89370-094)
- Trypsin/EDTA-500ml (Sigma T4049)
- Phosphate Buffered Saline
- Collagen Gel Media (Protocol at <http://bme.virginia.edu/holmes/downloads/index.html>)
- Serum Starving Media (Protocol at <http://bme.virginia.edu/holmes/downloads/index.html>)
- Zeiss LSM 780 Laser Scanning Microscope, found in the W.M. Keck Center for Cellular Imaging at the University of Virginia (http://artsandsciences.virginia.edu/kcci/signup/instructions/Zeiss780_Basic_Operation_Apr2016.pdf)

Protocol

- 1) Trypsinize fibroblasts and centrifuge them to create a cell pellet (refer to cell passaging protocol)
- 2) Culture fibroblasts in 24 well plates with glass bottoms at a density of 2.5 mill cells/175cm² in normal media with 10% Fetal Bovine Serum (FBS)
- 3) 3 days later, rinse and refeed cells with media, 10% FBS, and 100 µg/mL ascorbic acid.
- 4) On days 5 and 7, rinse and refeed cells with serum free media and 100 µg/mL ascorbic acid
- 5) On day 9, fix cells in 1mL 10% formalin
- 6) Stain F-actin or fibronectin, as needed (see Appendix 4.5.3)
- 7) Image collagen using SHG microscopy on the Zeiss 780 at a 900nm wavelength and a 30% power level

Appendix 4.5.3

Fibronectin Primary and Secondary Antibody Staining

+ Phalloidin Primary Antibody Staining Protocol

Materials:

- 10% Neutral Buffered Formalin (VWR 89370-094)
- Donkey Serum (Sigma D9336-10ML)
- Triton x100 (Sigma X100-100mL)
- BSA (Bovine Serum Albumin)
- Alexa Fluor 488 Phalloidin (Life Technologies Invitrogen A12379)
- Anti-Fibronectin Antibody, 100 ug (EMD Millipore AB2040)
- Goat anti-Rabbit IgG (H L) Cross-Absorbed Secondary Antibody (ThermoFisher A-11010) (H+L fragments have better penetration)
- PBS

Protocol

- 1) wash x3 (with PBS) then fix 20min in 10% Neutral Buffered Formalin
- 2) wash x3 then permeabilize in 0.2% Triton for 2min
- 3) wash x3 then block with block with 5-10% Donkey Serum (dilute in nanopure water)
 - i. Each 24 well plate = 0.5mL serum solution
- 4) stain (in blocking solution) overnight at 4°C on a rocker
 - i. stress fibers: Alexa Fluor 488 phalloidin 5ul/1mL = 1:200 dilution
 - ii. Fibronectin: Primary Anti-FN rat antibody (anti-rabbit) = 1:200 dilution
- 5) wash x3 for 30min rinses on a rocker at room temperature
- 6) Stain secondary antibody for 4 hours room temperature
 - i. Secondary antibody: donkey host, anti-rabbit 647
 - ii. Dilute 1:500

Chapter 5:

Multiscale Computational Model of

Achilles Tendon Wound Healing:

Untangling the Effects of Repair and Loading

The primary findings and conclusions of this chapter will be published:

Chen, K., Hu, X., Blemker, S.S., Holmes, J.W. "Multiscale Computational Model of Achilles Tendon Wound Healing: Untangling the Effects of Repair and Loading." (Accepted to PLOS Computational Biology)

5.1 Introduction

Many mechanically loaded tissues including skin, tendon, ligament, and heart respond to injury by forming a collagen-rich scar. Normally, tendons are comprised of highly aligned collagen fibers that help transmit forces between muscles and bones throughout the body and bear high loads. The Achilles tendon in particular can be exposed to loads up to 70 MPa, compared to 30 MPa in most other tendons (Kongsgaard et al. 2005). These high loads often lead to injury, with Achilles tendon ruptures accounting for up to 45% of all tendon ruptures (Jozsa et al. 1989) and afflicting up to 2.5 million annually (McCormack and Bovard 2015; Riggan et al. 2014). Many who suffer from an Achilles tendon rupture never regain complete function, especially because healing tendons form scar with reduced collagen fiber organization and stiffness compared to uninjured tendons (Soslowky et al. 2000).

While there seems to be general agreement that mechanical stimulation of the healing tendon, such as during physical therapy, influences scar mechanical properties (Thomopoulos, Williams, and Soslowky 2003), current treatments for patients with an Achilles tendon rupture have produced variable results (Freedman, Gordon, and Soslowky 2014; Twaddle and Poon 2007; McCormack and Bovard 2015; Kongsgaard et al. 2005; Olsson et al. 2013). To better understand the impact of loading, rat animal models of Achilles tendon rupture have been utilized so that scar tissue can be excised to determine quantitative biomechanical scar properties. Unfortunately, these studies have also led to a wide variety of results, with mechanical loading sometimes appearing to increase, but

at other times appearing to decrease, tendon properties such as stiffness or rupture strength. One of the potential explanations for this variability could be due to differences in mechanics during healing, which could be altered through unloading (e.g. cast immobilization) or loading (e.g. free cage activity) of the tendon (Andersson, Eliasson, and Aspenberg 2009; Tuzuner et al. 2013; Freedman et al. 2016; Schizas et al. 2010; Freedman et al. 2013) as well as through the choice to repair the tendon with suture versus allowing natural healing without repair (Freedman et al. 2016; Meier Bürgisser et al. 2016). In this work, we developed a multiscale computational model of the healing rat Achilles tendon that integrates information about how local mechanics influences cellular alignment and collagen remodeling to predict the effects of various repair and loading protocols on tendon structure. We found that the multiscale model predicted the major observed trends in the evolution of tissue-level scar properties across a wide variety of published rat studies. Furthermore, the model simulations identified a potential mechanism underlying the apparently paradoxical finding that mechanical loading enhances collagen alignment in unrepaired Achilles tendons yet decreases it in repaired tendons.

5.2 Methods

Our multiscale computational model simulated mechanics and associated responses at multiple scales. At the organ level, we simulated various healing and loading conditions in a musculoskeletal model of the right rat hindlimb (Johnson et al. 2008) implemented in OpenSim (Delp et al. 2007) to estimate associated strains

in the tendon (Fig 5.1A). At the cellular level, these strains affected cellular behavior in two ways (Fig 5.1B,C). First, cyclic strains determined cell alignment according to a thermodynamic model of stress fiber dynamics developed and validated against *in vitro* experiments by our group (Chen et al. 2018) (Fig 5.1B). Second, mean strains modulated fibroblast collagen synthesis according to a relationship fitted to data from multiple published studies (Fig 5.1C) (Atance, Yost, and Carver 2004; Guo et al. 2013; Husse et al. 2007; Papakrivopoulou et al. 2004). At the tissue level, we used an agent-based model (ABM) of wound healing similar to one published previously by our group (Rouillard and Holmes 2012) to integrate these cellular behaviors and predict the evolving collagen structure (Fig 5.1D).

5.2.1 Literature Collection

We searched PubMed and Google Scholar for all papers that included the keywords “rat Achilles tendon rupture injury” in the title or abstract and used a scalpel to perform a full transection of both the Achilles tendon and the plantaris tendon, a tendon parallel to the Achilles that is proportionally larger in rats than in humans and can act as an “internal splint” (Murrell et al. 1994). From these, we next identified studies that specifically compared the effects of unloading from intramuscular injection of Botox, tail suspension, or cast immobilization against loading due to free cage activity, or treadmill exercise. From these 30 identified papers, we then selected those that quantitatively measured the cross sectional area and/or the Young’s Modulus of the healing scar, leaving us with 10 studies

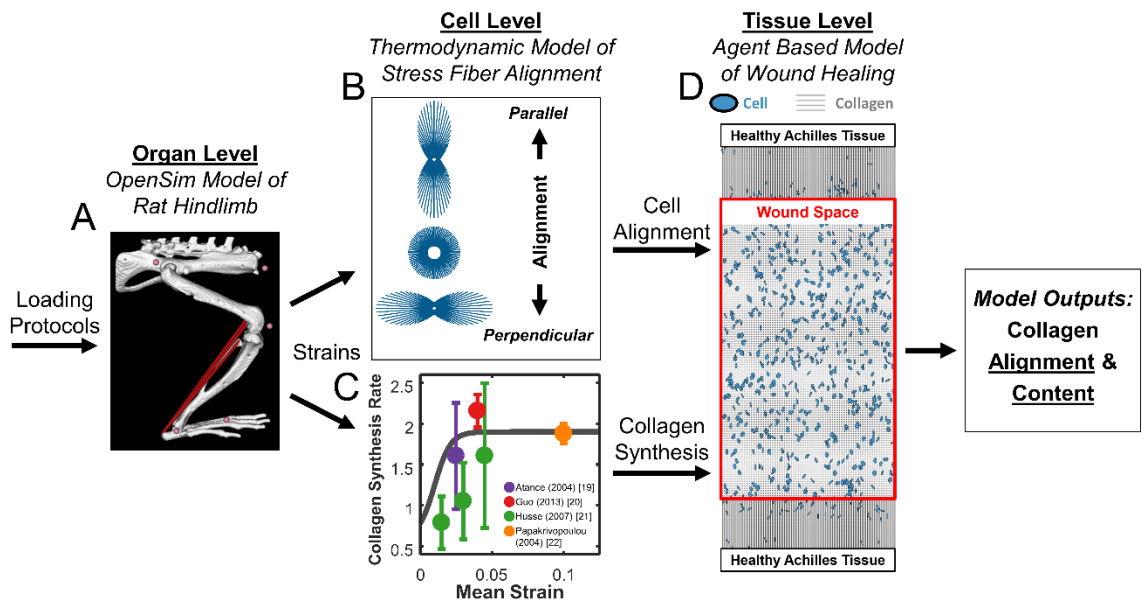


Figure 5.1

Flowchart depicting multiscale model. (A) OpenSim model of rat hindlimb adapted from Johnson 2008 (Johnson et al. 2008) simulates strains in the injured Achilles tendon. (B) Cell model predicts alignment based on the mechanical environment. (C) Fitted mean strain versus collagen I production curve (grey line) from four independent studies governs collagen production. (D) Agent-based model (ABM) of wound healing integrates migration, alignment, and collagen deposition by cells (blue) to predict scar collagen content and alignment (grey).

that met our search criteria (Eliasson, Andersson, and Aspenberg 2009; Eliasson, Andersson, and Aspenberg 2012a; Andersson et al. 2012; Andersson, Eliasson, and Aspenberg 2009; Tuzuner et al. 2013; Freedman et al. 2016; Schizas et al. 2010; Freedman et al. 2013; Freedman, Salka, et al. 2017; Freedman, Fryhofer, et al. 2017). We used cross sectional area (CSA) of the tendon as a surrogate measure for collagen production, based on previous studies showing that collagen concentration and tendon CSA rise in parallel (Woo et al. 1980; Eliasson, Andersson, and Aspenberg 2009; Buchanan and Marsh 2002), as well as the fact that tissue mass increases with tissue volume. Similarly, we used the Young's Modulus as a surrogate measure for collagen alignment based on the strong reported correlation between measured alignment and intrinsic material properties of the tissue (Freedman et al. 2013; Thomopoulos, Williams, and Soslowsky 2003), and the fact that Young's modulus was commonly measured in the studies we found while collagen alignment was not.

5.2.2 OpenSim Simulations and Strains

We adapted a previously published rat right hindlimb model to conduct our simulations (Fig 5.1A) (Johnson et al. 2008) (https://simtk.org/projects/rat_hlimb_model). Briefly, the model used anatomically accurate representations of the bones (spine, hip, femur, tibia, and foot), joints, and musculo-tendon units (each represented by one line segment from its origin to insertion) of the rat right hindlimb. Musculo-tendon units were represented as linear elements consisting of a muscle segment in series with a passive tendon segment. The muscle segment

consisted of its own passive element in parallel with an active contractile element that generated force depending on a Hill-type model. The mechanical properties of muscle fiber and tendon were defined using fiber force-length, fiber force-velocity, and tendon force-strain curves determined by Millard et al. (Millard et al. 2013). Muscle segments could be prescribed activation levels varying from 0 (rest) to 1 (full activation). Since muscles not attached to the Achilles tendon were irrelevant for this simulation, we simplified the model by only including the lateral and medial gastrocnemius and soleus muscles, the three musculo-tendon units that comprise the Achilles tendon. To predict Achilles tendon strains for the various cases simulated here, we prescribed experimentally measured joint angle profiles, muscle activation curves, and tendon mechanical properties as inputs, and obtained strain vs. time curves from forward dynamic simulations using custom MATLAB routines employed by two of the authors in a previous publication (Hu et al. 2017).

Passive tendon properties. To estimate physiologic strains for a ruptured tendon, we had to prescribe tendon parameters that reflected the early stages of healing. First, we decreased the slope of the linear portion of the tendon stress-strain curve by a factor of 5x, mimicking the decrease in material properties from a healthy tendon (~175 MPa) to an initial callus (~30 MPa) (Eliasson, Andersson, and Aspenberg 2009). Next, we mathematically estimated tendon slack length (TSL) values using a previously published numerical optimization algorithm (Manal and Buchanan 2004) that has also been previously utilized by two of the authors (Hu

et al. 2017) and by Charles et al. (Charles et al. 2016). The TSL is a value that represents the length at which the tendon begins to develop passive elastic force but is difficult to directly measure experimentally. Since the TSL must be a constant value for each tendon, if we know the optimal fiber length, the musculo-tendon lengths, and the normalized fiber lengths across a physiologic range of joint angles, we can numerically converge upon one TSL estimate using this algorithm. We used the calculated TSL values for our suture repaired tendons, since we assumed that suturing the two tendon stumps back together would form a ~0mm gap distance. In non-repaired tendons, we simulated the presence of a gap distance between the stumps by adding 7mm to each calculated TSL value, effectively shifting its reference (undeformed) length by 7mm. We used a gap distance of 7mm based on 3 separate studies that excised a 3mm section of the Achilles tendon and measured the gap distance between the stumps following excision to be ~10mm (Eliasson, Andersson, and Aspenberg 2012a; Eliasson, Andersson, and Aspenberg 2012b; Andersson, Eliasson, and Aspenberg 2009).

Prescribing loading and unloading using forward dynamic simulations. We categorized both free cage activity and treadmill exercise as loading conditions, since treadmill exercise conditions consisted of 23 hours of free cage activity + 1 hour of treadmill exercise prescribed at normal rat walking speeds (Freedman et al. 2016; Garnier, Falempin, and Canu 2009). We simulated loading by prescribing joint kinematics associated with the daily locomotion of a rat during a gait cycle. We used healthy knee and hip joint angles measured by Garnier et al. (Garnier, Falempin, and Canu 2009), as well as injured ankle joint angle data measured by

Liang et al. (Liang et al. 2012), who measured ankle motion following Achilles injury in both non-repaired and suture-repaired cases (Fig 5.2A). We limited the degrees of freedom of each joint to the sagittal plane, matching the plane of motion in the experimental flexion/extension data. All other available joints (e.g. ankle adduction/abduction, hip internal/external rotation, etc.) were held constant at the original rat hindlimb model angles determined for a healthy rat by Johnson 2008 (Johnson et al. 2008). We used stance and swing phases that comprised 75% and 25% of the total gait cycle (Garnier, Falempin, and Canu 2009), respectively. Based on studies conducted by Nicolopoulos-Stournaras et al. (Nicolopoulos-Stournaras and Iles 1984), we prescribed a maximum activation value of 1 to all three musculo-tendon units during the stance phases and minimum activation of 0.05 during the swing phases. Figure 5.2B shows the model at multiple phases of the gait cycle. For unloading conditions, we assumed that intramuscular botox injection, tail suspension, or cast immobilization of the tendon would leave the rats unable to move their knee and ankle on the injured side and unable to activate any of the muscles connected to the Achilles. With these assumptions, we fixed the knee joint at -50° flexion and the ankle at -30° plantar flexion (Schizas et al. 2010; Freedman et al. 2016), with all other joints held at original model angles. We prescribed a constant minimal muscle activation value of 0.05 to avoid numerical singularity in the muscle model when activation approaches 0 (Millard et al. 2013).

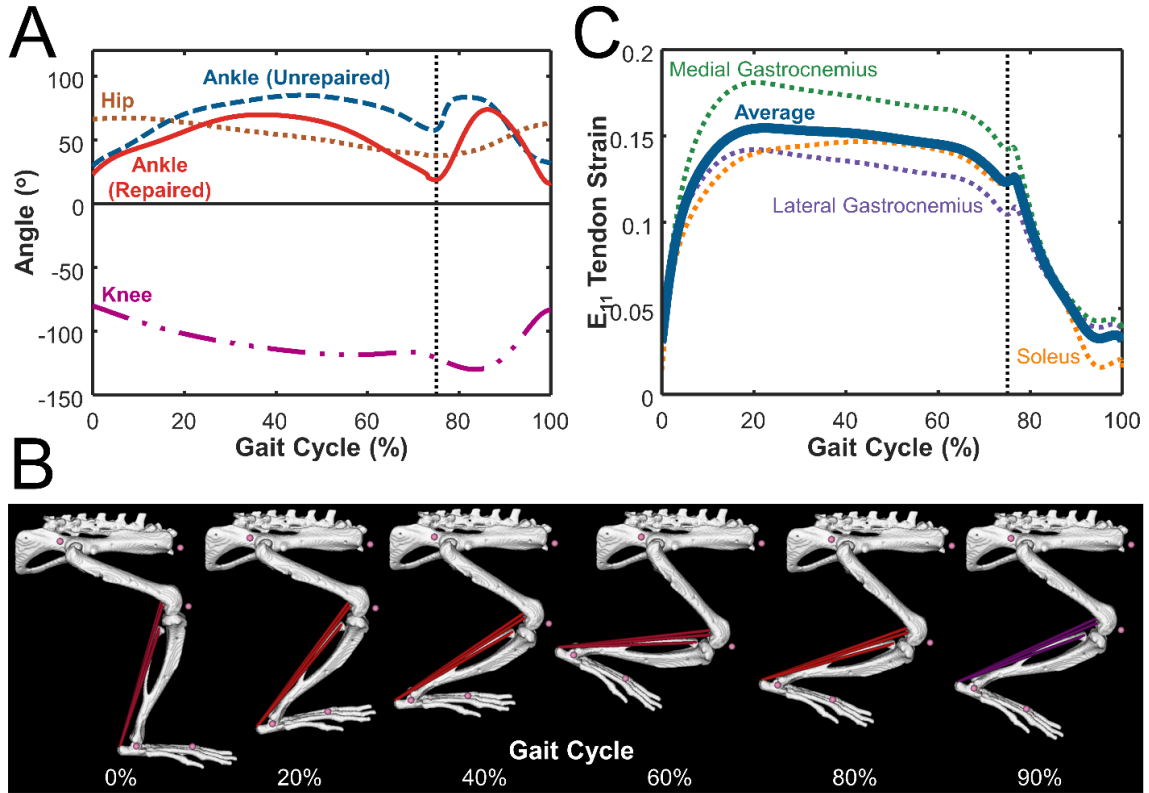


Figure 5.2

Rat Hindlimb Model implemented in OpenSim used joint angles, muscle activation, and passive tendon properties as inputs to determine tendon strains. (A) Hip (**brown**) and knee (**magenta**) angle data from healthy rat gait measured by Garnier et al. (Garnier, Falempin, and Canu 2009) and ankle angle data measured by Liang et al. (Liang et al. 2012) in both unrepaired (**blue**) and suture-repaired (**red**) tendons. Black dashed line separates stance phase (first 75%) from swing phase (last 25%). **(B)** Depiction of model motion during the prescribed gait cycle. The color of the muscle fiber depicts the activation during that part of the gait cycle, ranging from maximum activation (1, red) to minimum activation (0, blue). Purple fibers (shown during the swing phase at 90%) depict the transition from maximum to minimum activation. **(C)** Final tendon strain output was calculated by taking the average (**thick blue**) of tendon strains in the lateral (**purple**) and medial (**green**) gastrocnemius and soleus (**orange**) musculo-tendon units.

Outputs. We used the model-predicted changes in tendon lengths over time to calculate tendon strains as $(\text{tendon length} - \text{tendon slack length}) / (\text{tendon slack length})$. We calculated the strains over time for each of the tendon segments and averaged them to determine the final tendon strain (Fig 5.2C).

5.2.3 Thermodynamic Computational Model of Cell Alignment

We used a computational model of stress fiber remodeling published previously by our group to estimate cell alignment behavior (Chen et al. 2018) (Fig 5.1B). The model represents the thermodynamics of stress fiber (SF) assembly and disassembly, capturing features such as the ability of tension to promote assembly by altering the free energy of bound actin subunits. Two specific features of the model are important for the predictions shown in this manuscript. First, on the time scale of individual loading cycles, large negative strain rates reduce stress fiber tension through the force-velocity behavior of myosin, promoting SF disassembly in the direction of stretch and net SF (and cell) orientation perpendicular to that stretch. On a longer time scale, the model assumes that cells can remodel the extracellular matrix and/or their attachments to the ECM to attain an equilibrium strain state that minimizes the sum of the energies associated with elastic stretch and the chemical potential of the bound and unbound actin subunits. This aspect of the model drives the response to mean boundary conditions, upon which cyclic responses are then superimposed. Here, we used the average and spread of predicted SF distributions as surrogate measures of cell alignment, the same approach we used in the original model validation against *in vitro* data. For a more

complete description of the model and details on its validation, please see Chapter 3 and Chen et al. 2018 (Chen et al. 2018).

Integration of cell alignment model into the multiscale model. We used a uniaxial stretch boundary condition in all cellular simulations, prescribing stretch (or constraint, in the unloaded case) in one direction (x_1) while the transverse direction remained free (x_2). We estimated the strains experienced by individual cells as 0.28 times the tissue-level tendon strains computed in OpenSim. This empirically determined correction factor accounts for two effects we expect to reduce actual cell strains below the tissue strains we calculated here. First, in many tissues the surrounding matrix partially shields cells from strain; for example, Screen et al. (Screen et al. 2003) stretched rat tail tendons and observed cell nuclei strain to be about half of the imposed tendon strains. Second, due to lack of data on the actual magnitude of muscle activation during the rat gait cycle, we prescribed maximum (=1) activation to the muscle during stance phases in the rat hindlimb model (Nicolopoulos-Stournaras and Iles 1984). In reality, it seems improbable that these muscles are maximally activating during the normal gait cycle. We then used the maximum and minimum estimated cellular E_{11} and frequency of stretch as inputs to calculate the alignment of stress fibers within the cell. We devised a hypothetical loading profile to simulate a rat walking around its cage freely, alternating 1-hour periods of 1Hz walking with 1-hour rest periods for 12 hours of waking, followed by 12 hours of no activity to simulate sleep, consistent with the 12h/12h light/dark cycles employed by almost all rat studies used for

comparisons. In a typical rat gait cycle, injured rats walk with a gait cycle time of around 700ms (Liang et al. 2012), which corresponds to a stretch frequency between 1Hz and 2Hz; we chose the lower boundary of 1Hz. All other parameters in the cell alignment model remained unchanged from Chen et al. (Chen et al. 2018), and the model generated a predicted stress fiber orientation distribution for each strain state simulated. In order to quantitatively compare these stress fiber distributions, we used an order parameter (Chen et al. 2018; Hsu et al. 2010; Jungbauer et al. 2008):

$$S = \langle \cos 2\theta \rangle = \int h(\theta) \cos(2\theta) d\theta, \quad (1)$$

where $h(\theta)$ represents the probability distribution histogram of SFs in each angular bin. S ranges from $S = 1$, all cells or stress fibers aligned completely parallel to the stretch (x_1) direction, to $S = -1$, all cells or fibers aligned completely perpendicular to stretch, with $S = 0$ representing completely random alignment.

5.2.4 Agent Based Model of Achilles Tendon Wound Healing

We adapted an agent based model (ABM) originally published by Rouillard and Holmes (Rouillard and Holmes 2012; Rouillard and Holmes 2014) for infarct healing to integrate cellular-level responses and predict the evolving tendon scar structure (Fig 5.1D). Table 1 lists model parameters altered for these simulations, while Figure 5.3 shows a flowchart of a cell's decision tree within the model. Rouillard and Holmes modeled fibroblasts as circular discs free to move in a square, two-dimensional space divided into 10-micron-square patches. Each patch contained information about the local collagen alignment and density.

Fibroblasts could migrate, proliferate, undergo apoptosis, and remodel collagen. Fibroblast orientation guided fibroblast migration direction and deposition of collagen, and existing collagen fibers were degraded at a rate proportional to their local concentration. A local chemokine concentration gradient with a high concentration of chemokines within the wound area and a low chemokine concentration in the healthy tissue drove cell migration into the wound (Fig 5.4A). We made several modifications to this model to adapt it for Achilles tendon healing. We simulated healing of a rectangular wound area after complete transection or rupture (Fig 5.4B). The initial wound size, matrix structure, and collagen content within the wound depended on the healing condition (Table 1). A non-repaired transected tendon contained a low amount (0.1%) of randomly aligned collagen fibers, mimicking the randomly aligned provisional matrix in the wound area, while a suture-repaired tendon contained some aligned collagen (0.9%, alignment order parameter of 0.4), mimicking aligned collagen fibers from the healthy tendon stumps. Fibroblasts migrated into the wound space (Fig 5.4B,C,D) from the two opposing sides adjacent to healthy tissue. Rouillard determined cell alignment from a series of phenomenologic equations that represented the alignment response to stretch, contact guidance from surrounding collagen, and chemokine gradients, as well as their integration. Here, we replaced the original phenomenologic relationship governing stretch-induced alignment with the cell alignment predicted from the stress fiber model, and employed a more recent equation for integrating across the alignment cues published by Richardson et al. (Richardson et al. 2018).

Initial Wound	Value	Units
Width	1	mm
Length	0.5 (Repaired) 7 (Unrepaired)	mm
Collagen Fiber Area Fraction	0.001 (Unrepaired) 0.009 (Repaired)	
Collagen Fiber Alignment	0 (Unrepaired) 0.4 (Repaired)	MVL
Collagen	Value	Units
Collagen Synthesis	See Fig. 5.1C	collagen amount (arb.) per cell
Collagen Degradation	0.0025	h ⁻¹
Collagen Element Size	10x10	μm ²
Cell	Value	Units
Cell Radius	5	μm
Cell Initial Density	500	cells/mm ²
Time to apoptosis	240	hours
Time to mitosis	12 (quiescent) 240 (activated)	hours
Cell Speed	1 (quiescent) 50 (activated)	μm h ⁻¹

Table 1

Parameters used in ABM that differed from the ones initially employed by Rouillard and Holmes (Rouillard and Holmes 2012).

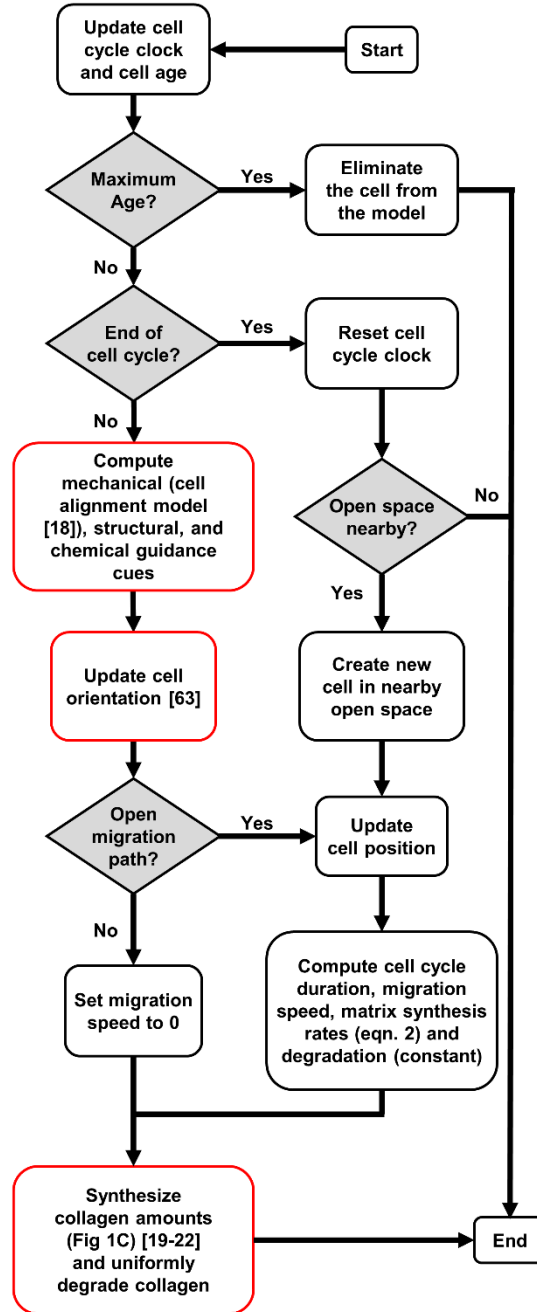


Figure 5.3

Flowchart adapted from Rouillard and Holmes (Rouillard and Holmes 2012) depicting the various decisions cells made in the agent-based model. Red bubbles indicate modifications introduced in the current study.

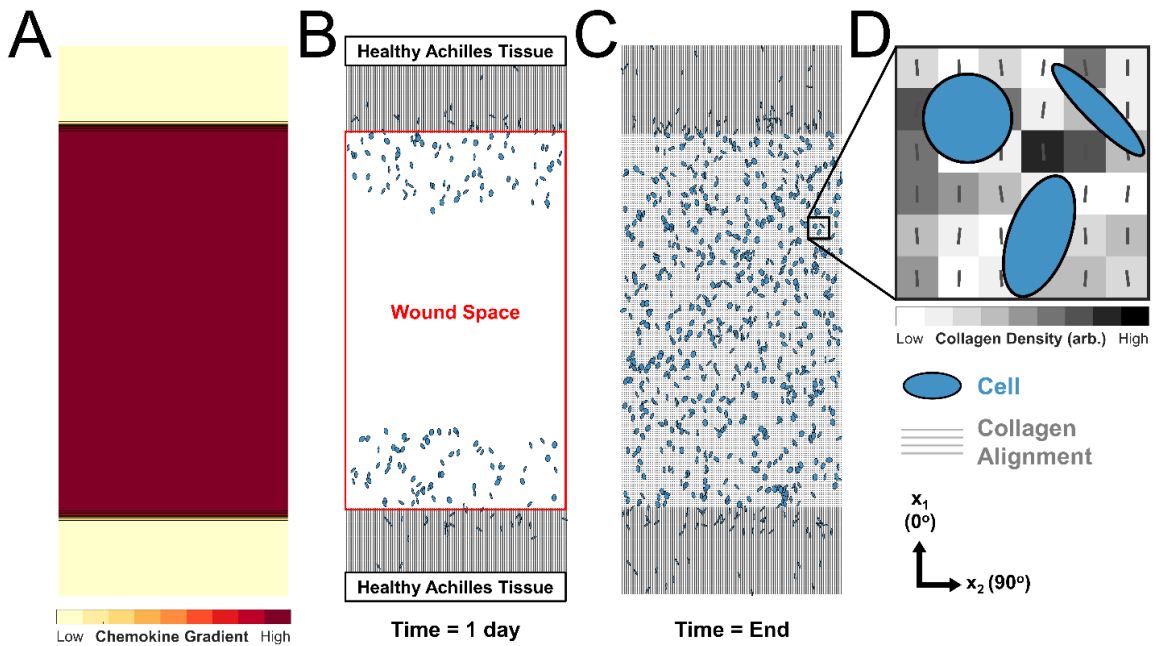


Figure 5.4

Schematic of the agent-based model of wound healing in the injured rat Achilles tendon. (A) Chemokine difference between the wound space and surrounding tissue drives cell migration into the wound. (B) Healthy Achilles tendon adjacent to the top and bottom of the wound space was comprised of fibroblasts (blue ovals) and highly aligned collagen (grey). The wound space was initially cell-free. (C) Cells migrated, proliferated, and synthesized and deposited collagen to create scar tissue within the wound area. (D) Magnification of the boxed area in (C) shows that the cells have different alignments and shapes determined by the cell alignment model and interact with $10\mu\text{m} \times 10\mu\text{m}$ collagen patches (grey boxes). Each patch stored information on local collagen density (grayscale tone) and collagen alignment (lines). Cell sizes have been increased for visibility in this schematic.

Based on previous studies showing that cells upregulate collagen production after exposure to both static (Lee et al. 1999) and cyclic stretch (Galatz et al. 2006; Magnusson, Langberg, and Kjaer 2010; Sullivan et al. 2009; Miller et al. 2005), cells synthesized collagen according to their mean strains, with higher strains corresponding to higher collagen synthesis rates. The mean strain was calculated by taking an average over one gait cycle period (1 second). In unloaded cases, this mean strain matched the static strain values. We determined the collagen synthesis amounts according to a sigmoidal curve fitted to data from four independent experiments in the literature (Fig 5.1C) (Galatz et al. 2006; Magnusson, Langberg, and Kjaer 2010; Sullivan et al. 2009; Miller et al. 2005):

$$CollagenSynthesis(\varepsilon_m) = \frac{1.3}{1 + \exp\left(-150\left(\frac{\varepsilon_m}{2} - 0.02\right)\right)} + 0.6 \quad (2)$$

Where ε_m is the mean strain felt by the cell. Cells deposited collagen aligned to their major axis of alignment. While the exact mechanisms by which fibroblasts deposit and orient collagen *in vivo* are still being debated, the general idea that collagen ends up locally aligned with the fibroblasts that deposit it remains strongly supported in the literature (Canty et al. 2004; Canty and Kadler 2005; Paten et al. 2016). At each time point for which collagen content and orientation are reported, the local collagen content and orientation histograms from each collagen patch were averaged to determine a single area fraction, mean angle, and order parameter for the entire scar region.

5.3 Results and Discussion

5.3.1 Effect of Unloading and Loading on Unrepaired Achilles Tendons

We searched the literature for studies of transected Achilles tendons in rats, the most common animal model used to mimic an Achilles tendon rupture. These studies used a variety of time courses and mechanical loading protocols to treat the rats during the wound healing process. First, we focused on studies that tested the effects of natural healing of unrepaired, transected tendons and imposed unloading by either botulinum toxin (Botox) injection into the gastrocnemius muscle or tail suspension (Eliasson, Andersson, and Aspenberg 2009; Eliasson, Andersson, and Aspenberg 2012a; Andersson et al. 2012; Andersson, Eliasson, and Aspenberg 2009) or loading by allowing the rat to freely walk around its cage (Andersson, Eliasson, and Aspenberg 2009; Schizas et al. 2010; Hammerman et al. 2015; Blomgran et al. 2016) (Fig 5.5A). Because no studies quantified both collagen alignment and total collagen mass, we then narrowed our search to include only studies that reported at least one of two quantitative measures that could act as surrogates for model comparisons. Based on the strong reported correlation between measured collagen alignment and intrinsic material properties of the tissue (Freedman et al. 2013; Thomopoulos, Williams, and Soslowsky 2003), we compared measured values of Young's Modulus (E_y in MPa) to the levels of collagen alignment predicted by our model.

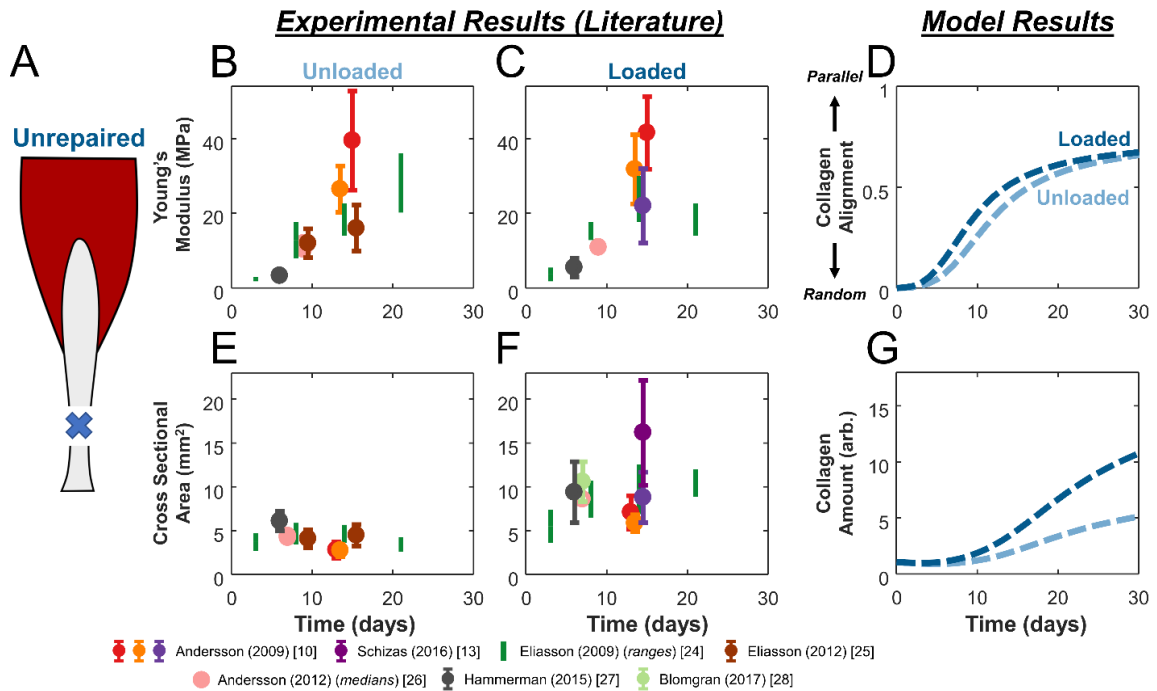


Figure 5.5

Model predictions of collagen alignment and content match trends in tissue-level properties reported in the literature during healing of unrepaired tendons. (A) Schematic of rat Achilles tendon transection injuries left to heal naturally. **(B,C,E,F)** We plotted data from studies (various colors) in which tendons healed unloaded **(B,E)** or loaded **(C,F)**. We compared our predictions of collagen alignment **(D)** and content **(G)** to experimentally measured Young's Moduli **(B,C)** and cross-sectional areas **(E,F)**, see text for details.

Similarly, based on previous studies showing that collagen concentration and tendon CSA rise in parallel (Woo et al. 1980; Eliasson, Andersson, and Aspenberg 2009; Buchanan and Marsh 2002), as well as the fact that tissue mass increases with tissue volume, we compared measured values of tendon cross-sectional area (CSA in mm^2) to the total collagen content predicted by the model. Despite considerable variability among the reported values of these metrics, two clear trends were apparent in the data. First, E_y started near 0 MPa at 3 days and rose to about 20-40 MPa at 14 days in both unloaded and loaded conditions (Fig 5.5B,C). Second, CSA values in unloaded conditions remained at around 5 mm^2 (Fig 5.5E), while loading increased CSA over time to around 10-20 mm^2 at day 14 (Fig 5.5F).

Next, we used the model of the rat hindlimb implemented in OpenSim (Johnson et al. 2008) to simulate these unloading and loading conditions and estimate strains in the healing region. We simulated unloading by fixing all joint ankles in plantar flexion, with minimum muscle activation and a 7mm gap distance between the tendon stumps (Eliasson, Andersson, and Aspenberg 2012a; Eliasson, Andersson, and Aspenberg 2012b; Andersson, Eliasson, and Aspenberg 2009), resulting in a predicted constant cell strain of $E_{11} = 0.002$ in the primary loading direction (Fig 5.6A). We simulated loading by prescribing joint angles and muscle activation corresponding to the rat gait cycle. Predicted strains oscillated between .009 and .043, reflecting the swing/stance phases of the gait cycle and yielding a

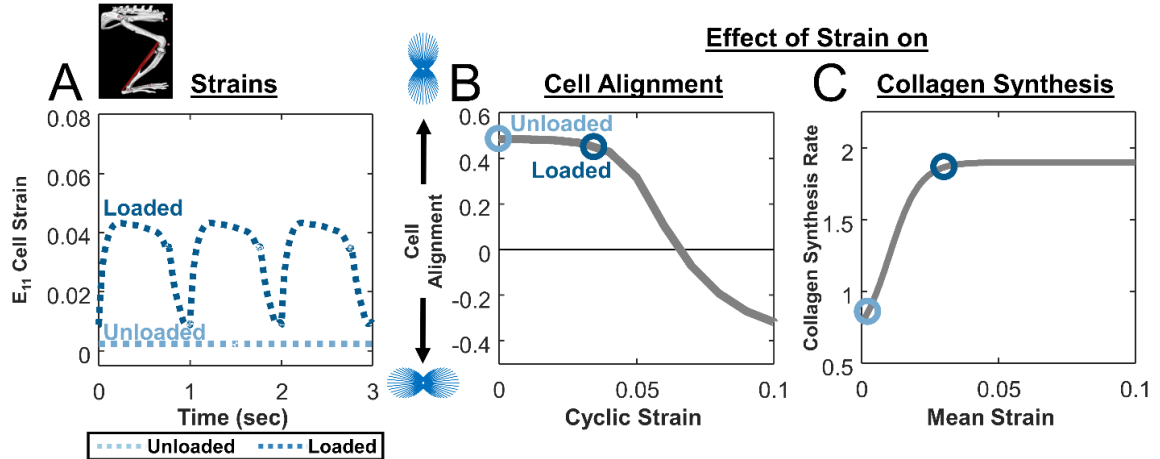


Figure 5.6

Effect of strain on cellular alignment and collagen synthesis. (A) Estimated cellular strain profiles derived from tendon strain profiles predicted by modified rat hindlimb model. **(B)** Cellular alignment response curve generated by model of stress fiber dynamics in response to cyclic stretching at various magnitudes and a frequency of 1 Hz with a 1h on, 1h off repeating cycle during waking hours (**gray line**); open circles show the operating points on this curve for simulated unloading (**light blue circle**) and loading conditions (**dark blue circle**) in unrepaired tendons. **(C)** Response curve showing the effect of mean strain on fibroblast collagen synthesis rate (**gray line**), again overlaid with circles showing the operating points for the specific cases simulated in Figure 5.5.

cyclic strain amplitude of 0.034 and a mean strain of 0.030 (Fig 5.6A). Using our published model of stress fiber dynamics (Chen et al. 2018), both strain states produced cell alignment along the loading axis, with slightly lower predicted alignment for the loaded case (Fig 5.6B). Using the collagen synthesis curve we fitted to published data (Galatz et al. 2006; Magnusson, Langberg, and Kjaer 2010; Sullivan et al. 2009; Miller et al. 2005), mean strain from the loaded case was associated with about 2x greater collagen production than the mean strain from the unloaded case (Fig 5.6C).

Integrating these two cellular behaviors in the ABM component, the multiscale model predicted that the specific loading protocols we simulated should produce little difference in collagen alignment (Fig 5.5D) but a substantial difference in collagen content (Fig 5.5G). Trends in predicted alignment agreed with literature reports showing similar E_y for both groups at all time points (Fig 5.5B,C). Furthermore, differences in model-predicted collagen accumulation in the two loading states qualitatively matched reported differences of the tendon CSA in loaded (Fig 5.5F) compared to unloaded (Fig 5.5E) conditions.

5.3.2 Effect of Unloading and Loading on Surgically Repaired Achilles

Tendons

In our next set of simulations, we explored how surgically repairing rat Achilles tendons would alter our predictions and the response to loading during healing (Fig 5.7A). We selected a set of studies that subjected experimental groups to either

unloading with cast immobilization or loading with an exercise protocol, defined as 60 min/day treadmill exercise + free cage activity for the rest of the time, compared surgically repaired and unrepaired groups, and reported Young's Modulus or cross-sectional area (Fig 5.7B,D) (Schizas et al. 2010; Freedman et al. 2016; Freedman, Salka, et al. 2017). For the unrepaired groups in this second set of studies, trends were similar to those shown in Figure 5.5, with loading enhancing CSA but not E_y . Similar to the unrepaired groups, loading of suture-repaired tendons increased tendon CSA compared to unloading (Fig 5.7D). However, loading in the suture-repaired groups surprisingly reduced Young's modulus below the values observed in any other group by the 42-day final time point (Fig 5.7B).

Assuming that surgical repair eliminated the gap distance between the tendon stumps, our hindlimb simulations in OpenSim predicted higher strains for repaired conditions compared to unrepaired, with repaired-unloaded tendons experiencing a static strain of $E_{11} = 0.012$ and repaired-loaded tendons oscillating between 0.011 and 0.075 (cyclic strain of 0.064, mean strain of 0.049; Fig. 5.8A). The much larger cyclic strains in the repaired-loaded group induced stress fiber disassembly along the loading axis in the cell alignment model, resulting in cells that were nearly randomly oriented (Fig 5.8B); the differences in predicted stress fiber orientation distributions for these four cases are shown in Figure 5.9. On the other hand, the large mean strains in the repaired-loaded group led to a higher rate of collagen synthesis in this group compared to the other conditions simulated (Fig 5.8C).

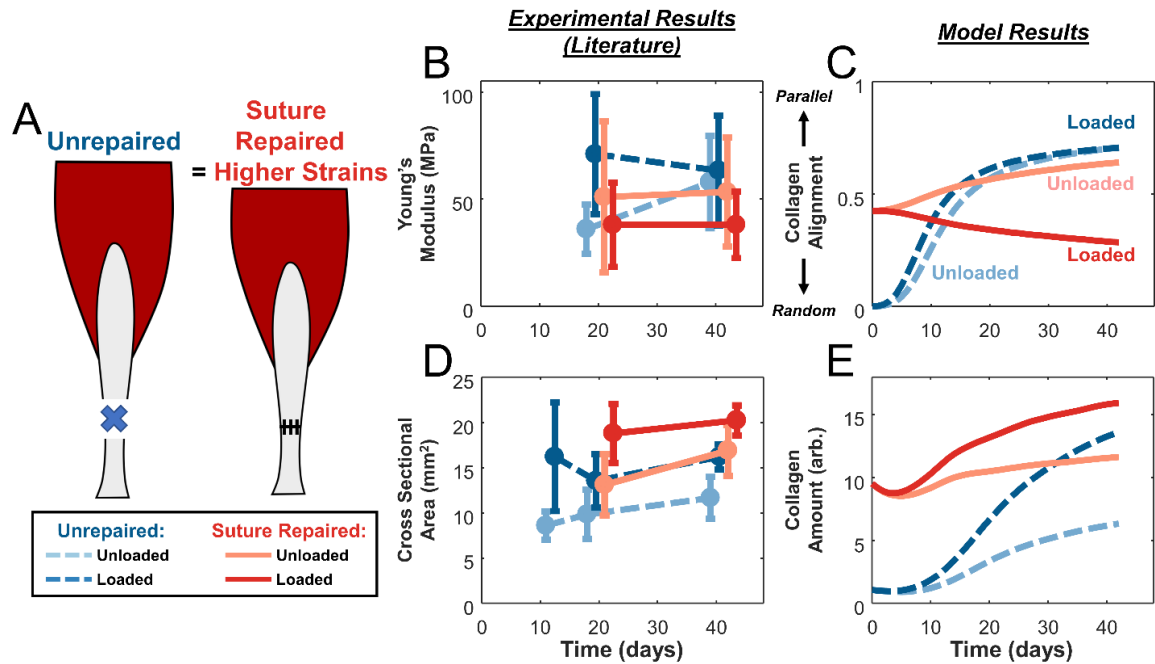


Figure 5.7

Model predictions of the effects of loading in unrepaired versus suture-repaired tendons also match experimentally observed tissue-level measures. (A) Schematic of rat Achilles tendon transection injuries left unrepaired or repaired with sutures. **(B,D)** Studies (Schizas et al. 2010; Freedman et al. 2016; Freedman, Salka, et al. 2017) that tested both unloading (**light color**) and loading (**dark color**) conditions in either unrepaired (**dashed blue lines**) or repaired (**solid red lines**) tendons showed a lower Young's modulus in the loaded, suture-repaired case and similar values in the other groups **(B)**, the same trend predicted for collagen alignment by the model **(C)**. Experimental data showed higher tendon cross-sectional area with loading regardless of repair status **(D)**, matching model predictions of total collagen **(E)**.

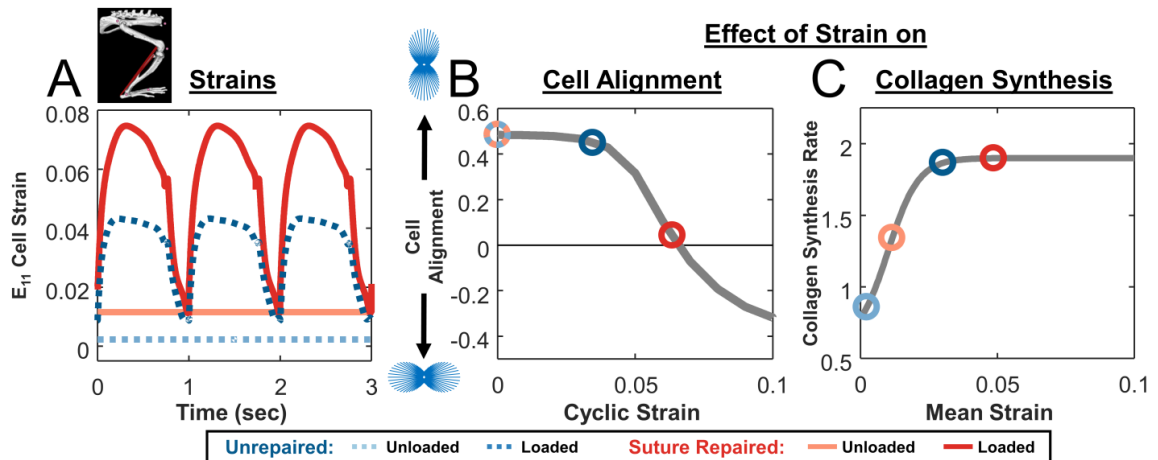


Figure 5.8

Cellular strain profiles and corresponding responses for simulations shown in Figure 5.7. (A) Estimated cellular strain profiles derived from tendon strain profiles predicted by hindlimb model in OpenSim. **(B)** Cellular alignment response curve generated by model of stress fiber dynamics (**gray line**, same as Figure 5.6) and operating points on that curve for unloading (**light color**) and loading (**dark color**) conditions in both unrepaired (**blue**) and suture-repaired (**red**) tendons. **(C)** Response curve showing the effect of mean strain on fibroblast collagen synthesis rate (**gray line**, same as Figure 5.6) and circles indicating the operating points for the different cases simulated.

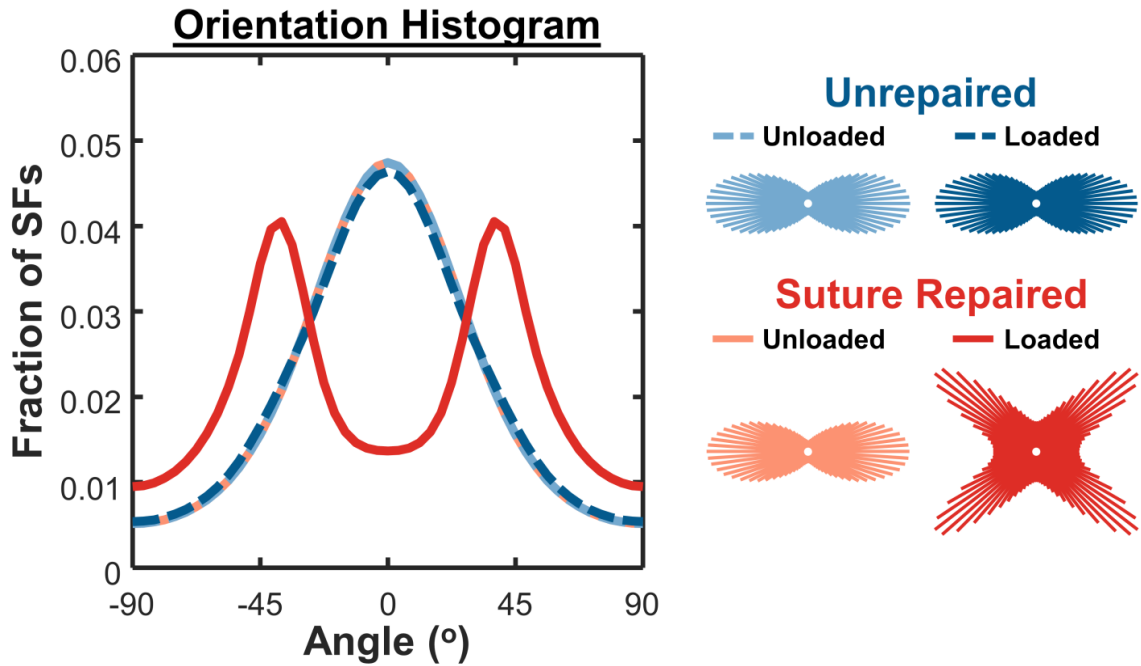


Figure 5.9

Angular histograms of cell stress fiber orientation from thermodynamic alignment model. Loaded, suture-repaired tendons exhibited lower cell alignment compared to other conditions. Insets underneath legend labels show corresponding circular histograms of SF orientation.

Integrating these predictions using the ABM component, overall our multiscale model correctly matched the apparently paradoxical reports that repaired, loaded tendons have the lowest collagen alignment of any of these four conditions (Fig 5.7B,C) despite having the highest collagen content (Fig 5.7D,E). In other words, a single set of cellular response curves can explain features of observed tendon healing across a wide array of reported experiments in rats without fitting model parameters to any data from those experiments. Rather, the key to the predictions in our multiscale model is simulating the specific loading and surgical protocols to predict tissue-level strains, which then guide cellular behaviors according to response curves based on *in vitro* experiments.

5.3.3 Effect of Intermittent Loading on Cell Alignment

Many of the studies we simulated here loaded healing tendons through unrestricted cage activity or through daily exercise added to normal cage activity. In these protocols, tendons are cyclically loaded in short bursts as the animals move about their cages, interspersed with short rest periods when they are standing still and longer rest periods when they sleep. We chose to model this situation by imposing cyclic loading at 1 Hz with a 1-hour on, 1-hour off protocol for 12 hours, followed by 12 hours of rest, and then repeating. To understand the effect of this choice on our results, we used the cell alignment model to simulate the effect of stretching with different protocols that all produced the same time-averaged frequency of 0.5Hz during a 24-hour period of wakefulness (Fig 5.10A).

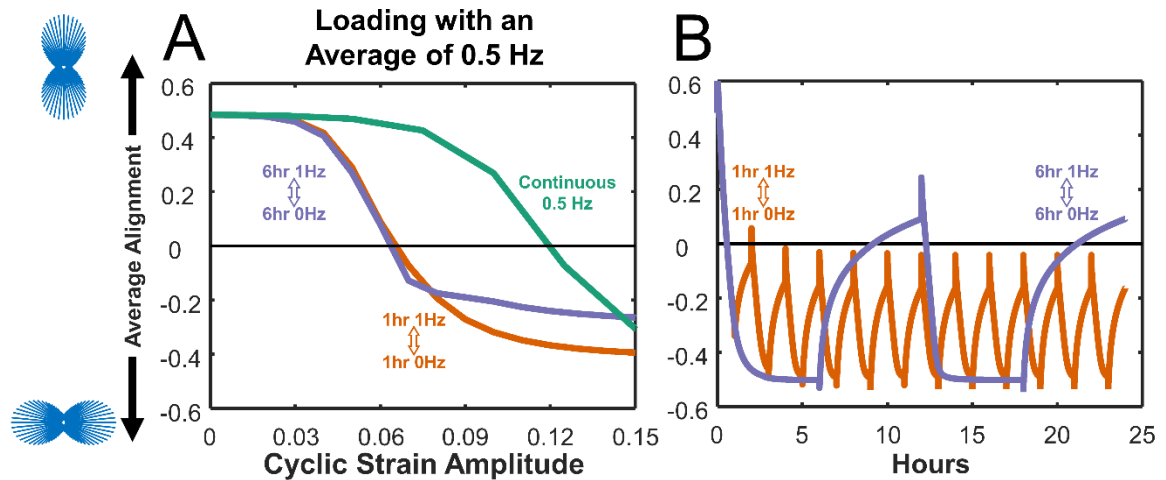


Figure 5.10

Identical average stretch frequencies result in varying cell alignment predictions using cell model. (A) Steady-state predicted alignment response curves for cells stretched in cycles of 6 hours at 1Hz followed by 6 hours of rest (0Hz) (**purple**), cycles of 1 hour at 1Hz followed by 1 hour of rest (**orange**), and continuous stretching at 0.5Hz (**green**). **(B)** Detailed time course of predicted alignment during 24 hours of intermittent stretch using two different duty cycles and a strain amplitude of 0.10. Each strain protocol was repeated until the difference in alignment at the end of each repetition was less than 0.01.

We compared stretching for repetitions of 6-hours at 1Hz followed by 6-hours of rest (0Hz), repetitions of 1-hour at 1Hz followed by 1-hour at rest, and continuous stretching for 24h at 0.5Hz. We simulated each repetition until steady state was reached, defined as the point when the difference in alignment at the end of two consecutive repetitions was less than 0.01 (5.10B). We found that the different stretching protocols produced different relationships between strain amplitude and predicted steady-state cell alignment, defined as the average order parameter over the last simulated cycle. At low strain amplitudes, all the protocols produced similar results, while at peak strains between 0.06 and 0.10 the three protocols resulted in predictions ranging from fairly strong alignment parallel to stretch (continuous stretching) to a modest degree of perpendicular alignment (1h on / 1h off and 6h on / 6h off). These differences arise from two features of the stress fiber model. First, stress fiber disassembly is triggered by high negative strain rates in the model, so much higher strains are required to influence alignment when loading is imposed at a lower frequency (Fig 5.10A). Second, because disassembly of stress fibers occurs on a much faster time scale than assembly, shorter durations of cyclic stretching can drive alignment down quickly, while much longer rest periods are needed to recover from each loading cycle (Fig 5.10B).

Our simulations of intermittent loading protocols raise the possibility that relatively minor differences in loading could have significant implications for fibroblast and collagen alignment. This could be an intriguing explanation for the surprising degree of variability we found in the literature among studies that employed

apparently identical experimental protocols and outcome metrics (see Fig. 5.5B,C,F), or even within groups in individual studies (see error bars in Fig. 5.7B,D). To date, most published experiments have not tracked movement of rats with the detail required to simulate more realistic or even animal-specific loading protocols. Sams-Dodd observed that healthy rats traveled around 5700 cm within a 10 minute observation period in one of the only studies we could find that attempted to track travel distances (Sams-Dodd 1995). Our simulations suggest that employing continuous movement tracking in future studies might provide additional insight into whether individual variability in activity and loading can explain some of the observed variability in tendon healing.

5.3.4 Limitations

The most serious limitation of the modeling studies reported here is that we were only able to validate them through qualitative comparisons of model-predicted trends to experimentally measured surrogates. The most novel prediction of our model was the degree of collagen fiber alignment. Experimentally, collagen alignment can be directly measured from ultrasound (Freedman et al. 2016; Riggins et al. 2014) or polarized microscopy (Fomovsky and Holmes 2010). However, these measurements were reported in so few studies that we were forced to use a more commonly reported surrogate, the Young's modulus (E_y), which has been shown to correlate with the degree of alignment. It is conceivable that other factors such as collagen density that might differ between the cases simulated here might have influenced E_y . Future studies may be able to draw on relationships between

alignment and modulus such as those reported by Lake et al. (Lake et al. 2009) and Li et al. (Li, Ogden, and Holzapfel 2018) to quantitatively estimate E_y . The comparison of total collagen content to tendon cross-sectional area (CSA) could also have limitations, since experimentally the rate of collagen production influences both collagen density (as assessed by biochemical assays or picrosirius red staining) and total CSA, but few studies provide data on both simultaneously. In addition, our collagen content predictions are in arbitrary units, since the studies we used to determine the effect of stretch on collagen synthesis reported relative changes rather than absolute synthesis rates.

The simplifications we made in the rat hindlimb model could also introduce some errors in the tendon-level strains we calculated. First, we included only the musculo-tendon units that directly comprise the Achilles tendon. Second, due to a lack of information in the literature about hip and knee motion during walking in the setting of rat Achilles tendon injury, we combined healthy hip and knee with injured ankle motion (Garnier, Falempin, and Canu 2009; Liang et al. 2012). However, we expect errors introduced by this choice to be small, since the gastrocnemius and soleus muscles do not cross the hip, the soleus does not cross the knee, and the moment arms around the ankle are larger than at the knee for the gastrocnemius. Furthermore, as long as simulated strains from repaired tendons are higher than unrepaired and strains from loading are higher than from unloading, the overall trends predicted from our model should be robust to small changes in the exact magnitude of the predicted tendon strains.

Our agent-based model assumes that cells deposit collagen aligned with their own axis, and this assumption was critical to translating cell alignment predictions from the cytoskeletal model into tissue-level predictions of collagen structure. While the exact mechanisms by which fibroblasts deposit and orient collagen *in vivo* are still being debated, the general idea that collagen ends up locally aligned with the fibroblasts that deposit it remains strongly supported in the literature (Canty et al. 2004; Canty and Kadler 2005; Paten et al. 2016). Furthermore, we have previously shown that agent-based models incorporating this same assumption correctly predict a range of scar structures observed following myocardial infarction in various animal models under different mechanical conditions (Rouillard and Holmes 2012). We also considered and simulated several other alternative methods of determining collagen alignment in the model but found that none could predict all the observed trends apparent in the data reviewed here. For instance, several experiments have theorized that surrounding collagen fibers could “structurally constrain” the formation of new fibers *in vivo* (Ruberti and Zieske 2008; Bhole et al. 2009; Giraud-Guille, Besseau, and Martin 2003). Others have demonstrated strain-dependent modulation of collagen degradation that could influence overall alignment under uniaxial loading by selectively degrading fibers with certain orientations faster than others (Wyatt, Bourne, and Torzilli 2009; Ruberti and Hallab 2005; Huang and Yannas 1977). While all these effects could be present within the actual tendon, we found that strain-dependent cell alignment, deposition of collagen aligned with the cells, and strain-dependent changes in

collagen synthesis rate were sufficient for capturing the major trends in the data as outlined above.

5.3.5 Conclusions

In this study, we used multiscale modeling to integrate information from the literature on fibroblast responses to stretch (alignment and collagen synthesis), scar formation following injury (collagen deposition and other features of the agent-based model), and musculoskeletal mechanics (rat hindlimb model implemented in OpenSim) to interpret apparently conflicting data from a range of experimental studies. We found that our computational model could reproduce several key features of observed tendon healing across a wide array of reported experiments in rats – including the paradoxical finding that repairing transected tendon reverses the effect of loading on alignment – without fitting model parameters to any data from those experiments. Rather, the key to the predictions in our multiscale model was simulating the specific loading and surgical protocols to predict tissue-level strains, which then guided cellular behaviors according to response curves based on *in vitro* experiments. These results suggest that the apparently conflicting data in the studies we reviewed may in fact reflect consistent biologic responses to local strains in the healing tendon, providing a new conceptual framework for interpreting existing data and devising potential therapies for Achilles tendon rupture.

5.4 References

- Andersson, Therese, Pernilla Eliasson, and Per Aspenberg. 2009. "Tissue Memory in Healing Tendons: Short Loading Episodes Stimulate Healing." *Journal of Applied Physiology (Bethesda, Md. : 1985)* 107 (2): 417–21. doi:10.1152/jappphysiol.00414.2009.
- Andersson, Therese, Pernilla Eliasson, Malin Hammerman, Olof Sandberg, and Per Aspenberg. 2012. "Low-Level Mechanical Stimulation Is Sufficient to Improve Tendon Healing in Rats." *Journal of Applied Physiology* 113 (9): 1398–1402. doi:10.1152/jappphysiol.00491.2012.
- Atance, Joel, Michael J. Yost, and Wayne Carver. 2004. "Influence of the Extracellular Matrix on the Regulation of Cardiac Fibroblast Behavior by Mechanical Stretch." *Journal of Cellular Physiology* 200 (3). Wiley-Blackwell: 377–86. doi:10.1002/jcp.20034.
- Bhole, A P, B P Flynn, M Liles, N Saeidi, C A Dimarzio, and J W Ruberti. 2009. "Mechanical Strain Enhances Survivability of Collagen Micronetworks in the Presence of Collagenase: Implications for Load-Bearing Matrix Growth and Stability." *Philosophical Transactions of the Royal Society A: Mathematical, Physical and Engineering Sciences* 367 (1902): 3339–62. doi:10.1098/rsta.2009.0093.
- Blomgran, Parmis, Robert Blomgran, Jan Ernerudh, and Per Aspenberg. 2016. "A Possible Link between Loading, Inflammation and Healing: Immune Cell Populations during Tendon Healing in the Rat." *Scientific Reports* 6 (1): 29824. doi:10.1038/srep29824.
- Buchanan, Cindy I., and Richard L. Marsh. 2002. "Effects of Exercise on the Biomechanical, Biochemical and Structural Properties of Tendons." *Comparative Biochemistry and Physiology Part A: Molecular & Integrative Physiology* 133 (4). Pergamon: 1101–7. doi:10.1016/S1095-6433(02)00139-3.
- Canty, Elizabeth G., Yinhui Lu, Roger S. Meadows, Michael K. Shaw, David F. Holmes, and Karl E. Kadler. 2004. "Coalignment of Plasma Membrane Channels and Protrusions (Fibropositors) Specifies the Parallelism of Tendon." *Journal of Cell Biology* 165 (4): 553–63. doi:10.1083/jcb.200312071.
- Canty, Elizabeth G, and Karl E Kadler. 2005. "Procollagen Trafficking, Processing and Fibrillogenesis." *Journal of Cell Science* 118 (Pt 7). The Company of Biologists Ltd: 1341–53. doi:10.1242/jcs.01731.
- Charles, James P., Ornella Cappellari, Andrew J. Spence, Dominic J. Wells, and John R. Hutchinson. 2016. "Muscle Moment Arms and Sensitivity Analysis of a Mouse Hindlimb Musculoskeletal Model." *Journal of Anatomy* 229 (4). Wiley/Blackwell (10.1111): 514–35. doi:10.1111/joa.12461.

- Chen, Kellen, Andrea Vigliotti, Mattia Bacca, Robert M. McMeeking, Vikram S. Deshpande, and Jeffrey W. Holmes. 2018. "Role of Boundary Conditions in Determining Cell Alignment in Response to Stretch." *Proceedings of the National Academy of Sciences* 115 (5). National Academy of Sciences: 986–91. doi:10.1073/pnas.1715059115.
- Delp, Scott L., Frank C. Anderson, Allison S. Arnold, Peter Loan, Ayman Habib, Chand T. John, Eran Guendelman, and Darryl G. Thelen. 2007. "OpenSim: Open-Source Software to Create and Analyze Dynamic Simulations of Movement." *IEEE Transactions on Biomedical Engineering* 54 (11): 1940–50. doi:10.1109/TBME.2007.901024.
- Eliasson, Pernilla, Therese Andersson, and Per Aspenberg. 2009. "Rat Achilles Tendon Healing: Mechanical Loading and Gene Expression." *Journal of Applied Physiology* 107 (2): 399–407. doi:10.1152/jappphysiol.91563.2008.
- . 2012a. "Influence of a Single Loading Episode on Gene Expression in Healing Rat Achilles Tendons." *Journal of Applied Physiology* 112 (2): 279–88. doi:10.1152/jappphysiol.00858.2011.
- . 2012b. "Achilles Tendon Healing in Rats Is Improved by Intermittent Mechanical Loading during the Inflammatory Phase." *Journal of Orthopaedic Research* 30 (2). Wiley Subscription Services, Inc., A Wiley Company: 274–79. doi:10.1002/jor.21511.
- Fomovsky, Gregory M., and Jeffrey W. Holmes. 2010. "Evolution of Scar Structure, Mechanics, and Ventricular Function after Myocardial Infarction in the Rat." *American Journal of Physiology. Heart and Circulatory Physiology* 298 (1): H221-8. doi:10.1152/ajpheart.00495.2009.
- Freedman, Benjamin R., George W. Fryhofer, Nabeel S. Salka, Harina A. Raja, Cody D. Hillin, Courtney A. Nuss, Daniel C. Farber, and Louis J. Soslowsky. 2017. "Mechanical, Histological, and Functional Properties Remain Inferior in Conservatively Treated Achilles Tendons in Rodents: Long Term Evaluation." *Journal of Biomechanics* 56. Elsevier Ltd: 55–60. doi:10.1016/j.jbiomech.2017.02.030.
- Freedman, Benjamin R., Joshua A. Gordon, Pankti R. Bhatt, Adam M. Pardes, Stephen J. Thomas, Joseph J. Sarver, Corinne N. Riggan, et al. 2016. "Nonsurgical Treatment and Early Return to Activity Leads to Improved Achilles Tendon Fatigue Mechanics and Functional Outcomes during Early Healing in an Animal Model." *Journal of Orthopaedic Research* 34 (12): 2172–80. doi:10.1002/jor.23253.
- Freedman, Benjamin R., Nabeel S. Salka, Tyler R. Morris, Pankti R. Bhatt, Adam M. Pardes, Joshua A. Gordon, Courtney A. Nuss, et al. 2017. "Temporal Healing of Achilles Tendons After Injury in Rodents Depends on Surgical Treatment and Activity." *Journal of the American Academy of Orthopaedic Surgeons* 25 (9): 635–47. doi:10.5435/JAAOS-D-16-00620.

- Freedman, Benjamin R, Joshua A Gordon, and Louis J Soslowsky. 2014. "The Achilles Tendon: Fundamental Properties and Mechanisms Governing Healing." *Muscles, Ligaments and Tendons Journal* 4 (2): 245–55. doi:10.11138/mltj/2014.4.2.245.
- Freedman, Benjamin R, Joseph J Sarver, Mark R Buckley, Pramod B Voleti, and Louis J Soslowsky. 2013. "Biomechanical and Structural Response of Healing Achilles Tendon to Fatigue Loading Following Acute Injury." *Journal of Biomechanics*, November. doi:10.1016/j.jbiomech.2013.10.054.
- Galatz, Leesa M., Linda J. Sandell, Stefan Y. Rothermich, Rosalina Das, Ava Mastny, Necat Havlioglu, Matthew J. Silva, and Stavros Thomopoulos. 2006. "Characteristics of the Rat Supraspinatus Tendon during Tendon-to-Bone Healing after Acute Injury." *Journal of Orthopaedic Research* 24 (3). Wiley Subscription Services, Inc., A Wiley Company: 541–50. doi:10.1002/jor.20067.
- Garnier, Cyril, Maurice Falempin, and Marie-Hélène Canu. 2009. "A 3D Analysis of Fore- and Hindlimb Motion during Overground and Ladder Walking: Comparison of Control and Unloaded Rats." *Experimental Neurology* 218 (1): 98–108. doi:10.1016/j.expneurol.2009.04.009.
- Giraud-Guille, Marie Madeleine, Laurence Besseau, and Raquel Martin. 2003. "Liquid Crystalline Assemblies of Collagen in Bone and in Vitro Systems." *Journal of Biomechanics* 36 (10): 1571–79. doi:10.1016/S0021-9290(03)00134-9.
- Guo, Yong, Qiang-cheng Zeng, Chun-qiu Zhang, Xi-zheng Zhang, Rui-xin Li, Jimin Wu, Jing Guan, et al. 2013. "Extracellular Matrix of Mechanically Stretched Cardiac Fibroblasts Improves Viability and Metabolic Activity of Ventricular Cells." *International Journal of Medical Sciences* 10 (13). Ivyspring International Publisher: 1837–45. doi:10.7150/ijms.6786.
- Hammerman, Malin, Parmis Blomgran, Sandra Ramstedt, and Per Aspenberg. 2015. "COX-2 Inhibition Impairs Mechanical Stimulation of Early Tendon Healing in Rats by Reducing the Response to Microdamage." *Journal of Applied Physiology* 119 (5). American Physiological Society Bethesda, MD: 534–40. doi:10.1152/japplphysiol.00239.2015.
- Hsu, Hui-Ju, Chin-Fu Lee, Andrea Locke, Susan Q. Vanderzyl, and Roland Kaunas. 2010. "Stretch-Induced Stress Fiber Remodeling and the Activations of JNK and ERK Depend on Mechanical Strain Rate, but Not FAK." Edited by Marc Vooijs. *PLoS ONE* 5 (8). Public Library of Science: e12470. doi:10.1371/journal.pone.0012470.
- Hu, Xiao, James P. Charles, Turgay Akay, John R. Hutchinson, and Silvia S. Blemker. 2017. "Are Mice Good Models for Human Neuromuscular Disease? Comparing Muscle Excursions in Walking between Mice and Humans." *Skeletal Muscle* 7 (1): 26. doi:10.1186/s13395-017-0143-9.

- Huang, C., and I. V. Yannas. 1977. "Mechanochemical Studies of Enzymatic Degradation of Insoluble Collagen Fibers." *Journal of Biomedical Materials Research* 11 (1): 137–54. doi:10.1002/jbm.820110113.
- Husse, Britta, Wilfried Briest, Lars Homagk, Gerrit Isenberg, and Michael Gekle. 2007. "Cyclical Mechanical Stretch Modulates Expression of Collagen I and Collagen III by PKC and Tyrosine Kinase in Cardiac Fibroblasts." *American Journal of Physiology-Regulatory, Integrative and Comparative Physiology* 293 (5). American Physiological Society: R1898–1907. doi:10.1152/ajpregu.00804.2006.
- Johnson, Will L., Devin L. Jindrich, Roland R. Roy, and V. Reggie Edgerton. 2008. "A Three-Dimensional Model of the Rat Hindlimb: Musculoskeletal Geometry and Muscle Moment Arms." *Journal of Biomechanics* 41 (3): 610–19. doi:10.1016/j.jbiomech.2007.10.004.
- Jozsa, L, M Kvist, BJ Balint, A Reffy, M Jarvinen, M. Lehto, and M. Barzo. 1989. "The Role of Recreational Sport Activity in Achilles Tendon Rupture." *The American Journal of Sports Medicine* 17 (3): 338–43. doi:10.1177/036354658901700305.
- Jungbauer, Simon, Huajian Gao, Joachim P. Spatz, and Ralf Kemkemer. 2008. "Two Characteristic Regimes in Frequency-Dependent Dynamic Reorientation of Fibroblasts on Cyclically Stretched Substrates." *Biophysical Journal* 95 (7): 3470–78. doi:10.1529/biophysj.107.128611.
- Kongsgaard, M, P Aagaard, M Kjaer, and S P Magnusson. 2005. "Structural Achilles Tendon Properties in Athletes Subjected to Different Exercise Modes and in Achilles Tendon Rupture Patients." *Journal of Applied Physiology* 99 (5): 1965–71. doi:10.1152/jappphysiol.00384.2005.
- Lake, Spencer P., Kristin S. Miller, Dawn M. Elliott, and Louis J. Soslowsky. 2009. "Effect of Fiber Distribution and Realignment on the Nonlinear and Inhomogeneous Mechanical Properties of Human Supraspinatus Tendon under Longitudinal Tensile Loading." *Journal of Orthopaedic Research* 27 (12). Wiley-Blackwell: 1596–1602. doi:10.1002/jor.20938.
- Lee, A A, T Delhaas, A D McCulloch, and F J Villarreal. 1999. "Differential Responses of Adult Cardiac Fibroblasts to in Vitro Biaxial Strain Patterns." *Journal of Molecular and Cellular Cardiology* 31 (10). Elsevier: 1833–43. doi:10.1006/jmcc.1999.1017.
- Li, Kewei, Ray W Ogden, and Gerhard A Holzapfel. 2018. "An Exponential Constitutive Model Excluding Fibres under Compression: Application to Extension–inflation of a Residually Stressed Carotid Artery." *Mathematics and Mechanics of Solids* 23 (8). SAGE PublicationsSage UK: London, England: 1206–24. doi:10.1177/1081286517712077.
- Liang, Jen-I, Meng-Yi Chen, Tsung-Hsun Hsieh, Chih-Yu Liu, Chen-Fuh Lam, Jia-

- Jin Jason Chen, and Ming-Long Yeh. 2012. "Video-Based Gait Analysis for Functional Evaluation of Healing Achilles Tendon in Rats." *Annals of Biomedical Engineering* 40 (12). Springer US: 2532–40. doi:10.1007/s10439-012-0619-z.
- Magnusson, S. Peter, Henning Langberg, and Michael Kjaer. 2010. "The Pathogenesis of Tendinopathy: Balancing the Response to Loading." *Nature Reviews Rheumatology* 6 (5). Nature Publishing Group: 262–68. doi:10.1038/nrrheum.2010.43.
- Manal, Kurt, and Thomas S. Buchanan. 2004. "Subject-Specific Estimates of Tendon Slack Length: A Numerical Method." *Journal of Applied Biomechanics* 20 (2): 195–203. doi:10.1123/jab.20.2.195.
- McCormack, R, and J Bovard. 2015. "Early Functional Rehabilitation or Cast Immobilisation for the Postoperative Management of Acute Achilles Tendon Rupture? A Systematic Review and Meta-Analysis of Randomised Controlled Trials." *British Journal of Sports Medicine* 49 (20): 1329–35. doi:10.1136/bjsports-2015-094935.
- Meier Bürgisser, Gabriella, Maurizio Calcagni, Elias Bachmann, Gion Fessel, Jess G Snedeker, Pietro Giovanoli, and Johanna Buschmann. 2016. "Rabbit Achilles Tendon Full Transection Model – Wound Healing, Adhesion Formation and Biomechanics at 3, 6 and 12 Weeks Post-Surgery." *Biology Open* 5 (9): 1324–33. doi:10.1242/bio.020644.
- Millard, Matthew, Thomas Uchida, Ajay Seth, and Scott L. Delp. 2013. "Flexing Computational Muscle: Modeling and Simulation of Musculotendon Dynamics." *Journal of Biomechanical Engineering* 135 (2): 021005. doi:10.1115/1.4023390.
- Miller, Benjamin F, Jens L Olesen, Mette Hansen, Simon Døssing, Regina M Cramer, Rasmus J Welling, Henning Langberg, et al. 2005. "Coordinated Collagen and Muscle Protein Synthesis in Human Patella Tendon and Quadriceps Muscle after Exercise." *J Physiol* 567 (3): 1021–33. doi:10.1113/jphysiol.2005.093690.
- Murrell, G A, E G Lilly, R D Goldner, A V Seaber, and T M Best. 1994. "Effects of Immobilization on Achilles Tendon Healing in a Rat Model." *Journal of Orthopaedic Research: Official Publication of the Orthopaedic Research Society* 12 (4): 582–91. doi:10.1002/jor.1100120415.
- Nicolopoulos-Stournaras, S., and J. F. Iles. 1984. "Hindlimb Muscle Activity during Locomotion in the Rat (*Rattus Norvegicus*) (Rodentia: Muridae)." *Journal of Zoology* 203 (3): 427–40. doi:10.1111/j.1469-7998.1984.tb02342.x.
- Olsson, N., K. Gravare Silbernagel, Bengt Eriksson, M. Sansone, A. Brorsson, K. Nilsson-Helander, and J. Karlsson. 2013. "Stable Surgical Repair with Accelerated Rehabilitation versus Nonsurgical Treatment for Acute Achilles

- Tendon Ruptures: A Randomized Controlled Study." *The American Journal of Sports Medicine* 41 (12): 2867–76. doi:10.1177/0363546513503282.
- Papakrivopoulou, J, Gisela E Lindahl, Jill E Bishop, and Geoffrey J Laurent. 2004. "Differential Roles of Extracellular Signal-Regulated Kinase 1/2 and P38MAPK in Mechanical Load-Induced Procollagen A1(I) Gene Expression in Cardiac Fibroblasts." *Cardiovascular Research* 61 (4). Oxford University Press: 736–44. doi:10.1016/j.cardiores.2003.12.018.
- Paten, Jeffrey A., Seyed Mohammad Siadat, Monica E. Susilo, Ebraheim N. Ismail, Jayson L. Stoner, Jonathan P. Rothstein, and Jeffrey W. Ruberti. 2016. "Flow-Induced Crystallization of Collagen: A Potentially Critical Mechanism in Early Tissue Formation." *ACS Nano* 10 (5). American Chemical Society: 5027–40. doi:10.1021/acsnano.5b07756.
- Richardson, William J., Brian Kegerreis, Stavros Thomopoulos, and Jeffrey W. Holmes. 2018. "Potential Strain-Dependent Mechanisms Defining Matrix Alignment in Healing Tendons." *Biomechanics and Modeling in Mechanobiology*, July. Springer Berlin Heidelberg, 1–12. doi:10.1007/s10237-018-1044-5.
- Riggin, Corinne N, Joseph J Sarver, Benjamin R Freedman, Stephen J Thomas, and Louis J Soslowsky. 2014. "Analysis of Collagen Organization in Mouse Achilles Tendon Using High-Frequency Ultrasound Imaging." *Journal of Biomechanical Engineering* 136 (2): 0210291-6. doi:10.1115/1.4026285.
- Rouillard, Andrew D., and Jeffrey W. Holmes. 2014. "Coupled Agent-Based and Finite-Element Models for Predicting Scar Structure Following Myocardial Infarction." *Progress in Biophysics and Molecular Biology* 115 (2–3). Elsevier Ltd: 235–43. doi:10.1016/j.pbiomolbio.2014.06.010.
- Rouillard, Andrew D, and Jeffrey W Holmes. 2012. "Mechanical Regulation of Fibroblast Migration and Collagen Remodelling in Healing Myocardial Infarcts." *The Journal of Physiology* 590 (Pt 18): 4585–4602. doi:10.1113/jphysiol.2012.229484.
- Ruberti, Jeffrey W., and Nadim J. Hallab. 2005. "Strain-Controlled Enzymatic Cleavage of Collagen in Loaded Matrix." *Biochemical and Biophysical Research Communications* 336 (2): 483–89. doi:10.1016/j.bbrc.2005.08.128.
- Ruberti, Jeffrey W., and James D. Zieske. 2008. "Prelude to Corneal Tissue Engineering - Gaining Control of Collagen Organization." *Progress in Retinal and Eye Research* 27 (5). Elsevier Ltd: 549–77. doi:10.1016/j.preteyeres.2008.08.001.
- Sams-Dodd, Frank. 1995. "Automation of the Social Interaction Test by a Video-Tracking System: Behavioural Effects of Repeated Phencyclidine Treatment." *Journal of Neuroscience Methods* 59 (2). Elsevier: 157–67. doi:10.1016/0165-0270(94)00173-E.

- Schizas, Nikos, Jian Li, Therese Andersson, Anna Fahlgren, Per Aspenberg, Mahmood Ahmed, and Paul W Ackermann. 2010. "Compression Therapy Promotes Proliferative Repair during Rat Achilles Tendon Immobilization." *Journal of Orthopaedic Research: Official Publication of the Orthopaedic Research Society* 28 (7): 852–58. doi:10.1002/jor.21066.
- Screen, H R, D A Lee, D L Bader, and J C Shelton. 2003. "Development of a Technique to Determine Strains in Tendons Using the Cell Nuclei." *Biorheology* 40 (1–3). IOS Press: 361–68. doi:10.1007/978-0-387-73906-9_8.
- Soslowsky, L.J., S. Thomopoulos, S. Tun, C.L. Flanagan, C.C. Keefer, J. Mastaw, and J.E. Carpenter. 2000. "Neer Award 1999: Overuse Activity Injures the Supraspinatus Tendon in an Animal Model: A Histologic and Biomechanical Study." *Journal of Shoulder and Elbow Surgery* 9 (2): 79–84. doi:10.1067/mse.2000.101962.
- Sullivan, Bridget E, Chad C Carroll, Bozena Jemiolo, Scott W Trappe, S Peter Magnusson, Simon Døssing, Michael Kjaer, and Todd A Trappe. 2009. "Effect of Acute Resistance Exercise and Sex on Human Patellar Tendon Structural and Regulatory mRNA Expression." *Journal of Applied Physiology (Bethesda, Md. : 1985)* 106 (2): 468–75. doi:10.1152/jappphysiol.91341.2008.
- Thomopoulos, S., G. R. Williams, and L. J. Soslowsky. 2003. "Tendon to Bone Healing: Differences in Biomechanical, Structural, and Compositional Properties Due to a Range of Activity Levels." *Journal of Biomechanical Engineering* 125 (1). American Society of Mechanical Engineers: 106–13. doi:10.1115/1.1536660.
- Tuzuner, Serdar, Ozlenen Ozkan, Nuray Erin, Sibel Ozkaynak, An Cinpolat, and Omer Ozkan. 2013. "Effects of Botulinum Toxin-A Injection on Healing and Tensile Strength of Ruptured Rabbit Achilles Tendons." *Annals of Plastic Surgery* 00 (00): 1–5. doi:10.1097/SAP.0b013e31829aa2e1.
- Twaddle, B. C., and P. Poon. 2007. "Early Motion for Achilles Tendon Ruptures: Is Surgery Important?: A Randomized, Prospective Study." *The American Journal of Sports Medicine* 35 (12): 2033–38. doi:10.1177/0363546507307503.
- Woo, S. L.-Y., M. A. Ritter, D. Amiel, T. M. Sanders, M. A. Gomez, S. C. Kuei, S. R. Garfin, and W. H. Akeson. 1980. "The Biomechanical and Biochemical Properties of Swine Tendons — Long Term Effects of Exercise on the Digital Extensors." *Connective Tissue Research* 7 (3). Taylor & Francis: 177–83. doi:10.3109/03008208009152109.
- Wyatt, Karla E-K, Jonathan W Bourne, and Peter A Torzilli. 2009. "Deformation-Dependent Enzyme Mechanokinetic Cleavage of Type I Collagen." *Journal of Biomechanical Engineering* 131 (5): 051004. doi:10.1115/1.3078177.

Chapter 6:

Summary and Final Conclusions

Motivation

Whether in a myocardial infarction, a tendon or ligament rupture, spinal-cord injury, or a burn wound, the wound healing process remains relatively similar across the body (Richardson et al. 2015; Gurtner et al. 2008), and we know that the structural and mechanical properties of the resultant scar tissue are critical in determining the overall function of the tissue. Within the heart, our lab has found that anisotropically reinforcing healing scar (stiffer longitudinally than circumferentially) can acutely improve cardiac output and pump function (Fomovsky et al. 2012; Fomovsky et al. 2011), leading us to believe that developing a longitudinally anisotropic scar could lead to better outcomes. For tendons and ligaments, we know that generating scar tissue comprised of highly aligned collagen fibers, similar to that in healthy tissue, will allow it to best maintain its original function. Fibroblasts align in response to their environment and synthesize, assemble, remodel, and cross-link collagen within the developing scar (Langberg et al. 1999; Layman, McGoodwin, and Martin 1971), mediating the development of scar mechanical properties. To fully uncover the principles governing scar structure formation, we must first understand how the mechanical environment affects fibroblast and collagen alignment.

The overall goal of this work was to develop predictive models of fibroblast alignment and scar formation during wound healing. The overall approach of this dissertation was to first develop a model of cell alignment and then utilize it to predict scar formation in the tendon. Improving our understanding of how

fibroblasts align and produce subsequent scar structures could give us better insights into how to optimize collagen alignment and scar anisotropy during wound healing.

Role of Boundary Conditions in Determining Cell

Alignment in Response to Stretch

Various studies have experimentally and computationally investigated the effects of the mechanical environment on cell alignment, and many others have studied how that alignment can determine collagen production to create various scar structures. In Chapter 2, we investigated current models of cell alignment and implemented the one that could seemingly capture alignment responses over a range of known conditions (Obbink-Huizer et al. 2014). This model used the theory of strain avoidance to drive its predictions of cell alignment, and we used our understanding of this model to design specific experimental conditions that would test the strain avoidance hypothesis. Next, in Chapter 3, we designed and developed a novel experimental setup to test those specific conditions. We loaded fibroblast-populated collagen hydrogels at various amplitudes and frequencies of cyclic stretch. We found that strain avoidance could not explain the alignment responses we observed and that cells did not seem to “remember” their strain history over long time periods. Instead, our experimental findings suggest that cell alignment was primarily determined by the cell’s current boundary conditions. Additionally, our experimental findings suggested that the

“transition frequency” at which cells begin to orient perpendicular to an applied cyclic stretch is higher in 3D conditions compared to on 2D substrates.

Using these experimental findings and in collaboration with the Deshpande and McMeeking groups, we then modified their computational model originally published by Vigliotti et al. (Vigliotti et al. 2016) to develop an improved model of cell alignment that could capture cellular alignment responses over the entire spectrum of both our experiments and in the literature. Our first modification to the original Vigliotti model was to assume that cells can remodel the surrounding collagen, their attachments to that collagen, and their cytoskeleton over time scales much longer than an individual loading cycle to achieve a state at which the increase in elastic energy due to stretching the cell beyond its reference configuration was balanced by the decrease in cytoskeletal free energy due to stress fiber assembly. Our second modification accounts for the fact that when cells are embedded in very soft gels, the cells and gel act as springs in series, and the cells experience only a fraction of the stretch applied globally to the gel (Ujihara et al. 2015). In Chapter 4, we explored potential experiments and generated preliminary data that supported our modifications to the computer model. We experimentally demonstrated that cells experience only a portion of an imposed tissue strain and that cells also can remodel their own cytoskeleton and their environment.

Overall, this improved computer model could be used to predict cellular responses to a range of loading conditions and enhanced our understanding of how cells adapt to their mechanical environment. Furthermore, our novel experimental setup to load collagen hydrogels could be used in the future to test additional experimental conditions or to mechanically load different types of tissue. These findings could improve understanding, modeling, and therapeutic modulation of tissue development, regeneration, and repair.

Effect of Repair and Loading on Achilles Tendon Wound

Healing

In Chapter 5, we used a multiscale computational modeling framework to simulate and predict how aligned fibroblasts could generate anisotropic scar tissue within healing tendons and ligaments. Tendons and ligaments transmit force between muscles and bones throughout the body and are comprised of highly aligned collagen fibers that help bear high loads. The Achilles tendon in particular is exposed to exceptionally high loads and is prone to rupture. When damaged Achilles tendons heal, they typically have reduced strength and stiffness, and while most believe that appropriate physical therapy can help improve these mechanical properties, both clinical and animal studies of mechanical loading following injury have produced highly variable and somewhat disappointing results. To help better understand the effects of mechanical loading on tendon healing and potentially guide future therapies, we developed a computational model of rat Achilles tendon healing and showed that we could

predict the main effects of different mechanical loading and surgical repair conditions reported across a wide range of published studies. This multiscale model incorporated the effect of changes in the mechanical environment on fibroblast behavior, collagen deposition, and scar formation.

We compared our model predictions to experimental data from ten different studies. We found that a single set of cellular response curves can explain features of observed tendon healing across a wide array of reported experiments in rats – including the paradoxical finding that repairing transected tendon reverses the effect of loading on alignment – without fitting model parameters to any data from those experiments. The key to these successful predictions was simulating the specific loading and surgical protocols to predict tissue-level strains, which then guided cellular behaviors according to response curves based on *in vitro* experiments. Our model results provide a potential explanation for the highly variable responses to mechanical loading reported in the tendon healing literature and may be useful in designing future therapies or experiments to test new therapies.

References

- Fomovsky, Gregory M., Samantha A. Clark, Katherine M. Parker, Gorav Ailawadi, and Jeffrey W. Holmes. 2012. "Anisotropic Reinforcement of Acute Anteroapical Infarcts Improves Pump Function." *Circulation: Heart Failure* 5 (4): 515–22. doi:10.1161/CIRCHEARTFAILURE.111.965731.
- Fomovsky, Gregory M., Jesse R. MacAdangdang, Gorav Ailawadi, and Jeffrey W. Holmes. 2011. "Model-Based Design of Mechanical Therapies for Myocardial Infarction." *Journal of Cardiovascular Translational Research* 4 (1): 82–91. doi:10.1007/s12265-010-9241-3.
- Gurtner, Geoffrey C., Sabine Werner, Yann Barrandon, and Michael T. Longaker. 2008. "Wound Repair and Regeneration." *Nature* 2008 453:7193, May. Nature Publishing Group.
- Langberg, Henning, Dorthe Skovgaard, Lars J Petersen, J Bulow, and M Kjaer. 1999. "Type I Collagen Synthesis and Degradation in Peritendinous Tissue after Exercise Determined by Microdialysis in Humans." *The Journal of Physiology* 521 Pt 1: 299–306. doi:10.1111/j.1469-7793.1999.00299.x.
- Layman, D L, E B McGoodwin, and G R Martin. 1971. "The Nature of the Collagen Synthesized by Cultured Human Fibroblasts." *Proceedings of the National Academy of Sciences of the United States of America* 68 (2): 454–58. doi:10.1073/pnas.68.2.454.
- Obbink-Huizer, Christine, Cees W J Oomens, Sandra Loerakker, Jasper Foolen, Carlijn V C Bouten, and Frank P T Baaijens. 2014. "Computational Model Predicts Cell Orientation in Response to a Range of Mechanical Stimuli." *Biomechanics and Modeling in Mechanobiology* 13 (1): 227–36. doi:10.1007/s10237-013-0501-4.
- Richardson, William J., Samantha A. Clarke, T. Alexander Quinn, and Jeffrey W. Holmes. 2015. "Physiological Implications of Myocardial Scar Structure." *Comprehensive Physiology* 5 (4): 1877–1909. doi:10.1002/cphy.c140067.
- Soslowsky, L.J., S. Thomopoulos, S. Tun, C.L. Flanagan, C.C. Keefer, J. Mastaw, and J.E. Carpenter. 2000. "Neer Award 1999: Overuse Activity Injures the Supraspinatus Tendon in an Animal Model: A Histologic and Biomechanical Study." *Journal of Shoulder and Elbow Surgery* 9 (2): 79–84. doi:10.1067/mse.2000.101962.
- Ujihara, Yoshihiro, Masanori Nakamura, Masatsugu Soga, Kenichiro Koshiyama, Hiroshi Miyazaki, and Shigeo Wada. 2015. "Computational Studies on Strain Transmission from a Collagen Gel Construct to a Cell and Its Internal Cytoskeletal Filaments." *Computers in Biology and Medicine* 56. Elsevier: 20–29. doi:10.1016/j.compbiomed.2014.10.015.

Vigliotti, A., W. Ronan, F. P. T. Baaijens, and V. S. Deshpande. 2016. "A Thermodynamically Motivated Model for Stress-Fiber Reorganization." *Biomechanics and Modeling in Mechanobiology* 15 (4). Springer Berlin Heidelberg: 761–89. doi:10.1007/s10237-015-0722-9.